ABSTRACT

LU, JIAN. Modeling and Controller Design of a Community Microgrid. (Under the direction of Dr. Ning Lu).

Microgrids are becoming increasingly popular in recent decades. The benefits of microgrids include accelerating improvement, increasing reliability, helping customers save money, reducing greenhouse gas emission, etc. Distributed energy resources (DER), e.g. combined heat and power (CHP) units, photovoltaics (PV), energy storage (ES) units, as well as thermal and electrical loads are commonly seen components in community-level microgrids. Commercial-residential hybrid buildings are commonly seen in high population density cities, especially in Asian countries, like China, Korea and Japan. With rapid growth of microgrid application, a community-level hybrid microgrid consisted of DG resources and demand response (DR) resources, commercial-residential hybrid buildings, will become possible in the future.

In this dissertation, four aspects of the modeling and controller design of a community-level hybrid microgrid are researched on. (1) A real-time dynamic CHP model for microgrid applications is presented. The CHP model includes three key components: generator, turbine, and absorption chiller. A new isochronous governor control strategy is proposed to provide zero-steady-state-error frequency regulation. The supply of building thermal loads is modeled to facilitate the calculation of the overall CHP system efficiency. The impact of ambient temperature on the maximum electrical output is considered. The developed model is implemented on OPAL-RT® for testing the microgrid controller performance in a microgrid system. (2) A data-driven, decoupled modeling method for Deriving model parameters of the thermostatically controlled appliance (TCA) is presented. HVAC is used as an example for demonstration. The method uses outdoor temperature and HVAC power consumption as inputs

to estimate the parameters of the HVAC equivalent thermal parameter (ETP) model. A novel decoupled-ETP model is proposed to decouple the modeling of the "ON" and "OFF" periods of an HVAC unit to improve the modeling accuracy. Then, an adjusted decoupled-ETP model is developed to allow users to derive the model parameters using only the midnight data. The last method fits for cases where the daytime HVAC consumptions are heavily distorted by occupant activities. The methods are tested and validated on 100 houses using actual 1-minute HVAC consumption data. (3) A novel measurement-based, data-driven residential household load forecasting algorithm is presented. Compared with traditional forecasting techniques, the proposed method adds in more measurements of individual appliances in a house, such that measurable appliances are divided into different types based on their characteristics. Different forecasting algorithms are designed for each type of appliance. The proposed forecasting algorithm is verified by a series of simulation case studies, including model-generated and field-measurement individual appliance validation, total household forecasting validation and cost-benefit studies, comparison with other traditional forecasting algorithms, etc. (4) An optimal dispatch strategy called "Microgrid Commitment" (MC) algorithm is presented to optimally dispatch and schedule the commands of all DG and DR resources while supplying both electrical and thermal loads under islanding operations. The MC algorithm is composed of 2 optimization problem to deal with the conditions when DG and DR resources can or cannot supply baseloads. Three cases are performed to verify the effectiveness of the MC algorithm and the influence of forecasting accuracy on the MC algorithm

© Copyright 2018 Jian Lu

All Rights Reserved

Modeling and Controller Design of a Community Microgrid

by
Jian Lu

A dissertation submitted to the Graduate Faculty of
North Carolina State University
in partial fulfillment of the
requirements for the degree of
Doctor of Philosophy

Electrical Engineering

Raleigh, North Carolina

2018

APPROVED BY:

_____	_____
Dr. Ning Lu Chair of Advisory Committee	Dr. David Lubkeman
_____	_____
Dr. Srdjan Lukic	Dr. Soolyeon Cho

DEDICATION

I would like to first thank my beloved mother and father, Canmei Zhang, Dr. Zhaoqin Lu. Without their support, I wouldn't be able to study at NC State University.

Specially thanks to Dr. Ning Lu, academic advisor of my Ph.D study. Dr. Lu gave me numerous suggestions and advices on my academic research as well as helps for my intern hunting, job hunting. Aside from the continuous guidance on my research, Dr. Lu also provided me with many useful supports on technical writing and presentation. I am very grateful that she accepted me as her Ph.D student in 2013.

I would also like to thank the rest of my committees: Dr. David Lubkeman, Dr. Srdjan Lukic, and Dr. Soolyeon Cho for their valuable and insightful guidance on my thesis. They have been my role models to inspire and encourage me to pursue scientific research.

Besides, I would like to thank Dr. Xiaoyuan Fan, research engineer at Pacific Northwest National Laboratory, for providing me with a summer internship opportunity and patient guidance with me during the internship in 2017. I would like to thank Mr. Carl Wilkins, vice president at Quanta Technology, LLC for providing me with an internship opportunity from Oct, 2017 to Jan, 2018. I would also like to thank my mentor Mr. Farbod Jahanbakhsh, my colleague Zhuoning Liu for their advice and support during my internship at Quanta.

Last, I would also like to express my thanks to my dear labmates: Xinda Ke, Maziar Vanouni, Jiahong Yan, Xiangqi Zhu, Weifeng Li, David Mulcahy, Gonzague Henri, Xiaoyu Wu, Tiankui Sun, Jiyu Wang, Fuhong Xie, Ming Liang. It's my great fortune to work with them during my graduate study.

BIOGRAPHY

Jian Lu was born in Taian, Shandong, China. He received the B.Sc degree in Electrical Engineering from Central South University, Changsha, China, in 2012, and the M.Sc. degree in Electrical Engineering from North Carolina State University, Raleigh, USA, in 2014. He is currently pursuing Ph.D. degree in Electric Power System Engineering in North Carolina State University, Raleigh, USA. His research interests include: microgrid modeling and control, load forecasting, renewable integration, home energy management, optimization, etc.

TABLE OF CONTENTS

LIST OF FIGURES

LIST OF TABLES

CHAPTER 1 Introduction

This chapter introduces the background of the research. New trends, state-of-the-art, challenges, and summary of the thesis are discussed in next few sections.

1.1 An Overview of mircogrids

Microgrid [1] is usually referred to a localized group of loads and sources that normally operate synchronously connected to traditional centralized grid (Macrogrid) or disconnect from traditional grid but still function autonomously. A microgrid system could include a series of distributed generators (DG) like diesel generators, combined heat and power units (CHP), photovoltaics (PV), wind or hydro turbines, energy storages, etc. Loads vary from industrial loads, commercial loads and residential loads depending on the characteristics of the microgrid. Besides benefiting the environment, DGs also increase the system reliability, reduce transmission losses and help enhance load management. The distributed sources in the microgrid can be called microsources. They are usually small units (up to several hundred kWs) with power electronic interfaces and placed at customer sites.

Microgrids usually have two main operation modes: grid-connected and islanding [2]. To operate a microgrid in the islanding mode, active distributed energy resources such as micro-generators, CHPs, PVs, wind or hydro turbines, and energy storage devices are needed. Among the DG options, the CHP unit has become increasingly popular. This is because the output of a CHP unit can be controlled within a wide range and its ramping capability is adequate. In addition, when generating electricity, a CHP unit can recycle waste heat to supply building cooling and heating loads. This greatly improves the efficiency of the overall system.

Smaller CHP units rated around several hundred kWs can be easily integrated into building energy supply systems, making them ideal generation resources for microgrid applications.

Commercial-residential hybrid buildings are commonly seen in high population density cities, especially in Asian countries, like China, Korea and Japan [3]. With rapid growth of microgrid development, a community-level hybrid microgrid consisted of DG resources (e.g. CHP units, PVs, ES units) and DR resources, commercial-residential hybrid buildings, will become possible in the future [4]. However, how to optimally dispatch of all the resources while maintaining the electrical demands and thermal demands in such a microgrid during islanding conditions has never been researched on.

In this dissertation, we mainly focus on hybrid community-level microgrids. An example of community-level microgrid one-line diagram is shown in Figure 1-1. As can be seen, the example microgrid consists of DGs such as CHP units, PVs and energy storage (ES) units. Energy storage can be used as both energy charging and discharging unit to facilitate the energy dispatch of the microgrid system. Microgrid loads include 2 types: electric loads and thermal loads. Electrical loads include all the devices supplied by electricity in both residential and commercial users. Thermal loads are usually referred to the loads which are able to add or remove heat from a space. The most commonly seen thermal loads are HVAC units. Generally, thermal loads can be fed by either heat or electricity or both. This dissertation researches on 4 aspects of the community-level microgrid: (1) modeling of a combined-heat and power unit; (2) modeling of residential HVAC units; (3) a load forecasting algorithm for residential houses; (4) a microgrid commitment algorithm to optimally dispatch all DG and demand response (DR) resources under islanding operations. The challenges and contributions of each aspect are introduced in the next section.

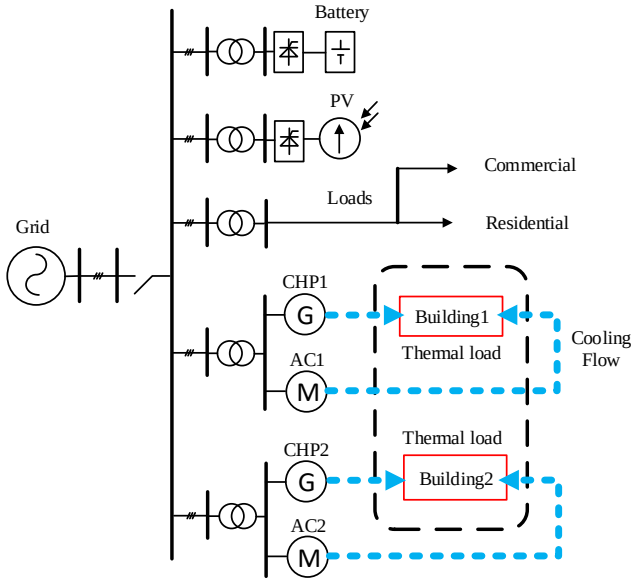

(a)

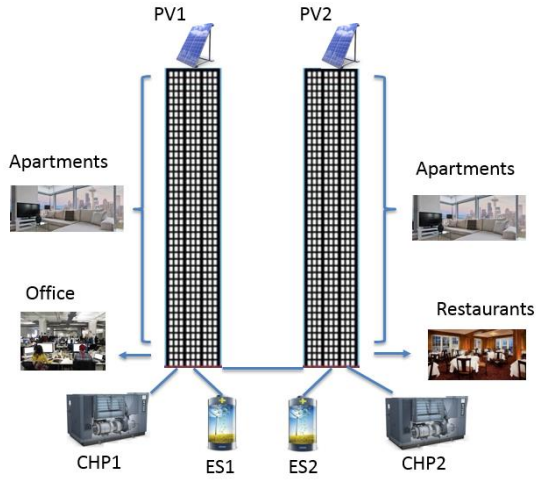

(b)

Figure 1-1. Topology of a community-level microgrid: (a) one-line diagram (b) physical view

1.2 Challenges and Contributions

The challenges of a hybrid community-level microgrid include:

- **Modeling an integrated combined heat and power (CHP) unit**

Although previous modeling efforts have enabled researchers to study the dynamic behavior of each component of a CHP unit [5]-[8], an integrated CHP model that is suitable to

run on a real-time simulation testbed for modeling both dynamic behaviors and steady-state operation of a CHP unit has not yet to be developed.

The main components of a CHP unit include a prime mover (e.g. turbine, engine or fuel cells), a generator, and heat recovery units (e.g. absorption chiller) for supplying the building heating or cooling loads. Past research efforts on modeling CHP units [5-15] have focused mainly on developing the prime movers, like turbine and generator models, for studying the thermal and electric dynamic behaviors when producing electricity for the power grid. The most influential turbine model when modeling the dynamics of heavy-duty gas turbines is the Rowen model proposed by Rowen in 1983 [14]. Many of the CHP turbine models described in the literature are based on the Rowen model [5, 17-19]. In 1994, an IEEE working group proposed another gas turbine model, known as the IEEE model [10]. Later on, a simplified Rowen turbine model, known as the GAST model [11], was developed and implemented in *PSS/E*. However, GAST and IEEE model are not as explicit as Rowen's model. Another commonly seen approach is the black-box modeling approach. Lazzaretto and Toffolo [2] designed the gas turbine model using artificial neural network (ANN) methods. Chiras, Evans and Reesa estimates the gas turbine model using another black-box method called NARMAX (nonlinear auto-regressive moving average with exogenous inputs) model [13, 19]. Sog-Kyun Kim builds a fuzzy modeling approach for a gas turbine using clustering and multi-objective optimization methods [12]. In this dissertation, we have adapted the Rowen model for modeling the turbine.

Turbine governors are crucial for regulating CHP power outputs and adjusting power system frequency. Proportional, integral and differential (PID) controllers and Woodward controllers are most commonly used for governor control. PID controllers, as described in [5,

14, 16] can reduce the steady-state error of frequency to zero but the controllers can only regulate frequency in response to load changes. Woodward controllers [7, 8] have the advantage of sharing load changes among multiple generators based on their droop characteristics but the frequency cannot be brought back to the nominal frequency. To adjust those problems, this paper proposes a new zero-steady-state-error (zero-SSE) governor based on the Woodward controller where load changes can be shared among different generators and the steady-state error of frequency regulation is zero under islanding conditions.

Absorption chiller is another important component of a CHP unit. When modeling the absorption chillers, an important consideration is the building thermal loads. When all the building thermal loads can be provided by the absorption chiller, then electric heating or cooling is no longer needed. This increases the overall efficiency of the CHP system. If only part of the building thermal load can be satisfied, one needs to calculate how much electricity is consumed for cooling or heating the building. Therefore, it is important to include the modeling of building thermal dynamics with respect to the ambient temperature when calculating the overall system efficiency.

Although previous modeling efforts have enabled researchers to study the dynamic behavior of each component of a CHP unit [7, 11, 14, 17], an integrated CHP model that is suitable to run on a real-time simulation testbed for modeling both dynamic behaviors and steady-state operation of a CHP unit has yet to be developed. Therefore, in this dissertation, a CHP model built in Simulink that can operate in both grid-connected mode and islanding mode is proposed. A real-time microgrid simulation test system consisting of a CHP unit, an energy storage unit (ES), a PV system, and electric loads, is used to demonstrate the performance of the proposed model. The test system runs on an OPAL-RT® testbed and is used as a tool for

developing and testing microgrid controllers. Gas turbines are one of the most commonly used prime mover of a CHP. Depending on the type of shaft, the gas turbine of a CHP system can be either single-shaft or two-shaft [8]. This dissertation focuses on modeling the single-shaft turbine.

The main contribution of combined heat and power unit modeling is summarized as follows. First, a new isochronous governor control strategy for zero-steady-state error frequency regulation in islanding mode is proposed. Second, an absorption chiller model that accounts for using waste heat from a CHP unit to supply building electric heating and cooling load when calculating the overall efficiency of the CHP system is proposed. Third, the derating phenomena of the CHP unit is simulated by modeling the impacts of ambient temperature variations on the maximum electrical output, fuel efficiency, and reusable heat outputs, which are neglected by most researchers.

- **Modeling of residential HVAC units**

Thermostatic-controlled appliances (TCA) such as heating, ventilation and air conditioning (HVAC) units, and water heaters, are the most commonly used residential appliances, and are considered to be perfect load-side resources for demand response programs and home energy management (HEM) systems. To control the electricity consumption of a TCA unit without tempering the user comfort, an equivalent thermal parameter (ETP) model of the TCA unit is normally needed to forecast the ON/OFF status of the unit for the next few hours. The ETP model uses the thermostat setpoint, outdoor temperature, and an initial room temperature as inputs to predict the subsequent ON/OFF cycles.

In [36-40], load detection methods are proposed based on signal processing methods such as signal extraction, neural networks, spectrum analysis, V-I trajectory, wavelet

transforms. However, those methods are used for detecting the loads instead of deriving a model that can forecast the load behaviors in subsequent intervals.

For residential applications, researchers normally apply 1st or 2nd order differential equations to represent the thermal dynamics of a single-family household when outdoor temperature changes [25]. The ETP model parameters are derived from one of the two general approaches: the physics-based approach or the measurement-based approach. The physics-based methods [26]-[31] usually model the house in detail. The inputs include the material and thickness of the wall, the size and number of windows, the thermal mass in the houses, the facing of the house, etc. This type of approach is usually used for modeling a typical residential home. When modeling an actual house for the HEM control purpose, it is impractical because many unforeseeable factors, such as construction material variations, tree covers, vent locations, can have significant impact on the accuracy of the model.

Thus, the measurement-based methods are often used to derive the ETP parameters. The method proposed in this dissertation belongs to the second approach. In [25], Lu proposed a data-driven HVAC model, the parameters of which are derived from curve-fitting the HVAC consumption curves. To account for the impact of outdoor temperature, an adjustment can be made by a look-up table that contains a set of HVAC parameters under each temperature range. However, this data-driven model was derived and tested primarily using the HVAC consumption data produced by higher-order physics-based ETP models because of the lack of sub-metered high-resolution HVAC consumption data. The accuracy of the model was not satisfactory when we validate it using metered 1-minute HVAC consumptions. This is the main reason for us to develop a refined parameter estimation method that uses the actual HVAC consumption data and corresponding outdoor temperatures as inputs for deriving the HVAC

ETP model. The derived model needs to accurately predict the ON/OFF cycles for an HVAC unit for the next few hours, which crucial for the HEM and demand response controllers to adjust the HVAC consumptions without compromise the user comfort.

The main contribution of HVAC modeling is summarized as follows: we first present a data-driven method to estimate the parameters of the ETP model. Then, a decoupled-ETP model is proposed to improve the modeling accuracy of both the ON and OFF cycles. Because in actual data sets, daytime HVAC consumptions are often heavily distorted by human activities, a tuning method, called the adjusted decoupled-ETP model, is proposed to allow users to use only the midnight data (where user behaviors are minimum) to estimate the 24-hour operations status.

- **Short term residential load forecasting**

Load forecasting is considered to be vital to meet supply and demand equilibrium. In Home Energy Management System and microgrid islanding operations, short term residential load forecasting (15 minutes to 2 hours ahead) is essential to assist the scheduling and dispatching algorithms to optimize the whole microgrid's operation and stability.

Traditionally, a lot of short term load forecasting algorithms can be found in literature reviews. Commonly seen load forecasting algorithms include: multi-linear regression [41], similar day [42], time series approaches, such as ARIMA and NARMAX [43]-[44], and artificial intelligence such as neural networks [45], etc. Most of the load forecasting techniques require inputs such as historical power consumption, outdoor temperature, humidity, time of the day, weekday or weekend, holiday or workday, etc. to increase the forecasting accuracy. However, these techniques are suitable for integrated load forecasting such as utility level, substation level, or community level, but not suitable for single residential household loads.

This is because aggregated loads tend to have similar trends based on the type of day and weather. And also aggregated loads tend to be smooth, which makes it easier to forecast, as is shown in Figure 1-2. However, for a single residential household, as is shown in Figure 1-3, load changes very frequently in an hour. Besides, the peaks are spiky and shows no obvious trend. Also, the load consumptions depend heavily on residents' personal habits and schedules, e.g., different users may have very different load patterns. Therefore, using traditional load forecasting techniques will generate huge errors in single household load forecasting.

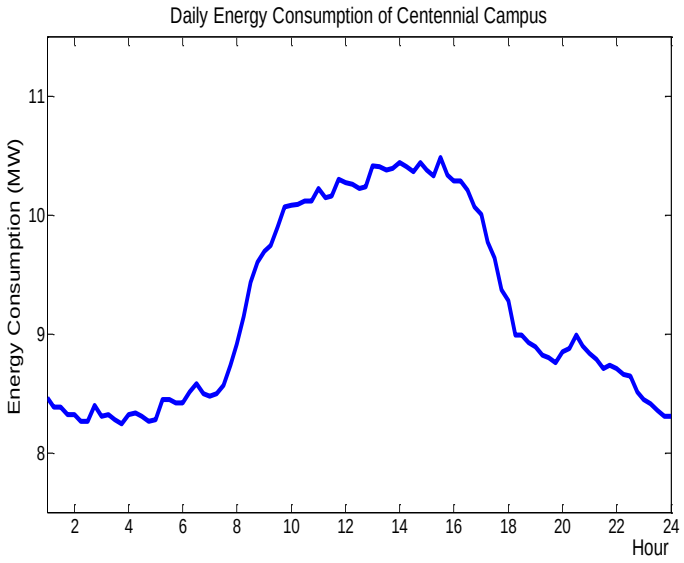

Figure 1-2. Daily energy consumption of centennial campus

So in this dissertation, we propose a novel measurement-based, data-driven residential load forecasting algorithm to improve the forecasting accuracy of traditional load forecasting techniques. In the proposed forecasting algorithm, measurable appliances are divided into different groups based on their characteristic. Every group has its own forecasting algorithm. A cost-benefit study on forecasting accuracy versus number of appliances measurable is also performed to look for the best combination of appliances measurable.

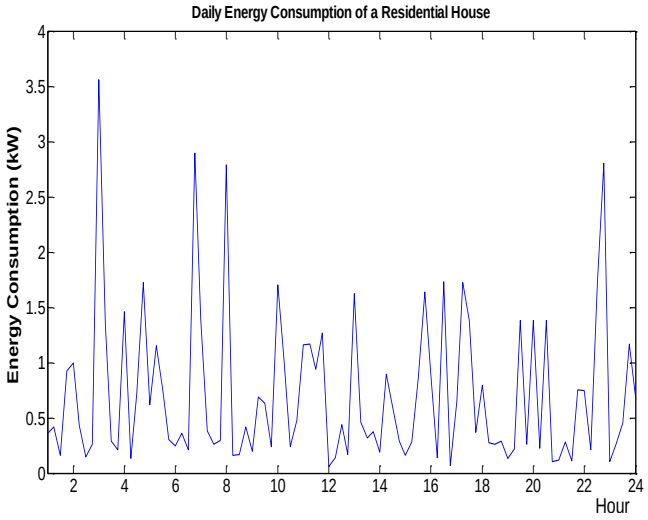

Figure 1-3. Daily energy consumption of a residential house

- **Energy dispatch between multi-CHP units in islanding conditions**

A series of papers on microgrid optimal dispatch have been published recently. J. Sohn proposed a generation applications package for CHP in on-grid and off-grid energy management system [55]. But [55] oversimplified the thermal output of the CHP unit to be proportional to its electrical output, which is not reasonable [21]. Z. Wu proposed an economic optimal schedule of CHP microgrid system using chance constrained programming and particle swarm optimization [5]. But it only considered the optimization of grid-connected condition. X. Lin proposed a dynamic optimal dispatch of CHP microgrid based on Leapfrog Firefly algorithm [56]. However, the authors did not consider impact of the ambient temperature on fuel efficiency and the exhaust heat output is also oversimplified. Besides, none of the papers talk about the dispatch of resources in commercial-residential hybrid microgrids.

In Chapter 5, a microgrid system which is consisted of several commercial-residential hybrid buildings, and scheduled to operate under islanding conditions for a period of time is studied. A microgrid commitment (MC) algorithm is designed to optimally dispatch the DG resources (PV and ES) as well as the DR resources while maintaining the electrical and thermal

balance of the microgrid system. Compared with previous published papers, the contribution of our paper lies in the following aspects: (1) this is the first research on the optimal dispatch strategy of commercial-residential hybrid microgrids under islanding operations. (2) our method depicts the generation of exhaust heat and fuel efficiency more accurately such that the thermal balance can be modeled in a more practical way; (3) controllable loads, especially TCAs can bid in the market such that demand response will not create an aftermath peak after being controlled.

The overall contribution of the dissertation is summarized as follows:

1. Develop a dynamic model of combined heat and power unit that can operate under both grid-connected and islanding mode.
2. Develop a data-driven HVAC model based on only ambient temperature and power consumptions which estimates the HVAC operations during daytime and nighttime.
3. Develop a novel, data-driven residential load forecasting algorithm which benefits the energy dispatch of the microgrid. A cost-benefit study on forecasting accuracy versus number of appliances measurable is also performed to look for the best combination measurements.
4. A microgrid commitment (MC) algorithm is designed to optimally dispatch all the DG resources (CHP, PV and ES) as well as the DR resources while maintaining the electrical and thermal balance of the microgrid system under islanding operations.

1.3 Organization of the dissertation

The rest of the dissertation is organized as follows. Chapter 2 presents detailed modeling strategies of each component of in the microgrid, including CHP unit, loads, PV and energy

storage. Chapter 3 presents a decoupled, data-driven TCA model based on only ambient temperature and power consumptions to estimate operations of residential TCAs. Chapter 4 presents a novel, data-driven household load forecasting algorithm. Chapter 5 introduces the MC algorithm in microgrid islanding conditions. Chapter 6 summarizes the report.

CHAPTER 2 Modeling Combined Heat and Power Units for Microgrid Applications

This chapter introduces the detailed modeling methodology of each component in the CHP unit. The microgrid is composed of multi-CHP units, loads, PVs and ES units. Electric load models are simplified to be a time series of real and reactive power and can be replaced with a current source or a dynamic load block in Simulink. Other units like PVs and ES units can also be treated in the same way.

The CHP unit discussed in this dissertation consists of three main components: a gas turbine, a synchronous generator, and an absorption chiller, as shown in Figure 2-1. In this section, we will discuss the modeling of each component for the real-time operation of a CHP unit in both grid-connected and islanding modes.

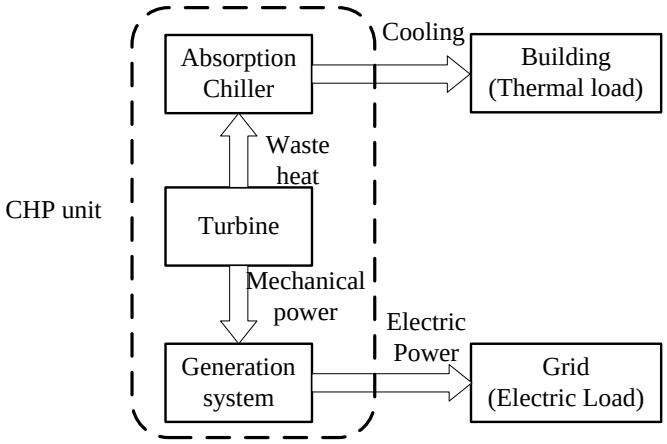

Figure 2-1. Configuration of a CHP unit

2.1 Modeling Considerations

Because the CHP model is developed for a real-time simulation system that can be used to develop and test microgrid controllers, the following five functionalities need to be implemented:

(1) *Following power dispatch command:* The steady-state power operation point needs to follow the power setpoint and dynamic responses resulting from setpoint changes needs to be correctly reflected.

(2) *Providing frequency regulation:* In grid-connected mode, the CHP unit is assumed to operate in constant power mode. However, in islanding mode, the CHP unit can enter frequency regulation mode to maintain system frequency.

(3) *Supplying building thermal loads:* The turbine model outputs need to include the amount of reusable waste heat entering the absorption chiller. The building heat transfer process needs to be modeled so that the building thermal loads can be assessed. These loads will first be supplied by the absorption chiller and any unmet thermal loads will be supplied by the electrical systems. Thus, the efficiency of the overall CHP unit for supplying both the electrical load and the building thermal load can be calculated.

(4) *Maximum power output:* The maximum power output of the CHP unit needs to be correlated to the ambient temperature so that the derating caused by high outdoor temperature can be modeled.

(5) *CHP model runtime:* The CHP model can be run for real-time simulation, so the computational speed must meet the real-time simulation requirements.

Section 2.2 to 2.6 describe the model of each CHP component, including turbine model, generator model, microgrid coordinator controller model, absorption chiller model and efficiency calculation methods.

2.2 Turbine Model

The gas turbine model shown in this section is derived based on the Rowen model [14], which is a single-shaft microturbine. Figure 2-2 shows the components of the microturbine

system model. The model consists of a speed governor, fuel system, compressor, temperature control and acceleration control [14, 17]. The following subsections introduce the details of each component of the microturbine system.

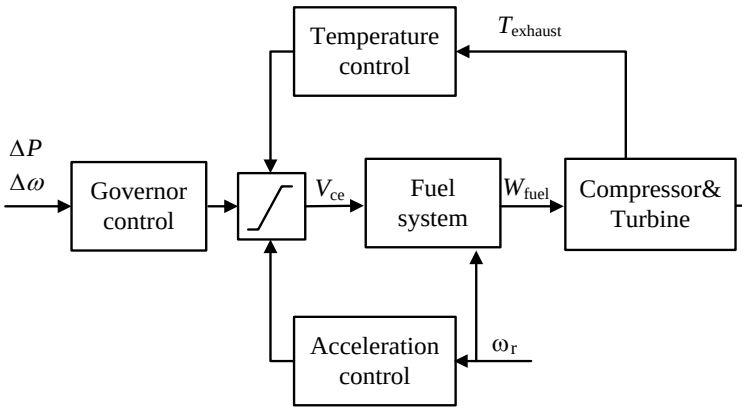

Figure 2-2. Main components of a CHP natural gas turbine model

2.2.1 Governor Control

The CHP turbine governor has two control modes: droop control and isochronous control [14]. In grid-connected mode, the turbine governor is in droop control mode. In islanding mode, the turbine governor can either be in droop mode to follow a power dispatch command or in isochronous control mode to provide frequency regulation.

The block diagram for the droop-control mode of the CHP governor is shown in Figure 2-3(a) [14]. Usually the frequency variation of the bulk grid is very small. When the slope of the droop curve K_{droop} is very small, the electrical output of the microturbine-generator will follow the reference signal P_{set}. Therefore, the CHP will provide constant power based on the dispatch command received from a central controller.

The zero-SSE governor developed for this paper is based on the Woodward controller [7] by adding an integral block (highlighted in red), as shown in Figure 2-3(b). K_p and K_I are

the corresponding PI controller's proportional gain and integral gain parameters. The zero-SSE governor feeds the frequency error into the integral block (i.e. the block highlighted in red in Figure. 3(b)) so that the steady-state error of frequency regulation is driven to zero. Thus, when there is more than one CHP unit or there are other generators in the microgrid, the zero-SSE controller can adjust the CHP power output setpoint while performing frequency regulation around the setpoint.

The control inputs of the zero-SSE controller are the frequency reference ω_{ref} (usually 1 p.u.) and power dispatch command P_{set} from a microgrid coordination controller, described below in Section 2.3.

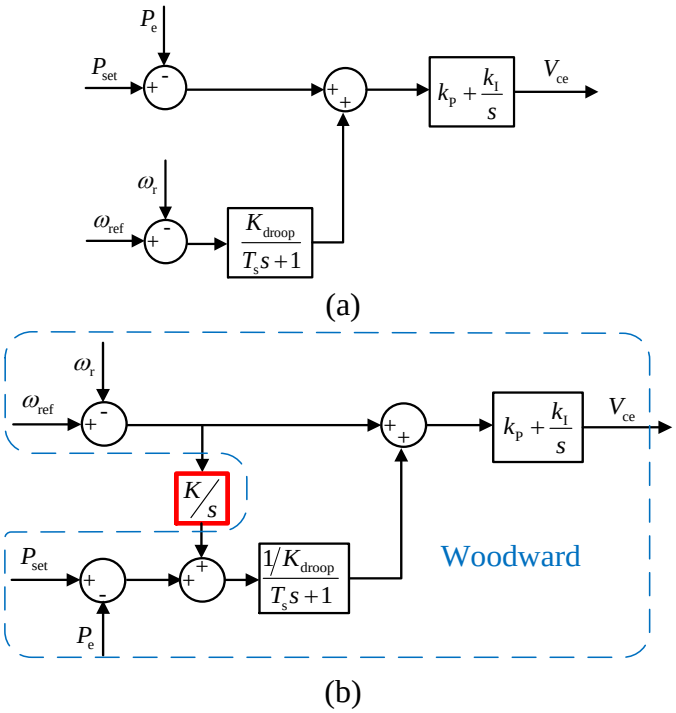

Figure 2-3. Governor control blocks: (a) Droop control governor blocks (grid-connected operation); (b) Zero-SSE governor control blocks (islanding operation)

2.2.2 Temperature Control

The temperature control block consists of three components: radiation shield, thermal coupling, and a PI controller [14], as shown in Figure 2-4. The goal of this control block is to

maintain the turbine waste heat at the reference temperature. In our case, the reference temperature is 950°F. T_{rs1}, T_{rs2}, T_{th} are the coefficients of radiation shield and thermal coupling. Typical values are $T_{rs1} = 12s$, $T_{rs2} = 15s$, and $T_{th} = 2.5s$ [137].

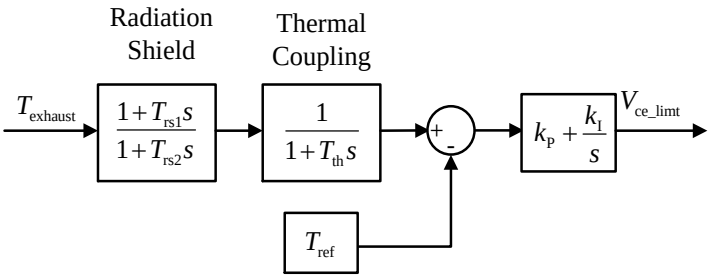

Figure 2-4. Temperature control block diagram [10]

2.2.3 Acceleration Control

An acceleration control block (see Figure 2-5) is used to limit the rate of rotor acceleration during startup in order to alleviate the thermal stress [14]. The most commonly used acceleration reference $T_{inertia}$ is 0.01 p.u. value. If the operating speed is close to its rated speed then this block can be omitted.

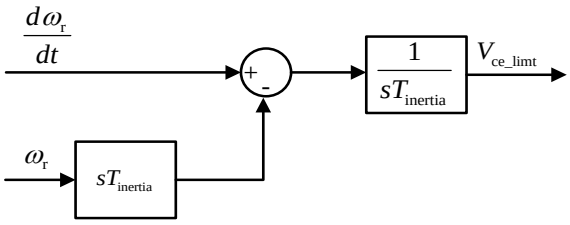

Figure 2-5. Acceleration control block diagram [14]

2.2.4 Fuel System

The fuel system used in this dissertation is Derived from [14]. The outputs of the speed governor, temperature controller and acceleration controller will be evaluated by a low-value gate (LVG) so that the minimum value of these 3 outputs is selected [14]. Thus, the output of

the LVG will represent the least amount of fuel needed for a particular operating point [17]. The fuel system consists of a valve positioner and a fuel regulator, as shown in Figure 2-6. The initial fuel rate represents the minimum amount of fuel needed to maintain the normal turbine operation. The time constants of the valve positioner T_{vp} and the fuel regulator T_{fs} reflect the time delays of the two processes. Typical values are $T_{vp} = 0.05s$, $T_{fs} = 0.4s$ and $K_{init} = 0.23$ p.u. [17].

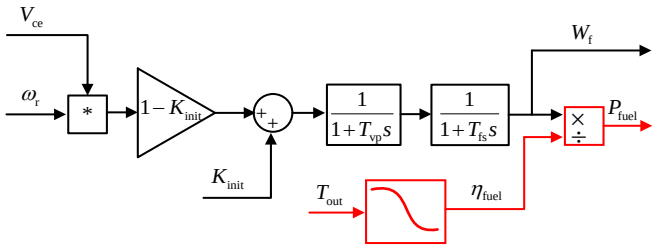

Figure 2-6. Fuel system block diagram [14]

To calculate actual fuel input, two additional blocks are added (highlighted in red in Fig. 6). As shown in Figure 2-7, the fuel combustion efficiency can be represented as a function of ambient temperature T_{out}. Therefore, a look-up table is used to calculate the total amount of fuel required P_{fuel} for generating electrical output P_e at a given ambient temperature.

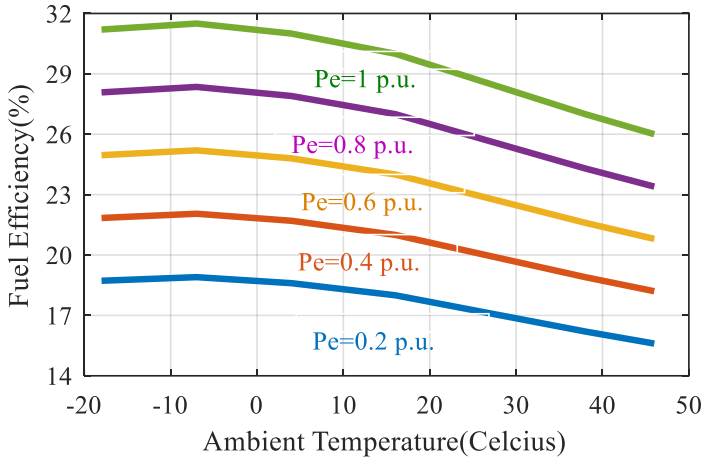

Figure 2-7. Fuel efficiency curves of a 250 kW microturbine-generator under different electrical output levels and ambient temperature levels [20]

2.2.5 Compressor and Turbine Model

The compressor and turbine models are the key components of the turbine model. As is shown in Figure 2-8, the turbine output torque and exhaust temperature are determined by [14]:

$$T_{\text{exhaust}} = T_{\text{ref}} - af_1 \times (1 - W_{\text{f1}} + af_2 \times (1 - \omega_{\text{r}})) \tag{2.1}$$

$$T_{\text{m}} = K_{\text{HHV}}(W_{\text{f2}} - bf_1) + bf_2 \times (1 - \omega_{\text{r}}) \tag{2.2}$$

where K_{HHV} is a coefficient depending on the enthalpy and T_{ref} is the reference exhaust temperature. The most commonly used value of K_{HHV} is 1.3 and T_{ref} is 950 °F. Constant values are $af_1 = 700$, $af_2 = 550$, $bf_1 = 0.23$ and $bf_2 = 0.5$. The input of the compressor and turbine model is the fuel demand in per unit value, W_{f}. Typical values of delay constants are $T_{\text{TD}} = 0.04s$, $T_{\text{CD}} = 0.2s$, $T_{\text{CR}} = 0.01s$, and $C = 1$ [17].The outputs are per unit turbine torque T_{m} and exhaust temperature T_{exhaust} [5, 14]. However, when system frequency is constant at steady-state, the maximum torque is limited by the ambient temperature T_{out} as shown in

Figure 2-9 [20]. In the model, a block is added (highlighted in red in Figure 2-8) to limit the turbine torque.

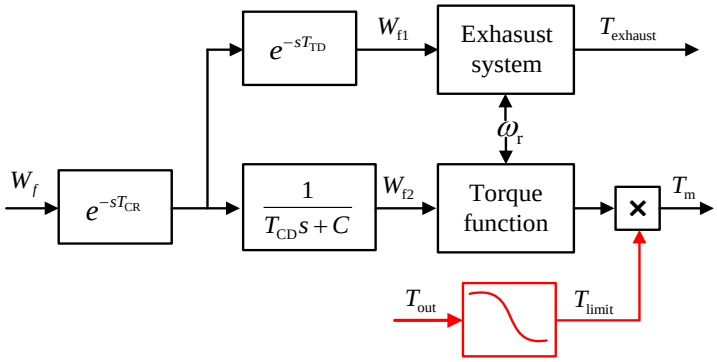

Figure 2-8. Compressor and turbine block diagrams [14]

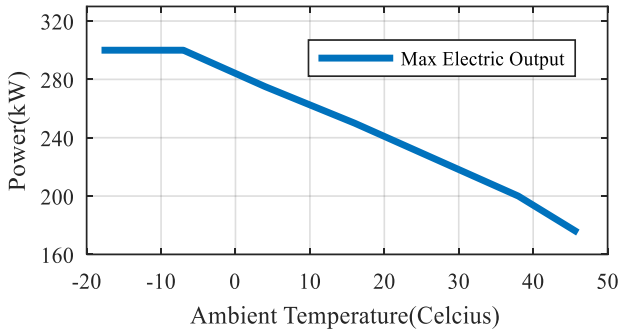

Figure 2-9. Maximum electrical output of a gas turbine at different ambient temperature [20]

The amount of the waste heat energy fed to the absorption chiller is calculated using (3.3) - (3.5) [21].

$$Q_{\text{exhaust}} = p_1(T_{\text{out}}) \times P_{\text{fuel}} + q_1(T_{\text{out}}) \times \delta \tag{3.3}$$

$$p_1(T_{\text{out}}) = a_1 T_{\text{out}} + b_1 \tag{3.4}$$

$$q_1(T_{\text{out}}) = c_1 T_{\text{out}} + d_1 \tag{3.5}$$

where Q_{exhaust} is the reusable waste heat from the turbine and δ is a binary variable representing the operation status of the gas turbine (1-on and 0-off). Typical values for the coefficients are $a_1 = 0.00028$, $b_1 = 0.2067$, $c_1 = 2.1609$ and $d_1 = 66.564$ for a 250 kW natural gas CHP unit

[21]. In this case, the thermal dynamic is neglected because it has very little influence on calculating the steady-state thermal output and the overall system efficiency.

2.3 Microgrid Coordination Controller

A coordination controller is utilized to operate multiple CHPs for the islanding operation of a microgrid. As shown in Figure 2-10, the power operation points of all CHP units are dispatched by the microgrid coordination controller. Different control strategies can be implemented in this block to determine the preferred operation point of each CHP unit. For example, based on the fuel storage and the loading condition of each CHP supplied system, the coordination controller may execute a unit commitment program to determine the power operation points of all CHP unit in the next few hours. In real-time, it can execute an economic dispatch algorithm to adjust the CHP operation setpoints. The coordinative controller also determines the output of each CHP unit, i.e. how the frequency regulation service or power dispatch should be shared among the CHPs. Because the focus of this paper is to illustrate the modeling of the CHP operation, the control strategies used in the coordination controller are not discussed in detail here.

The coordination controller has 2 main operating modes A and B. Mode A is to dispatch the power command P_{set} between CHPs based on a predetermined proportion $k_1 : k_2 : \ldots : k_n$, where n is the number of CHPs in the system. Mode B is used to fix the power dispatch points of some CHPs and let the other CHPs respond to load variations. A detailed dispatch algorithm is introduced in Chapter 5.

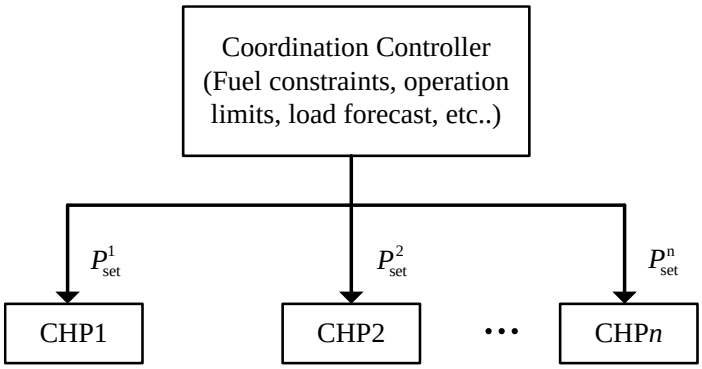

Figure 2-10. Diagram of coordination controller

2.4 **Generator Model**

The generator model used in this dissertation is a standard synchronous machine model where voltage, flux, and mechanical equations can be found in [22].

The generator excitation system model (see Figure 2-11) has two operating modes: voltage control and reactive power control. The excitation system model is simplified by representing it using a PI controller with a filter. In the voltage control mode, the input is a voltage error between the voltage reference and the filtered generator voltage output. In reactive power control mode, the input is a power error between the reactive power reference and the filtered generator reactive power output. The output V_f is the voltage of the field winding in both modes. Note that the PI controller parameters k_p, k_I and time constant T_s are not the same for the voltage control and reactive power control modes.

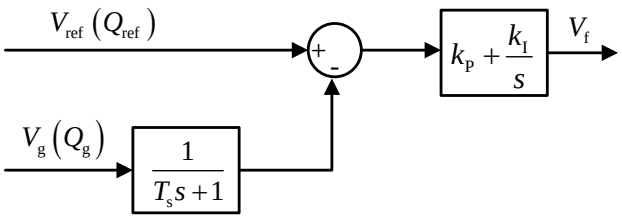

Figure 2-11. Excitation system block diagram

The generator in several kW range can be a permanent magnet synchronous machine, electrical excitation synchronous machine, or asynchronous machine with an inverter. Because the electrically excited synchronous generator has low equipment cost and high reliability, we built our generator model for this type of generators using the default model provided in the *SimPower* model package in which the voltage, flux, and mechanical equations are represented by [22]

$$\begin{cases} u_a = \dfrac{d\psi_a}{dt} + r_a i_a \\ u_b = \dfrac{d\psi_b}{dt} + r_b i_b \\ u_c = \dfrac{d\psi_c}{dt} + r_c i_c \end{cases} \tag{3.6}$$

$$\begin{cases} \psi_a = L_{ia} - M_{ib} - M_{ic} + M_{ad} i_d \\ \psi_b = L_{ib} - M_{ia} - M_{ic} + M_{bd} i_d \\ \psi_c = L_{ic} - M_{ia} - M_{ib} + M_{cd} i_d \\ \psi_f = L_f i_f + M_{df} i_d + M_{af} i_a + M_{bf} i_b + M_{cf} i_c \\ \psi_d = L_d i_d + M_{df} i_f + M_{ad} i_a + M_{bd} i_b + M_{cd} i_c \end{cases} \tag{3.7}$$

$$\begin{cases} T_e = \dfrac{1}{\sqrt{3}} n_p \left[\psi_a \left(i_b - i_c \right) + \psi_b \left(i_c - i_a \right) + \psi_c \left(i_a - i_b \right) \right] \\ J \dfrac{d\omega_r}{dt} = T_m - T_e \end{cases} \tag{3.8}$$

where u is the terminal voltage; i is the output current, r is the resistance of the winding; ψ is the flux produced by the winding; L is the self-inductance; M is the mutual inductance; T_e is the electrical torque; T_m is the mechanical torque; n_p is the number of pole pair; J is the inertia of the rotor (including the generator and turbine); ω_r is the mechanical speed of rotor.

2.5 **Absorption Chiller Model**

The main objective in the modeling of the absorption chiller is to facilitate the calculation of the overall system efficiency of the CHP unit. The inputs to the absorption chiller

model are the amount of exhaust heat Q_{exhaust} and the exhaust heat temperature T_{exhaust}. The output of the model is the equivalent electric power consumption P_{abs}, which is the electric power consumption of an electric chiller for supplying the same building thermal load. Converting the thermal load supplied by an absorption chiller to the equivalent electrical load will facilitate the calculation of the overall system efficiency. This is because we calculate the total thermal need of a building as if the whole building will be supplied by an electric chiller. Thus, if the absorption chiller will be able to supply the total load, the electric chiller is off and the electricity consumption is zero. Otherwise, the unmet thermal load will be supplied by the electric chiller. For this reason, we ignored the modeling of the thermal dynamics of the absorption chiller because only the total amount of thermal load is relevant to the efficiency calculation.

The absorption chiller will start to operate only if the exhaust heat temperature T_{exhaust} is higher than a certain value. The thermal efficiency of an absorption chiller is defined as the coefficient of performance COP_{a} shown in (3.6):

$$COP_{\text{a}} = Q_{\text{cool}} / Q_{\text{exhaust}} \tag{3.6}$$

where Q_{cool} is the cooling capacity. Normally, the COP_{a} for a single-effect absorption chiller ranges from 0.6 to 0.8 and the COP_{a} of a double-effect absorption chiller ranges from 1.4 to 1.6 [23].

If the same thermal load is supplied by an electric chiller, the efficiency of the chiller COP_{e} is defined as

$$COP_{\text{e}} = Q_{\text{cool}} / P_{\text{abs}} \tag{3.7}$$

Normally COP_e of an electric chiller ranges from 2.0 to 6.1 [23].

Therefore, the input of the absorption chiller efficiency model is the exhaust reusable heat from the turbine in kW and the output is its equivalent electricity consumption in kW. Thus, the equivalent electric power consumption is

$$P_{abs} = \frac{Q_{exhaust} \times COP_a}{COP_e} \tag{3.8}$$

2.6 CHP Efficiency Calculation

The efficiency of a CHP unit at time t can be calculated by

$$P_{reused}(t) = \min\{P_{abs}(t), P_{thermal}(t)\} \tag{3.9}$$

$$\eta_{CHP}(t) = (P_e(t) + P_{reused}(t)) / P_{fuel}(t) \tag{3.10}$$

where $P_{thermal}$ is the thermal load demand; P_e is the electric output power from generator, and P_{fuel} is the gas turbine input fuel heat power. The efficiency of the CHP unit over a time period t can be calculated by

$$\eta_{CHP} = (\int_t P_e dt + \int_t P_{reused} dt) / \int_t P_{fuel} dt \tag{3.11}$$

2.7 Simulation Tests

In this section, two case studies are presented to evaluate the performance of the proposed CHP model in grid-connected and islanding modes, respectively. As shown in Figure 2-12, the microgrid test system has two identical CHP units, a photovoltaic generator, a battery storage unit, and electrical loads connected to an ideal grid supply. Each CHP is connected to a thermal load representing the air conditioning (AC) system in a commercial building.

Modeling parameters of the distribution circuits, transformers, and each piece of equipment are shown in Table 2-1.

2.7.1 Grid Connected Mode

In grid-connected mode, the building thermal load varies with respect to the ambient temperature and the PV outputs vary with respect to the solar radiation. The electrical loads vary every second. The output of the CHP unit can follow the operation setpoint sent by a microgrid controller. In the grid connected mode, we want to verify: (1) the CHP model functions properly with other models; (2) the energy efficiency of the CHP system under different loading conditions can be calculated.

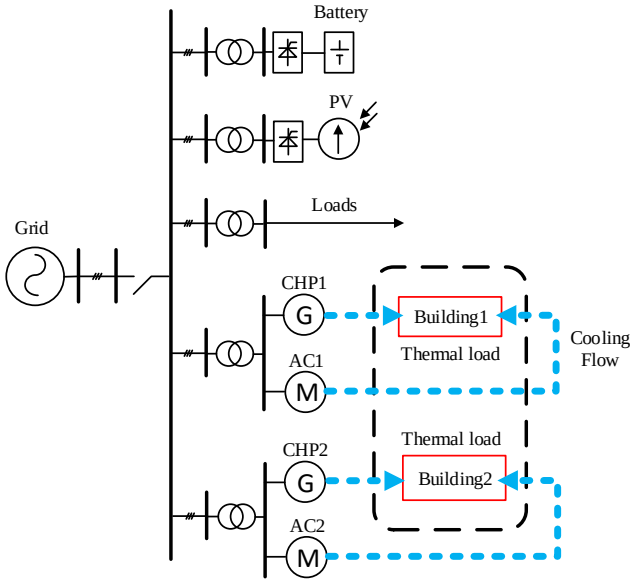

Figure 2-12. One-line diagram of the microgrid test system

Table 2-1 Parameter of the microgrid

Parameters	**Parameter values**
Base power (kW)	250
Base frequency (Hz)	60
Electric loads (kW)	varies second by second
Thermal loads in P_{abs} (kW)	varies from 37 to 78
Energy storage capacity (kWh)	258
Energy storage maximum charge/discharge rate (kW)	129
Photovoltaics (kW)	varies from 0 to 380
CHP generator capacity (kW)	250
Absorption chiller COP_a	1.4
Electric chiller COP_e	4
Line impedance (ohms/ km)	0.123+j0.3637
Transformer impedance	2.09% p.u.

The simulation results are shown in Figure 2-13 to Figure 2-16. The dispatch curves of the battery and the CHP systems (Figure 2-13) are calculated based on the time-of-use rate using a coordination algorithm. The power setpoints sent to the CHP as well as the actual CHP power outputs are shown in Figure 2-14. A zoom-in plot of the dynamic responses of the microgrid system in the grid-connected mode is shown Figure 2-15. Note that because the same dispatch command is sent to the 2 CHP units, then their performances are the same. Therefore, only the performance of CHP1 is shown in the following figures.

The following observations are made from the results:

- The CHP system follows dispatch commands precisely and the dynamic responses between the setpoint changes are reflected (See Figure 2-13).
- The derating effect can be properly represented. As shown in Figure 2-13, the CHP system is required to generate 250 kW between 14:00 to 18:00. However, because of the high ambient temperature, the maximum output of the CHP is DGated to approximately 220 kW.

- Figure 2-13 shows the total power output at the point of common coupling (PCC) P_{PCC} as well as the power output of each component in the microgrid system. When the control objective is to minimize the cost based on the TOU price, P_{PCC} will be minimized during peak price periods. The overall system works seamlessly over the 24-hr simulation periods.

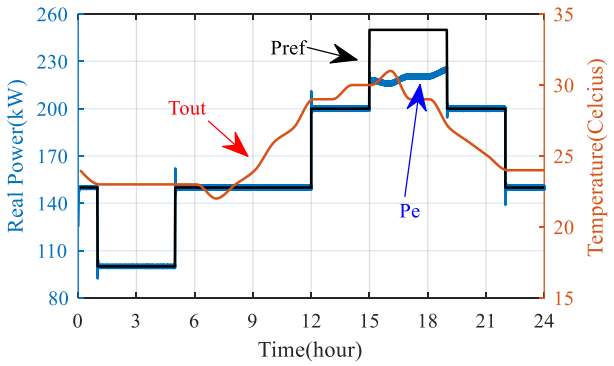

Figure 2-13. CHP power output with respect to ambient temperature and power reference command

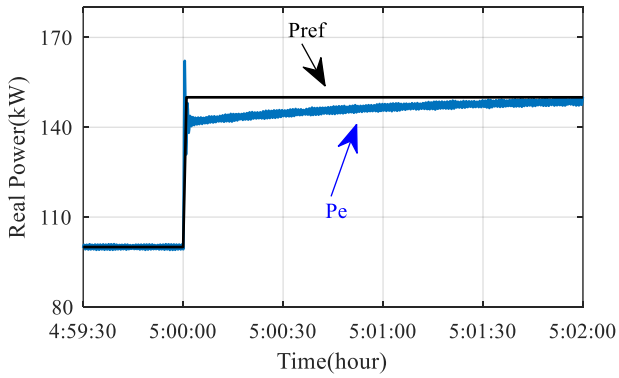

Figure 2-14. Dynamic responses of transitions between two setpoints in the grid-connected mode

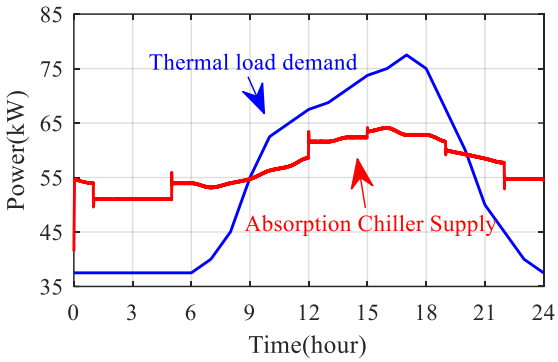

Figure 2-15. Comparison of reusable heat from absorption chiller and thermal loads

Note that in this simulation, it is assumed that the building thermal loads can be supplied by either the absorption chiller or the electric chiller. However, the absorption chiller will supply the thermal load as much as possible, so that only the unsatisfied thermal load of the absorption chiller will be supplied by the electrical chiller to achieve a higher overall system efficiency. As shown in Figure 2-15, when the building thermal load exceeds the absorption chiller supply capability between 9 a.m. to 20 p.m., the electrical chiller will have to be brought online to supply the cooling load.

Based on (2.14), the efficiency of CHP over 24 hours is 32.1%. If one does not consider the thermal loads supplied by the absorption chiller, then the efficiency is only 24.7%. Note that the overall system efficiency when using the CHP unit depends heavily on COP_a and COP_e as well as the CHP output. At a lower power setpoint, a CHP unit has less capability to supply building thermal load. So there may be a tradeoff between the needs to supply the building thermal load and the need to reduce the CHP electrical power outputs.

2.7.2 Islanding Mode

In islanding mode, microgrid generators need to not only follow power setpoints sent from a microgrid controller but also provide primary and secondary frequency regulation. In this subsection, we use the same microgrid topology (see Figure 2-12) to test the CHP model

performance. Seven operational cases are presented. Cases 1 to 4 demonstrate the performance of the zero-SSE governor for frequency regulation. Cases 5 to 7 demonstrate the coordination between two CHPs. In the following case studies, we define P_l^i as electric power output demand of the i^{th} CHP in the microgrid and P_{set}^i as the power setpoint of the i^{th} CHP; P_e^i electric power output of the i^{th} CHP; ω_r^i is the rotor speed of the i^{th} CHP.

2.7.2.1 Case 1: Response to a large step load change

In Case 1, the response of the zero-SSE governor to a large step load change is tested. It is assumed that only CHP1 is used to supply the microgrid and CHP2 is disconnected. The zero-SSE governor of CHP1 will regulate the CHP1 power output to supply load and maintain the nominal frequency. Figure 2-16 shows when P_l^1 increases from 100kW (0.4 p.u.) to 200kW (0.8 p.u.) at 30s, that the dynamic responses of electrical output P_e^1 and rotor speed ω_r^1 are stable and all the steady-state values are within operational limits.

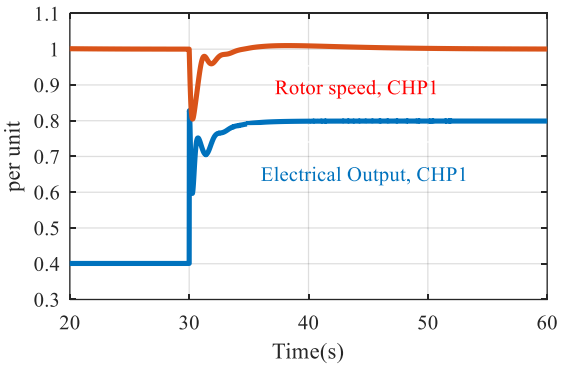

Figure 2-16. Electrical output and rotor speed of CHP1 in Case 1

2.7.2.2 Case 2: Response to Continuous Step Load Changes

In this case, it is assumed that only CHP1 is used to supply the microgrid and CHP2 is disconnected. The electrical power demand of CHP1 P_l^1 first increases from 115 kW to 190 kW and then drops to 115 kW in steps of 15 kW per second. The goal is to demonstrate the

CHP dynamic response to continuous step load changes. The electrical output P_e^1 and rotor speed ω_r^1 shown in Figure 2-17. The results show that the zero-SSE governor response is stable and the CHP unit can maintain the frequency and voltage within the acceptable ranges.

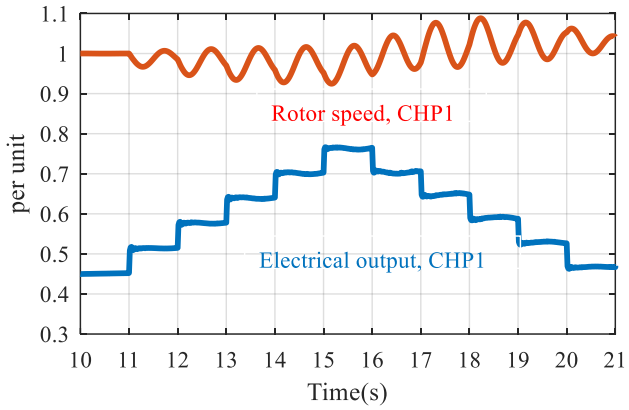

Figure 2-17. Rotor speed and electrical output in Case 2

2.7.2.3 Case 3: Response to Continuous Load Changes

In this case, CHP performance is tested using continuous actual load data. The initial settings of CHP units are the same as those used in Cases 1 and 2. As shown in Figure 2-18, the zero-SSE governor response is stable and the CHP can maintain the microgrid frequency and voltage within the acceptable ranges.

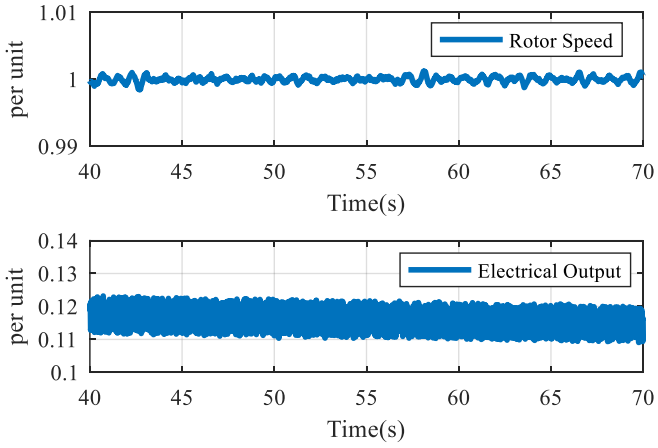

Figure 2-18. Frequency and voltage outputs in Case 3

2.7.2.4 Case 4: Frequency Regulation: Zero Steady-State Error

In this case, it is assumed that only CHP1 is used to supply the microgrid and CHP2 is disconnected. The frequency regulation characteristics of the proposed zero-SSE governor is compared with that of the Woodward governor. In this case, the electrical power output is set to rise from 0.5 p.u. to 0.8 p.u. at t=100s and drops to 0.5 p.u. at 0.1 p.u./20 seconds rate. The electrical power output and rotor speed comparison of both governors are shown in Figure 2-19.

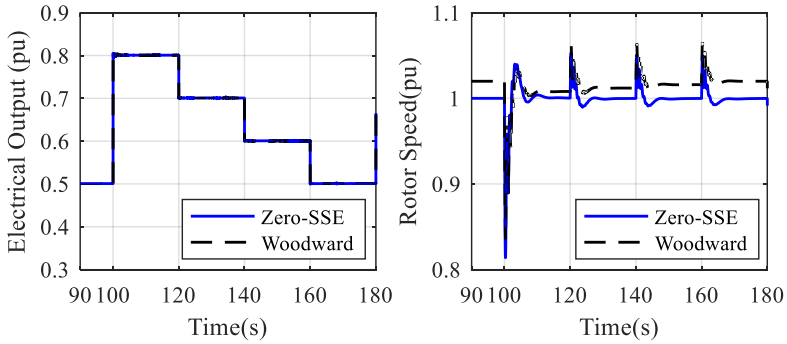

(a) (b)

Figure 2-19. Rotor speed and electrical output of CHP1 and CHP2 in Case 4: (a) Comparison of electrical power outputs in Case 4 (b) Comparison of rotor speed in Case 4

As shown in Figure 2-19, both the Woodward governor and zero-SSE governor can respond to the load change correctly. The electrical power output response of both governors are almost the same. However, it is obvious that the Woodward governor has a steady-state error in frequency regulation while the zero-SSE governor has none. This is because zero-SSE governor has an integral block to mitigate the steady state error of Woodward governor (shown in Figure 2-3(b)). The advantage of using the proposed non-SSE governor is to regulate the frequency of the microgrid in islanding situation at exactly at 1.0 p.u. while Woodward governor still needs an "AGC (Automatic generation control)" mechanism to achieve the same goal, which is usually hard to implement during islanding situations.

2.7.2.5 Case 5: Coordination Controller: Fixed Sharing Ratios among CHP units

In this case, it is assumed that the coordination controller works under *Mode A* and the power sharing ratio between CHP1 and CHP2 is 6:4, i.e. $P_{set}^{1} : P_{set}^{2} = 0.6 : 0.4$. Initially, the total demand of CHP1 and CHP2 P_l is 250 kW, P_e^1=150 kW (0.6 p.u.) and P_e^2=100 kW (0.4 p.u.). At t=10s, P_l has a large step change from 250 kW to 400 kW. As shown in Figure 2-20, the rotor speeds are stable and the power sharing ratio is as expected.

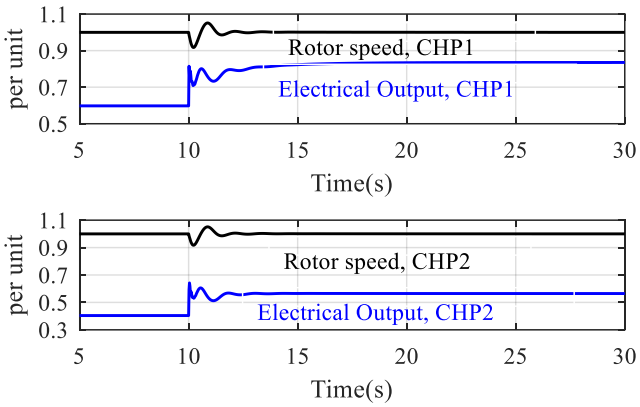

Figure 2-20. Rotor speed and electrical output of CHP1 and CHP2 in Case 5

2.7.2.6 Case 6: Coordination Controller: Balancing the Power Sharing Ratios among CHP Units

In this case, the coordination controller still works under *Mode A*. Initially the power sharing ratio between CHP1 and CHP2 is 0.6:0.4. It is assumed that during the microgrid operation one needs to balance the electrical outputs among generators so that both CHPs are generating at 0.5 p.u. A command is issued at 300s so that the power sharing ratio changes from $P_{set}^{1} : P_{set}^{2}$ = 0.6:0.4 to $P_{set}^{1} : P_{set}^{2}$ = 0.5:0.5. As shown in Figure 2-21, the electrical output of CHP1 starts to drop while CHP2 starts to rise at 300s when the command is issued. The power

outputs of both CHPs reach 125 kW in response to the coordination controller's command. The transition is stable and the whole process takes about 60 seconds.

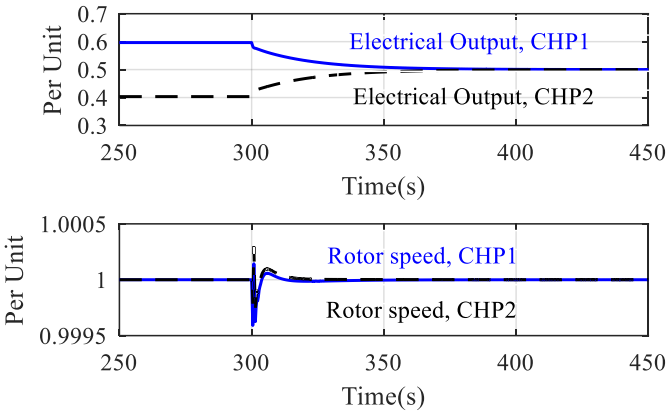

Figure 2-21. Electrical output and rotor speed of CHP1 and CHP2 in Case 6

2.7.2.7 Case 7: Master and Slave Operation Mode

In this case, it is assumed that the total electric power output demand P_l of 2 CHPs is 250 kW initially with P_e^1 =175 kW (0.7 p.u.) and P_e^2 =75 kW (0.3 p.u.). At t=10s, P_l has a step change from 250 kW to 350 kW. Coordination controller is set at *Mode B* such that CHP1 is at constant power mode (P_{set}^1 is fixed to be 0.7 p.u.) and CHP2 will meet all the load changes ($P_{set}^2 = P_l / P_{base} - P_{set}^1$). As shown in Figure 2-22, the transition is stable. As expected, CHP1 power output remains the same and CHP2 power output is increased to meet the additional demand.

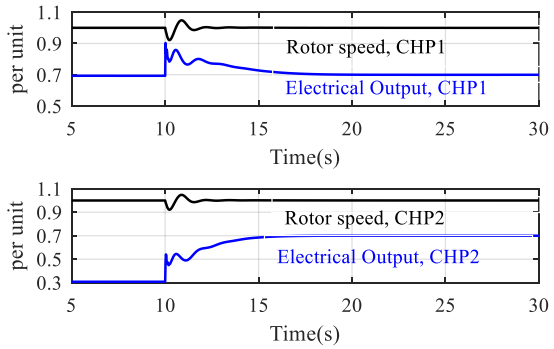

Figure 2-22. Rotor speed and electrical output of CHP1 and CHP2 in Case 7

2.8 Conclusion

This chapter proposes a CHP model for meeting different microgrid operational needs. In the grid-connected mode, the CHP unit will follow a power dispatch command from the central controller. In the microgrid operation mode, depending on the coordination command, the CHP unit will either operate as a master unit for load following and frequency regulation or as a slave unit that follows a power setpoint. The new isochronous governor control strategy allows the CHP unit to realize zero-steady-state-error frequency regulation in the islanding mode. Because the building thermal loads and the thermal exchange process of the absorption chiller is modeled, it is possible to calculate the efficiency of the overall CHP systems and model the derating phenomena. The case studies show that the proposed CHP model performs as expected in all operating modes. Future work will focus on developing the coordination controller further so that the CHP units can operate in a microgrid with energy storage, smart inverters, and controllable loads.

CHAPTER 3 A Data-Driven Decoupled Modeling Method for Thermostatically Controlled Appliances

In this chapter, we first present a data-driven method to estimate the parameters of the 1st order ETP model. Then, a decoupled-ETP model is proposed to improve the modeling accuracy of both the ON and OFF cycles. Because in actual data sets, daytime HVAC consumptions are often heavily distorted by human activities, a tuning method, called the adjusted decoupled-ETP model, is proposed to allow users to use only the midnight data (where user behaviors are minimum) to estimate the 24-hour operations status. The rest of this chapter is organized as follows. Section 3.1 introduces the methodologies. Section 3.2 shows simulation results and Section 3.3 is the conclusion.

3.1 Modeling Methodologies

We use HVAC as an example to illustrate model parameter estimation process and the adjustment algorithms. Because we focus on modeling the residential households, models of the HVAC units with variable frequency drives are not considered.

3.1.1 The 1st order HVAC ETP Model [25]

As shown in Figure 3-1, assuming that the current time step is $t = k$, the indoor room temperature T_{room} at $t = k+1$ can be represented by a 1st order ETP model as:

$$T_{room}(k+1) = \begin{cases} T_{out}(k+1) + Q \times R - e^{-\Delta t/(R \times C)} \times (T_{out}(k) + Q \times R - T_{room}(k)) & \text{when } u_{ac}(k) = 1 \text{ i.e. HVAC is on} \\ T_{out}(k) - (T_{out}(k) - T_{room}(k)) \times e^{-\Delta t/(R \times C)} & \text{when } u_{ac}(k) = 0 \text{ i.e. HVAC is off} \end{cases} \quad (3.1)$$

where T_{out} and T_{room} are the outdoor and room temperature, respectively; u_{ac} is the HVAC ON/OFF status; Δt is the duration of each time step; R represents thermal resistance; C represents thermal capacitance; and Q represents the heat flow provided by the HVAC unit. Thus, the HVAC status u_{ac} at next time step $k+1$ can be determined by

$$u_{ac}(k+1)=\begin{cases} 1 & T_{room}(k+1)<T^{-} \\ 0 & T_{room}(k+1)>T^{+} \\ u_{ac}(k) & T^{+}>T_{room}(k+1)>T^{-} \end{cases} \tag{3.2}$$

where T^{-} and T^{+} refer to the lower and upper bounds of the HVAC temperature deadband.

If T_{out} remains constant, (1) can be rewritten as

$$T^{-}=T_{out}+Q\times R-(T_{out}+Q\times R-T^{+})\times e^{-t_{ON}/(R\times C)} \tag{3.3}$$

$$T^{+}=T_{out}-(T_{out}-T^{-})\times e^{-t_{OFF}/(R\times C)} \tag{3.4}$$

where t_{ON} and t_{OFF} refers to a complete ON and OFF cycle, as shown in Figure 3-1.

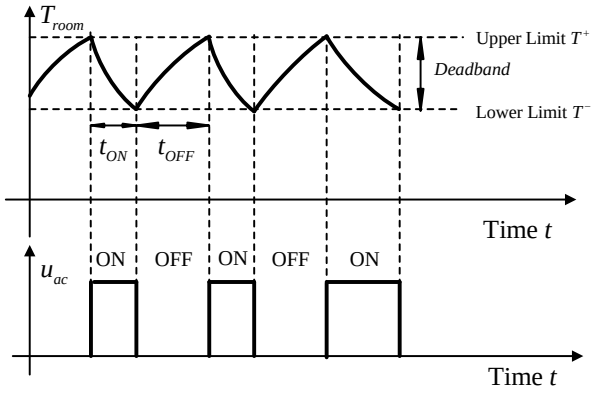

Figure 3-1. Cycling characteristics of an HVAC unit.

The biggest advantage of using the 1st order ETP model for data-driven modeling is its simplicity. RCQ values can easily be derived from the set of five variables: T^{+}, T^{-}, T_{out}, t_{ON} and t_{OFF}. The disadvantage of the model is that t_{ON} and t_{OFF} will change when T_{out} changes. So for each T_{out} range, we need one set of *RCQ* values to meet modeling accuracy requirements. In addition, because of solar radiation, day-time and night-time *RCQ* values may not be the

same even though they are Derived at the same T_{out}. For example, one set of RCQ values can only be used for a T_{out} range of 5~10 °F for the nighttime of the day. In this chapter, we developed a decoupled-ETP model with a tuning method to resolve these modeling issues, which is the main contribution of this chapter.

3.1.2 Data Preparation

The HVAC consumption, P_{ac}, and the outdoor temperature, T_{out}, were collected by researchers in the PECAN street project [54]. We selected 100 houses (located in Austin, Texas) with 1-minute sub-metered HVAC power consumption and outdoor temperature data for conducting the study. Because we want to model an HVAC unit in its cooling mode, the data length we used is from July to August, 2015.

To derive the RCQ parameters, we need to screen the data to exclude the periods where the HVAC power consumption is significantly distorted by occupants' activities such as manually turning ON/OFF the HVAC unit, frequent changes of the thermostat setpoints, opening doors/windows for a prolonged period, etc. Therefore, we separated the data into three types. The first type is the *Midnight data* from 12 a.m. to 5 a.m. where the residents' activities that can influence the HVAC operations are at the minimum, as shown in Figure 3-2 (a). The second type set is the 24-hr *Whole-day data* in which cases occupants show very little interference on HVAC operations, as shown in Figure 3-2 (b). The third type is the discarded data set where HVAC unit operation is either erratic or always ON/OFF, as shown in Figure 3-2 (c). Note that when a household has an under-sized or multiple HVAC units, we cannot model the HVAC operation appropriately by the RCQ parameter based ETP model.

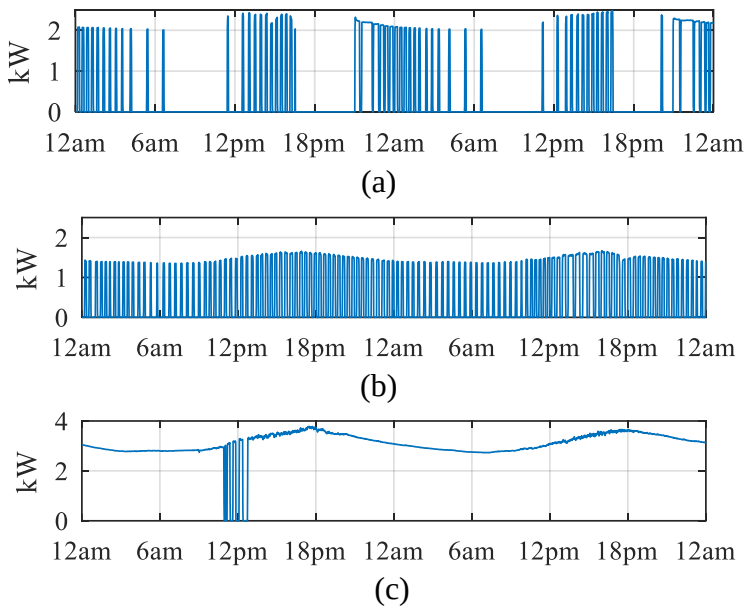

Figure 3-2. Examples of HVAC power consumptions data collected in the PECAN street project. (a) Only Midnight data can be used because the HVAC unit is OFF most of the time during the day; (b) Both whole-day data and Midnight data can be used because the HVAC unit has consistent ON/OFF cycles; (c) A discarded data set (The HVAC is always ON, so modeling it using an ETP model is no longer valid).

3.1.3 1st order ETP Model RCQ Parameter Estimation

A flow chart is introduced in Fig. 3 to illustrate the six steps in the RCQ parameter estimation process for the 1st order ETP model of an HVAC unit.

- **Step 1: Obtain the HVAC ON/OFF curves**

  In this step, the HVAC power consumption data is converted into HVAC status using

$$u_{ac}(t)=\begin{cases}1 & \text{if } P_{ac}(t)>0.5\times P_{ac,\max}\\ 0 & \text{if } P_{ac}(t)\le 0.5\times P_{ac,\max}\end{cases} \tag{3.5}$$

where $P_{ac,\max}$ is the maximum power consumption during $t\in\tau$ and τ is the set of total time horizon of input data; u_{ac} is the HVAC status.

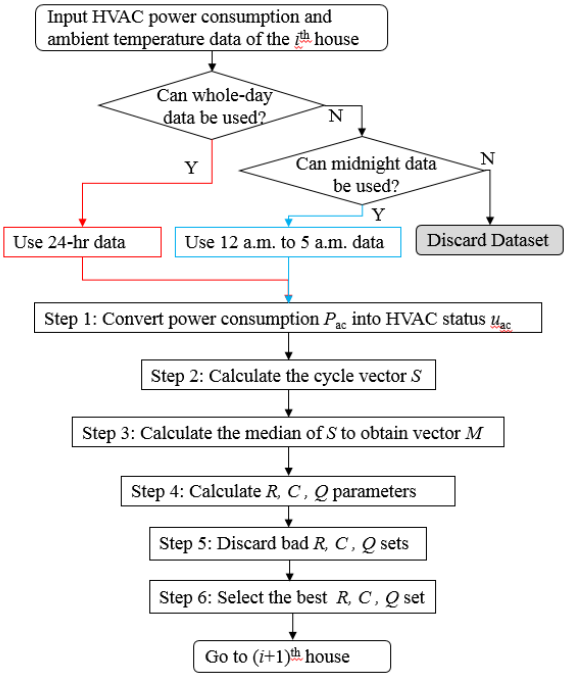

Figure 3-3. Flow chart of the RCQ parameter estimation process.

- **Step 2: Build a cycling characteristic vector S**

From the HVAC ON/OFF curves, calculate the duration of each ON and OFF cycle, t_{ON} and t_{OFF}, as well as the corresponding average outdoor temperature T_{out_avg} during each ON or OFF cycle. Note that each T_{out_avg} will be rounded to its nearest integer value. Store $t_{ON}(i)$, $t_{OFF}(i)$, and $T_{out\_avg}(i)$ in the cycling characteristic vector, $S(i)$, for the cycle i.

To eliminate the outliers, when the difference between the maximum and minimum outdoor temperatures in an ON or OFF cycle is greater than a threshold, ΔT_{out}, this cycle will be discarded. We recommend $\Delta T_{out} = 4\text{F}°$. This is because when temperature varies a lot in a cycle, the RCQ values may not be representative. An example of the *S* matrix is shown in Figure 3-4 and Table 3-1.

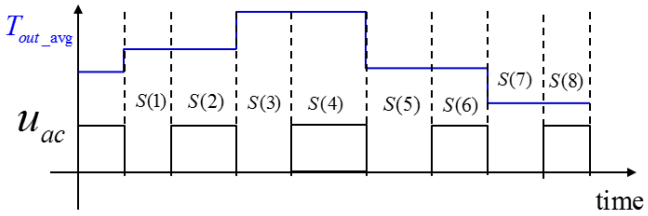

Figure 3-4. Illustration of vector $S(i)$ over a period of time

Table 3-1 An Example of Dataset S

$S(i)$	$S(1)$	$S(2)$	$S(3)$	$S(4)$	$S(5)$	$S(6)$	...
$t_{ON}(i)$	NA	14 min	NA	17 min	NA	13 min	…
$t_{OFF}(i)$	10 min	NA	11 min	NA	15 min	NA	…
$T_{out\_avg}(i)$	85 °F	85 °F	89 °F	89 °F	84 °F	81 °F	…

- **Step 3: Correlate t_{ON} and t_{OFF} with T_{out_avg}**

Select the median values of t_{ON} and t_{OFF} for each T_{out_avg} in S to obtain a new vector M. M will be used to derive the correlation between (t_{ON}, t_{OFF}) and T_{out_avg}. Note that if t_{ON} or t_{OFF} is missing for a certain T_{out_avg}, the T_{out_avg} will not be included in M. An example of M is shown in Table 3-2. The outdoor temperature set in M is renamed as T_o. The median value sets of t_{ON} and t_{OFF} are named as t_{ON}^{M} and t_{OFF}^{M}. Example boxplots of the ON and OFF durations with respect to different outdoor temperatures are plotted in Figure 3-5 (a) (b). The median value is selected and shown in Figure 3-5 (c).

Table 3-2 An Example of Dataset M

M(i)	$M(1)$	$M(2)$	$M(3)$	$M(4)$	$M(5)$	$M(6)$	...
$t_{ON}^{M}(i)$	10 min	10 min	11 min	11 min	12 min	13 min	…
$t_{OFF}^{M}(i)$	35 min	30 min	27 min	27 min	18 min	19 min	…
$T_o(i)$	75 °F	76 °F	77 °F	78 °F	88 °F	89 °F	…

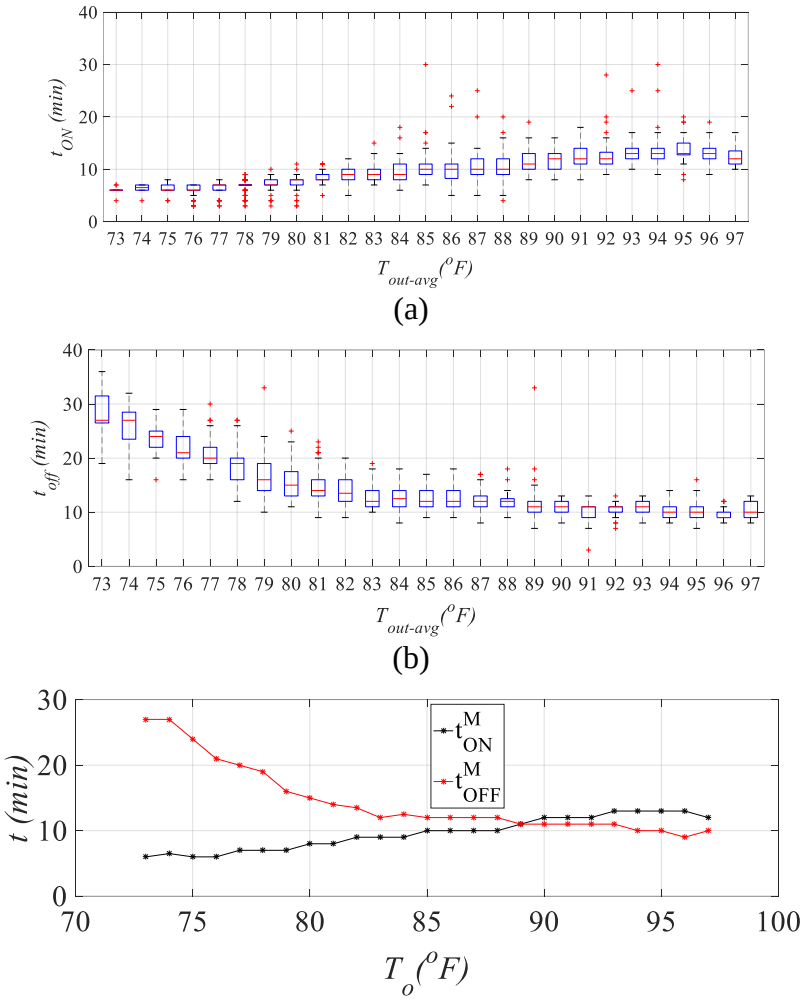

Figure 3-5. ON/OFF cycles durations under different outside temperature: (a) Boxplot of t_{ON}, (b) Boxplot of t_{OFF}, (c) t^M_{ON} and t^M_{OFF} with respect to T_{out}.

- **Step 4: derive RCQ parameters**

  Now, at each outdoor temperature $T_{out} \in T_o$, we have a set of t^M_{ON} and t^M_{OFF}. Because Q represents the heat flow contributed by the HVAC unit, the value of Q only influences the ON cycles. Note that in a curve fitting process, the RCQ values no longer represent accurately their physical characteristics as does in a physics-based model approach. So, we select Q to be -500 for all the households and tune only the values of R and C. Thus, from (3.3) and (3.4), once the value of Q is fixed, R and C can be calculated as

$$R = \frac{T^- - T_{out} + (T^+ - T_{out}) \times \mathrm{e}^{-t_{ON}^M \times \ln(\frac{T^- - T_{out}}{T^+ - T_{out}})/t_{OFF}^M}}{Q \times (1 - \mathrm{e}^{-t_{ON}^M \times \ln(\frac{T^- - T_{out}}{T^+ - T_{out}})/t_{OFF}^M})} \tag{3.6}$$

$$C = \frac{t_{OFF}^M}{\ln(\frac{T^- - T_{out}}{T^+ - T_{out}}) \times R} \tag{3.7}$$

In this dissertation, we assume that for each HVAC unit, T^+ and T^- are chosen to be $72\ ^\circ F$ and $70\ ^\circ F$, respectively. There are two observations when selecting the value for *Q*. First, *Q* is only a variable that influences the length of the HVAC ON cycle because in the OFF cycle, the room temperature decay is unrelated with the HVAC power consumption. Second, from (3.6) and (3.7), one can deduce that if we treat the problem as a curve fitting problem instead of considering the physical meanings of RCQ parameters, an arbitrary value can be selected for *Q* to calculate a corresponding set of values for *R* and *C* while the measured ON/OFF cycling characteristics can still be reproduced by the corresponding decoupled-ETP model. Therefore, although we selected -500 as the value of *Q*, others can select another value, for example -1000 or -1500. They will obtain another set of *R* and *C* values that can also produce the same curve fitting results at the given T_{out}. However, in Step 5, we will vary T_{out} from $\min(T_o)$ to $\max(T_o)$ and the RCQ values fail to produce satisfactory results under other outdoor temperatures will be excluded in Step 5.

- **Step 5: Discard the bad RCQ sets**

A bad set of RCQ value will fail to reproduce the HVAC cycling characteristic when T_{out} varies from $\min(T_o)$ to $\max(T_o)$. The following two criterion are used to exclude the bad set of RCQ values obtained in Step 4.

(1) Criterion A: meet the HVAC capacity requirement

If we rewrite (1) as

$$t_{ON} = -R \times C \times \ln(\frac{T_{out} + Q \times R - T^{-}}{T_{out} + Q \times R - T^{+}}) \tag{3.8}$$

$$t_{OFF} = -R \times C \times \ln(\frac{T_{out} - T^{+}}{T_{out} - T^{-}}) \tag{3.9}$$

Because the antilogarithm of a logarithm function in (3.8) and (3.9) must be positive when T_{out} ranges from $\min(T_o)$ to $\max(T_o)$, we have

$$Q \times R > T^{+} - T_{out} \tag{3.10}$$

As shown in Figure 3-6, when a set of RCQ values cannot meet *Criterion A*, the physical meaning behind it is that the HVAC unit is undersized and it can no longer bring the room temperature down to T^{-} when the outdoor temperature is too high. Therefore, any set of RCQ values that violate the *Criterion A* need to be discarded.

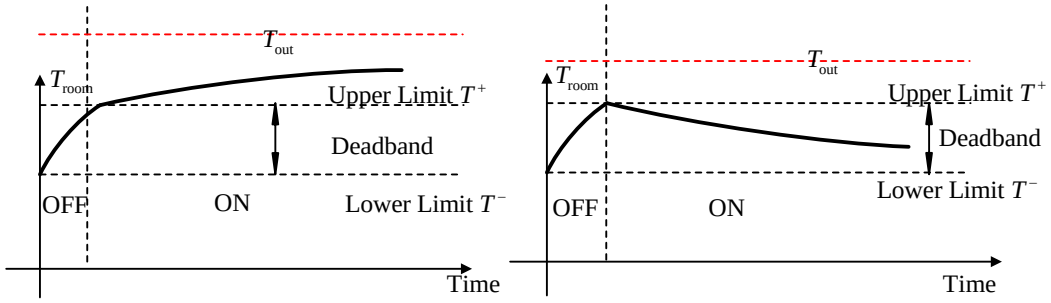

(a) (b)

Figure 3-6. Examples of cases when Criterion A is violated: (a) Room temperature rises above T^{+}; (b) room temperature fails to reach T^{-}

(2) Criterion B: Meet modeling setpoint change requirement

This criterion is made to ensure that when modeling the HVAC setpoint changes (e.g. $[T^{-}, T^{+}]$ changes to $[\bar{T}^{-}, \bar{T}^{+}]$), t_{ON} and t_{OFF} will change accordingly. Mathematically, if $\bar{T}^{+} = T^{+} + \Delta T$ and $\bar{T}^{-} = T^{-} + \Delta T$, the following equations must hold:

$$\bar{t}_{ON} - t_{ON} > f_{ON}(\Delta T, T_{out}) \tag{3.11}$$

$$\bar{t}_{OFF} - t_{OFF} > f_{OFF}(\Delta T, T_{out}) \tag{3.12}$$

where $f_{ON}(\Delta T, T_{out})$ and $f_{OFF}(\Delta T, T_{out})$ are functions that determine the minimum changes of t_{ON} and t_{OFF} with respect to the HVAC setpoint change, ΔT, and T_{out}. Note that $\bar{t}_{ON}$ and $\bar{t}_{OFF}$ are calculated from (3.8) and (3.9) by replacing T^- and T^+ with $\bar{T}^-$ and $\bar{T}^+$. Any set of RCQ values that violate *Criterion B* will be discarded.

- **Step 6: Select the best RCQ set**

After the bad sets are eliminated, the best RCQ set (defined as R_f, C_f, and Q_f obtained at outdoor temperature T_f) in the *N* remaining sets can be selected by minimizing the error between the estimated and actual ON/OFF durations using:

$$\min \sum_{T_{out} \in T_o} [(\hat{t}_{ON}(T_{out}) - t_{ON}^M(T_{out}))^2 + (\hat{t}_{OFF}(T_{out}) - t_{OFF}^M(T_{out}))^2] \tag{3.13}$$

where $\hat{t}_{ON}(T_{out})$ and $\hat{t}_{OFF}(T_{out})$ are the estimated ON and OFF durations under outdoor temperature T_{out} calculated using (3.8) and (3.9); $t_{ON}^M(T_{out})$ and $t_{OFF}^M(T_{out})$ are the median value of ON/OFF durations under T_{out} from actual measurements, which can be found in dataset M in Step 3.

Figure 3-7 compares the median of the measured ON/OFF durations, t_{ON}^M and t_{OFF}^M (ON,m and OFF,m in Figure 3-6) and the estimated ON/OFF durations, $\hat{t}_{ON}$ and $\hat{t}_{OFF}$ (ON,e and OFF,e in Figure 3-7) using the best RCQ set. In this case, the RCQ values are derived when the outdoor temperature is $84°F$.

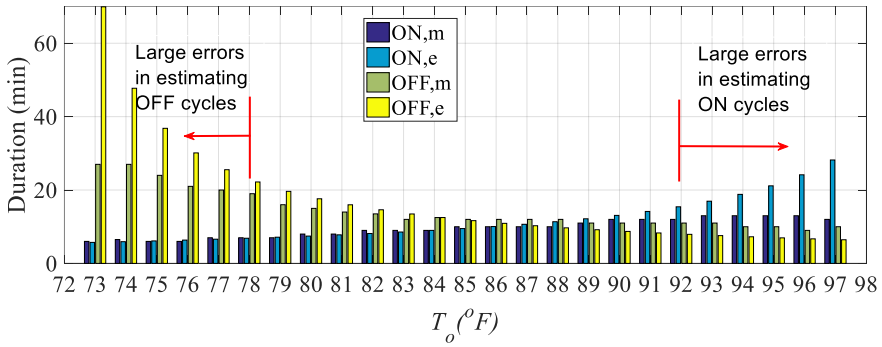

Figure 3-7. A comparison between the actual and estimated HVAC ON/OFF durations (Data source: PECAN Street Data Set. House #: 5395. Location: Austin, Texas. Duration: July 1 to Aug 31, 2015).

From the comparison, in this example, we made the following observations:

1. As expected, the model calculated ON/OFF durations fit the measurements well when $80°F \le T_{out} \le 93°F$.
2. However, when $T_{out} < 80°F$, the estimated OFF cycle durations will be significantly longer than the measured ones; while when $T_{out} > 93°F$, the estimated ON cycle durations will be significantly longer than measured ones.

This is because when using the 1st order to approximate a higher order thermal dynamic process, the nonlinearity of the actual thermal dynamic process will cause the estimated $t_{ON}^{\%}$ and $t_{OFF}^{\%}$ to deviate from the measured t_{ON}^{M} and t_{OFF}^{M} further and further when T_{out} is significantly higher or lower than T_f , at which temperature the RCQ parameters were derived. To resolve this modeling issue, we propose a decoupled-ETP model in the next subsection.

3.1.4 Derivation of the Decoupled-ETP model

As shown in Figure 3-6, the estimation errors of $t_{ON}^{\%}$ and $t_{OFF}^{\%}$ have different trends. This shows that if we focus on using one RCQ set for modeling both the ON and OFF cycles, a simple parameter adjustment is not feasible because when errors in $t_{ON}^{\%}$ is reduced, errors in

t_{OFF} will increase. From (3.8) and (3.9), we observed that t_{ON} is related with R,C,Q but t_{OFF} is only related with $R \times C$. Therefore, we propose a decoupled-ETP model so that the modeling of ON and OFF cycles are separated. Then, we can make RCQ parameters a function of T_{out} to reduce the modeling error corresponding to the T_{out} variations. Different from (3.1) and (3.2), in the decoupled-ETP model, T_{room} and u_{ac} at $t = k+1$ are calculated as:

$$T_{room}(k+1) = \begin{cases} T_{out}(k+1) + f_Q(T_{out}(k)) \times R_f - e^{-\Delta t/(R_f \times C_f)} \times & \text{if } u_{ac}(k) = 1 \\ (T_{out}(k) + f_Q(T_{out}(k)) \times R_f - T_{room}(k)) & \\ T_{out}(k) - (T_{out}(k) - T_{room}(i)) \times e^{-\Delta t / f_{RC}(T_{out}(k))} & \text{if } u_{ac}(k) = 0 \end{cases} \tag{3.14}$$

$$u_{ac}(k+1) = \begin{cases} 1 & \text{if } T_{room}(k+1) < T^- \\ 0 & \text{if } T_{room}(k+1) > T^+ \\ u_{ac}(k) & \text{else} \end{cases} \tag{3.15}$$

When T_{out} is constant, (3.14) can be rewritten as:

$$T^- = T_{out} + f_Q(T_{out}) \times R_f - (T_{out} + f_Q(T_{out}) \times R_f - T^+) \times e^{-t_{ON}/(R_f \times C_f)} \tag{3.16}$$

$$T^+ = T_{out} - (T_{out} - T^-) \times e^{-t_{OFF}/f_{RC}(T_{out})} \tag{3.17}$$

where R_f, C_f can be obtained in Section 3.1.3.Step 6. The modifications are explained in detail as follows.

3.1.4.1 Derivation of OFF cycle RCQ parameters

For the OFF cycle, define $R \times C = f_{RC}(T_{out})$ so the *RC* value is a function of T_{out}. First, from (3.17), we have

$$\hat{t}_{OFF} = -f_{RC}(T_{out}) \times \ln\left(\frac{T_{out} - T^+}{T_{out} - T^-}\right) \tag{3.18}$$

where $\hat{t}_{OFF}$ is the estimated OFF duration by using decoupled-ETP model. Second, we need to find the relationship between f_{RC} and T_{out}. By calculating $R \times C$ values under each T_{out} using

the method shown in Section 3.1.3.Step4, the linear correlation between $R \times C$ and T_{out} derived from 100 houses data is calculated. The mean correlation coefficient is 0.973 and the standard deviation is 0.0253. An example is shown in Figure 3-8(a). Thus, the linear regression model used to calculate $f_{RC}(T_{out})$ is

$$f_{RC}(T_{out}) = k_{RC} \times T_{out} + b_{RC} \tag{3.19}$$

3.1.4.2 Derivation of the ON cycle RCQ parameter

To avoid modeling temperature sensitivity of all three RCQ parameters, we choose to let $R = R_f$ and $C = C_f$ (obtained in Section 3.1.3.Step5). Once the values of *R* and *C* are fixed, we only need to make Q a function of T_{out} so that

$$Q(T_{out}) = \frac{(T_{out} - T^{+}) \times e^{-t_{ON}^{M}/(R \times C)} + T^{-} - T_{out}}{R \times [1 - e^{-t_{ON}^{M}/(R \times C)}]} \tag{3.20}$$

The correlation between Q and T_{out} derived from 100 houses are calculated. The mean of correlation coefficient is 0.941 and the standard deviation is 0.048. An example is plotted in Figure 3-8(b). The linear regression model used to calculate *Q* for each T_{out} is

$$f_Q(T_{out}) = k_Q \times T_{out} + b_Q \tag{3.21}$$

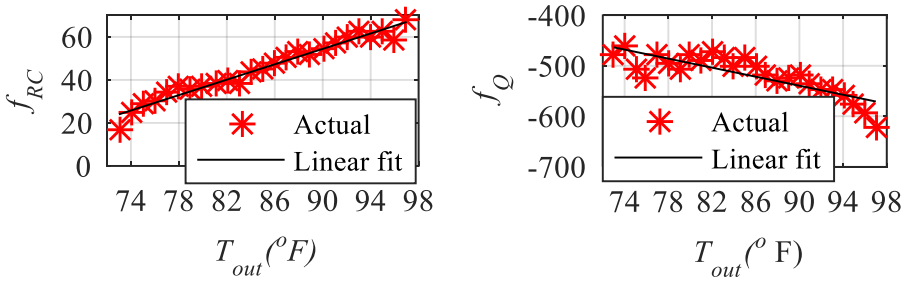

(a) (b)

Figure 3-8. RC parameters under different outside temperature: (a) *RC* with respect to T_{out} (b) *Q* with respect to T_{out}. (Data source: PECAN Street. House #: 5395. Location: Austin, Texas. Duration: from 16:18 pm, July 16 to 17:08 pm, July 29, 2015.)

After Q is calculated for each T_{out} using (3.21), the estimated ON cycle duration, $\hat{t}_{ON}$, can be calculated as

$$\hat{t}_{ON} = -R_f \times C_f \times \ln\left(\frac{T_{out} + f_Q(T_{out}) \times R_f - T^-}{T_{out} + f_Q(T_{out}) \times R_f - T^+}\right) \tag{3.22}$$

Figure 3-9 shows a comparison between the estimated ON and OFF durations and the median of the actual ON/OFF durations with respect to outdoor temperature.

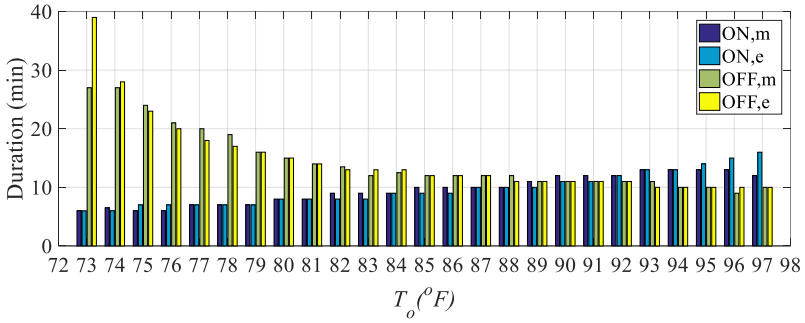

Figure 3-9. A comparison between the actual and estimated HVAC ON/OFF durations (Data source: PECAN Street Data Set. House #: 5395. Location: Austin, Texas. Duration: July 1 to Aug 31, 2015).

Compared with Figure 3-7, the accuracy of the prediction of the proposed decoupled-ETP model is significantly improved. We run the validation test for 100 homes using the PECAN street data set. The average errors between actual median of t_{ON} and t_{OFF} and the estimated $\hat{t}_{ON}$ and $\hat{t}_{OFF}$ are calculated. The average error among 100 houses over the full range of T_{out} values are 4.02 and 2.05 minutes for the ETP model and the decoupled-ETP model, respectively. If considering only the low (T_{out} <76°F) or the high (T_{out} >95°F) outdoor temperature cases, the modeling error of the decoupled-ETP model is normally 10~20 minutes less than that of the ETP model.

3.1.5 Adjusted Decoupled-ETP Model

The proposed decoupled-ETP model can be applied to model all TCAs as long as the consumptions are regulated by a consistent thermostat setting without being distorted by occupants' activities such as opening the doors or windows for a prolonged period, frequently changing thermostat setpoints or manually shutting down the TCA devices, etc. However, in practice, TCA operations during daytime can heavily be distorted by human activities, as shown in Figure 3-2 (a) and (c). For most houses, the most usable data for Deriving TCA models are the data measured between midnight and early morning when the occupants are asleep so the influence of their activities are at the minimum. However, for an HVAC unit, using only the midnight data will cause inaccuracy because we will not be able to account for the impact of the solar radiations on the thermal dynamics of the house. To address this issue, we propose the adjusted decoupled-ETP model to tune the parameters of the decoupled-ETP model derived using only the midnight data so that the day-time operation can also be accurately modeled.

When the HVAC unit is ON, T_{room} at $t = k+1$ can be calculated as

$$\begin{aligned} T_{room}(k+1) &= T_{out}(k) + \hat{f}_Q(T_{out}) \times \hat{R}_f \\ &-(T_{out}(k) + \hat{f}_Q(T_{out}(k)) \times \hat{R}_f - T_{room}(k)) \times e^{-\Delta t/(\hat{R}_f \times \hat{C}_f)} \end{aligned} \tag{3.23}$$

When the HVAC unit is OFF, T_{room} at $t = k+1$ can be calculated as

$$T_{room}(k+1) = T_{out}(k) - (T_{out}(k) - T_{room}(k)) \times e^{-\Delta t/\hat{f}_{RC}(T_{out}(k))} \tag{3.24}$$

where

$$\hat{R}_f = K_{R_f} \times R_{f,N}$$
$$\hat{C}_f = K_{C_f} \times C_{f,N}$$
$$\hat{f}_Q(T_{out}) = K_Q(T_{out}) \times f_{Q,N}(T_{out})$$
$$\hat{f}_{RC}(T_{out}) = K_{RC}(T_{out}) \times f_{RC,N}(T_{out})$$

In (3.23) and (3.24), $R_{f,N}$, $C_{f,N}$, $f_{Q,N}(T_{out})$, and $f_{RC,N}(T_{out})$ are the parameters of the decoupled-ETP model calculated using the midnight data set and K_{R_f}, K_{C_f}, $K_Q(T_{out})$ and $K_{RC}(T_{out})$ are the adjustment coefficients for modeling daytime HVAC cycling behaviors.

To derive those coefficients, we first select n households with at least 5 days 24-hour HVAC consumptions during which period there is no obvious distortion caused by occupants' activities. Let NIGHT model and WHOLE-DAY model represent the decoupled-ETP model derived using the midnight data and the whole-day data, respectively. Then, the NIGHT model parameters of the i^{th} HVAC unit are named as $R^i_{f,N}$, $C^i_{f,N}$, $f^i_{Q,N}(T_{out})$, and $f^i_{RC,N}(T_{out})$. The WHOLE-DAY model parameters are named as $R^i_{f,D}$, $C^i_{f,D}$, $f^i_{Q,D}(T_{out})$, and $f^i_{RC,D}(T_{out})$.

The adjustment coefficients can be calculated as follows

$$K_{R_f} = \text{median}\{\frac{R^1_{f,D}}{R^1_{f,N}}, \frac{R^2_{f,D}}{R^2_{f,N}}, \ldots, \frac{R^n_{f,D}}{R^n_{f,N}}\} \tag{3.25}$$

$$K_{C_f} = \text{median}\{\frac{C^1_{f,D}}{C^1_{f,N}}, \frac{C^2_{f,D}}{C^2_{f,N}}, \ldots, \frac{C^n_{f,D}}{C^n_{f,N}}\} \tag{3.26}$$

$$K_Q(T_{out}) = \text{median}\{\frac{g^1_{Q,D}(T_{out})}{f^1_{Q,N}(T_{out})}, \frac{g^2_{Q,D}(T_{out})}{f^2_{Q,N}(T_{out})}, \ldots, \frac{g^n_{Q,D}(T_{out})}{f^n_{Q,N}(T_{out})}\} \tag{3.27}$$

$$g^i_{Q,D}(T_{out}) = \frac{(T_{out} - T^+) \times e^{-t^M_{ON}/(R^i_{f,N} \times C^i_{f,N})} + T^- - T_{out}}{R^i_{f,N} \times [1 - e^{-t^M_{ON}/(R^i_{f,N} \times C^i_{f,N})}]} \tag{3.28}$$

where $T_{out} \in T_o$.

To account for the saturation effect of the HVAC unit in low or high temperature ranges, a capped linear regression model is used so that

$$\overline{K}_Q(T_{out}) = \begin{cases} \overline{k}_Q \times \min(T_o) + \overline{b}_Q & \text{if } T_{out} < \min(T_o) \\ \overline{k}_Q \times T_{out} + \overline{b}_Q & \text{if } \min(T_o) \le T_{out} \le \max(T_o) \\ \overline{k}_Q \times \max(T_o) + \overline{b}_Q & \text{if } T_{out} > \max(T_o) \end{cases} \tag{3.29}$$

An example of $\frac{g^i_{Q,D}(T_{out})}{f^i_{Q,N}(T_{out})}$ when i ranges from 1 to 10 and K_Q with respect to T_{out} is shown in Figure 3-10(a). The linear fit model $\hat{K}_Q$ with respect to T_{out} is shown in Figure 3-10(b).

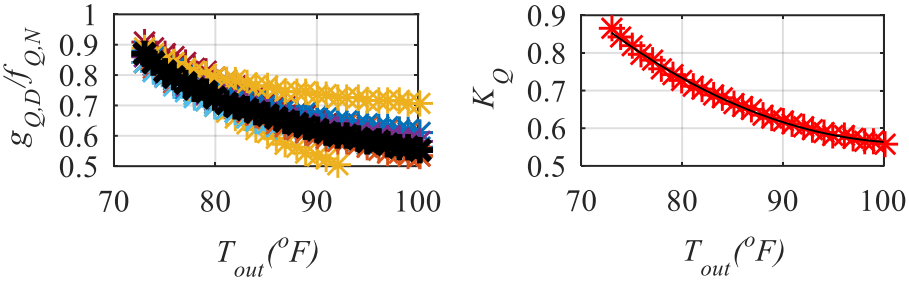

(a) (b)

Figure 3-10. Q parameter under different outside temperature: (a) *Q* ratios between *WHOLE-DAY* and *NIGHT* models of 10 houses (Black dots are the median values of K_Q); (b) Comparison between K_Q (black line) and a linear fit $\hat{K}_Q$ (red stars) with respect to outdoor temperatures.

$K_{RC}(T_{out})$ is calculated as

$$K_{RC}(T_{out}) = \text{median}\{\frac{f^1_{RC,D}(T_{out})}{f^1_{RC,N}(T_{out})}, \frac{f^2_{RC,D}(T_{out})}{f^2_{RC,N}(T_{out})}, \ldots, \frac{f^n_{RC,D}(T_{out})}{f^n_{RC,N}(T_{out})}\} \tag{3.30}$$

where $T_{out} \in T_o$. A capped 2nd order polynomial regression model $\hat{K}_{RC}(T_{out})$ is used to fit the relationship between K_{RC} and T_{out} so that

$$\hat{K}_{RC}(T_{out}) = \begin{cases} a_0 \times (\min(T_o))^2 + a_1 \times \min(T_o) + a_2 & \text{if } T_{out} < \min(T_o) \\ a_0 \times T_{out}{}^2 + a_1 \times T_{out} + a_2 & \text{if } \min(T_o) \le T_{out} \le \max(T_o) \\ a_0 \times (\max(T_o))^2 + a_1 \times \max(T_o) + a_2 & \text{if } T_{out} > \max(T_o) \end{cases} \tag{3.31}$$

An example of $\frac{f^i_{RC,D}(T_{out})}{f^i_{RC,N}(T_{out})}$ when i ranges from 1 to 10 and K_Q with respect to T_{out} is shown in Figure 3-10 (a). The 2nd order polynomial model $\hat{K}_Q$ versus T_{out} is shown in Figure 3-11(b).

Once the adjustment coefficients are derived, one can use only the middle night data to derive the decoupled-ETP model parameters. Then, the *NIGHT* model parameters are adjusted using (3.23) and (3.24) so that when modeling the daytime HVAC cycling behaviors, the solar radiation impacts can be reflected appropriately.

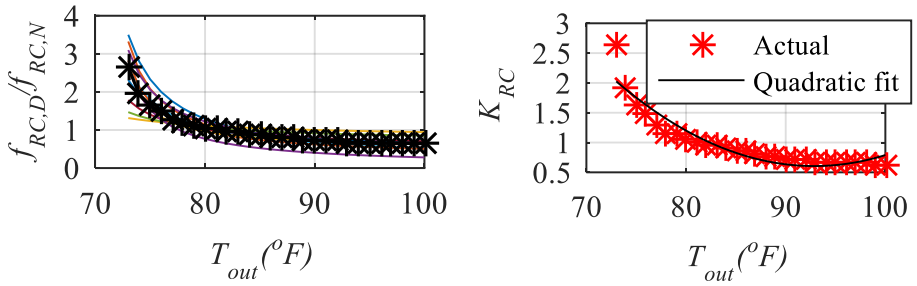

(a) (b)

Figure 3-11. *RC* ratios under different outside temperature: (a) *RC* ratios between *WHOLE-DAY* and *NIGHT* model of 10 houses (Black dots are the median values of K_{RC}); (b) Comparison between K_{RC} (red dots) and the quadratic fit $\hat{K}_{RC}$ (the black line) with respect to T_{out}.

3.2 Simulation Results

In this section, we present the simulation results to compare the performance of the ETP model with the decoupled-ETP model and the adjusted decoupled-ETP model. Two performance criteria are used. The first criterion is the error in the measured and estimated total ON time durations and the second is the total number of switching. The total ON duration reflects the accuracy of the model when estimating the total power consumptions. The total number of switching indicates the accuracy of the model when estimating the switching behaviors.

3.2.1 Verification Results of the Midnight Model

In this section, we verify the accuracy of the ETP models and the decoupled-ETP models using midnight data.

3.2.1.1 Case 1: Verification Results using House #3192 Data

Table 3-3 shows the results comparison of the errors in the total ON time and the total number of switching when using the ETP model and the decoupled-ETP model, respectively. Define *APE* as the absolute percentage error we have

$$APE = \left| \frac{\hat{x} - x}{x} \right| \tag{3.35}$$

where x is the actual measurement and $\hat{x}$ is the estimation using the ETP model or the decoupled ETP model. As shown in Table 3-3, the performance of the decoupled-ETP model is much better than that of the ETP model.

Table 3-3. Performance Comparison

House #3192	Total ON time		Total switchings	
	time(min)	APE	times	APE
Actual	6788	NA	751	NA
ETP Model	6471	4.66%	702	6.52%
Decoupled ETP	6784	0.01%	766	2.00%

3.2.1.2 Case 2: Verification Results using 100 HVAC units

In this case, the mean absolute percentage error (*MAPE*) and standard deviation (*SD*) of the total ON time and the total number of switching of 100 HVAC units at Austin, Texas (Data range: July 1st to Aug. 31st, 2015) are shown in Table 3-4. From the results, we can see that the total ON time and the total number of switching of the decoupled-ETP model has a much lower MAPE and SD than those of the ETP model. The error distribution shown in Figure 3-12 also confirms that the decoupled-ETP model performs significantly better than the ETP model and its performance is consistent across the households.

Table 3-4 Performance Comparison Using 100 Houses Data

100 Houses	Total On Time		Total Swtiching times	
	MAPE	SD	MAPE	SD
ETP Model	14.52%	10.55%	12.69%	12.56%
Decoupled ETP	4.23%	3.35%	3.49%	2.95%

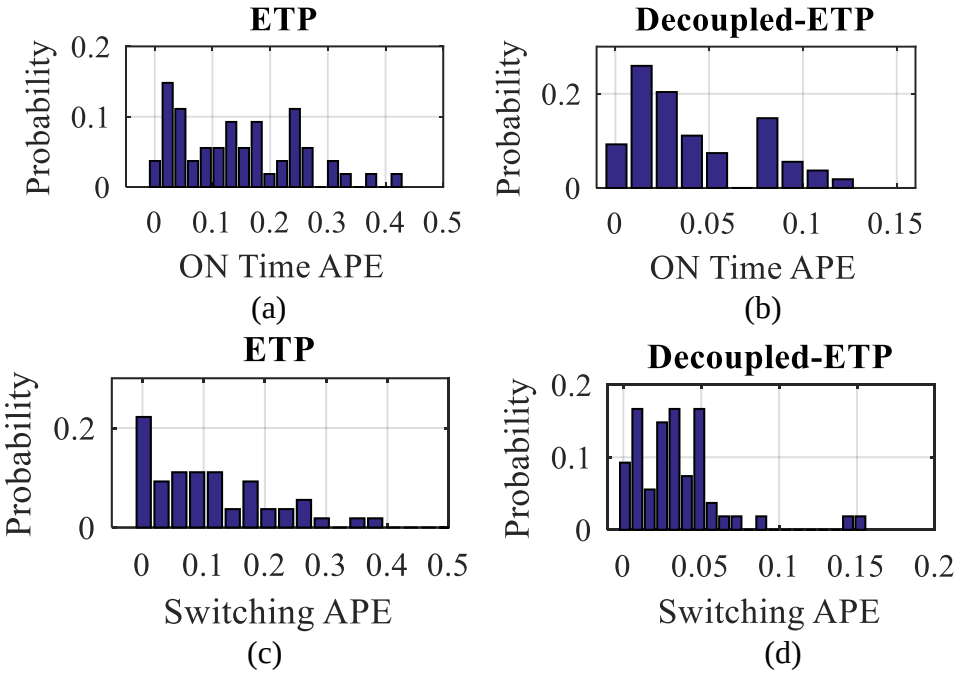

Figure 3-12. Absolute percentage error (APE) distribution of ETP and decoupled-ETP: (a) Total On time of the ETP model; (b) Total number of switching of the ETP model; (c) Total On time of the decoupled-ETP model; (d) Total number of switching of the decoupled-ETP model.

3.2.2 Verification Results of the Whole-day Model

In this section, we first verify the performance of the Whole-day model using the 24-hour whole-day data. Then, we will verify the performance of the adjusted decoupled-ETP models when only the midnight data can be used.

3.2.2.1 Case 1: Verification Results using House #3456 Data

Table V shows the comparison of the errors in the total ON time and the number of switching for different models.

Table 3-5. Results Comparison, House #3456 at Austin, Texas; From 15:18 Pm, July 12th To 21:57 Pm, Aug 2nd, 2015

House #3456	Data Input	Total ON time		Total Number of Switchings	
		time(min)	APE	times	APE
Actual	NA	5779	NA	669	NA
ETP1	Midnight	11713	102.68%	946	41.30%
ETP2	Wholeday	5487	5.05%	583	12.86%
Decoupled-ETP1	Midnight	6338	9.68%	733	9.62%
Decoupled-ETP2	Wholeday	5765	0.25%	335	0.10%
Adjusted Decoupled-ETP	Midnight	6152	6.46%	708	5.77%

Column "Data Input" refers to the type of data that are used to build the model. Note that the Whole-day data uses the 24-hr consumption of the HVAC unit in house #3456 as inputs and the Night data uses 12 a.m. to 5 a.m. HVAC consumption as inputs. Obviously, the decoupled-ETP model using the whole-day data as inputs has the best performance with the lowest errors. When the Midnight model is used without being adjusted, the modeling error increases sharply. When using the adjusted decoupled-ETP model, the error can be reduced by close to 50%. Note that the error is the cumulated error of 21 days, the average daily modeling errors in the total ON time are within 18 minutes and the average errors in modeling the number of switch are within 2 times. This is an outstanding performance when modeling the HVAC switching characteristics.

3.2.2.2 Case 2: verification of 100 HVAC units

Table 3-6 and Figure 3.13 verify the Case 1 results using data collected from 50 homes at Austin, Texas, between July 1st and Aug. 31st, 2015. The results show that all three decoupled-ETP model performances are consistent across households. From the results, we conclude that if only the midnight data are usable, the adjusted decoupled-ETP model can be used for modeling the day-time HVAC behaviors.

Table 3-5. Performance Comparison Using 50 Houses Data

50 Houses	Data Input	Total ON time		Total Number of Switchings	
		MAPE	SD	MAPE	SD
ETP1	Midnight	85.72%	38.96%	46.69%	15.70%
ETP2	Wholeday	9.16%	7.44%	8.61%	7.61%
Decoupled-ETP1	Midnight	17.84%	14.73%	13.07%	12.77%
Decoupled-ETP2	Wholeday	2.31%	1.79%	3.00%	1.81%
Adjusted decoupled-ETP	Midnight	8.86%	7.09%	7.92%	6.33%

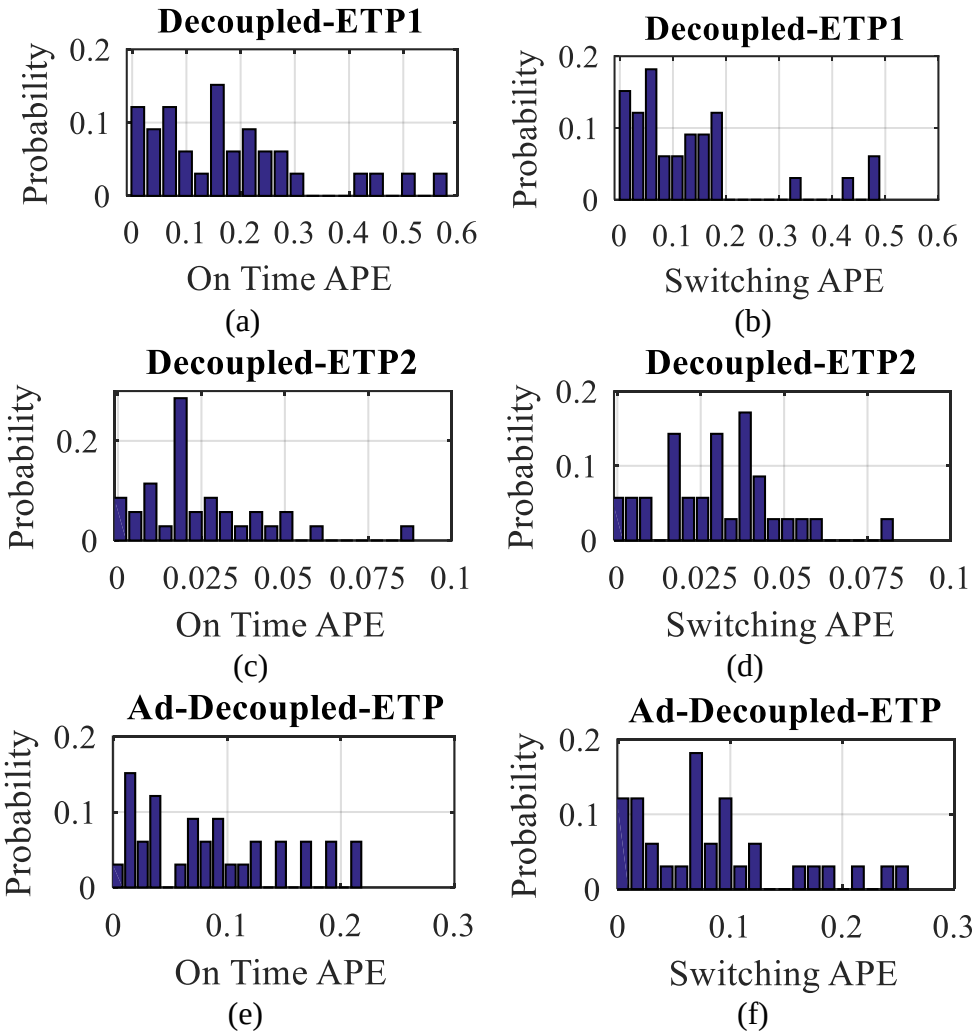

Figure 3-13. Probability distribution function of the absolute percentage error (APE) of different models (a) Total ON time of the decoupled-ETP1 model; (b) Total number of switching of the decoupled-ETP1 model; (c) Total ON time of the decoupled-ETP1 model; (d) Total number of switching of the decoupled-ETP1 model; (e) Total ON time of the adjusted decoupled-ETP model; (f) Total number of switching of the adjusted decoupled-ETP model.

3.3 Conclusions

This chapter presents a data-driven method to estimate the ETP model parameters of TCAs using their power consumptions and ambient temperature data as inputs. We use the modeling of HVAC units as an example to demonstrate that by decoupling the modeling of the ON and OFF cycles, we can simplify the derivation of modeling parameters and significantly improve the modeling accuracy. To adjust the distortion of the human activities on HVAC cycling behaviors, midnight data can be used for ETP model parameter estimation. However, a tuning process will be needed to adjust the nighttime models so that the impact of the solar radiation can be accounted for. By testing the proposed methods using the minute-by-minute HVAC data collected from 100 household at Austin, Texas in summer 2015, we verified the performance of the decoupled ETP models and the adjustment process.

CHAPTER 4 A Data-Driven Household Load Forecasting Algorithm

In this chapter, a data-driven load forecasting algorithm for residential household is proposed. Each type of measurable appliance in the house has a unique forecasting algorithm and the total household power consumption forecast is the sum of all forecasting.

Generally, residential appliances can be divided into TCAs and Non-TCAs depending on whether their operation statuses are determined by temperatures. TCAs include heating, ventilating and air conditioning (HVAC) units, water heaters, fridges, etc. All other appliances can be considered as Non-TCAs. Non-TCAs are further categorized into 3 types depending on their characteristics. Forecasting algorithms of TCAs and each type of non-TCAs are shown in this chapter. Figure 4-1 shows the overall structure of the whole forecasting procedure. If an appliance is measurable, for TCAs, measurements include temperatures and power consumptions while for measurable Non-TCAs, measurements only include power consumptions of each appliance.

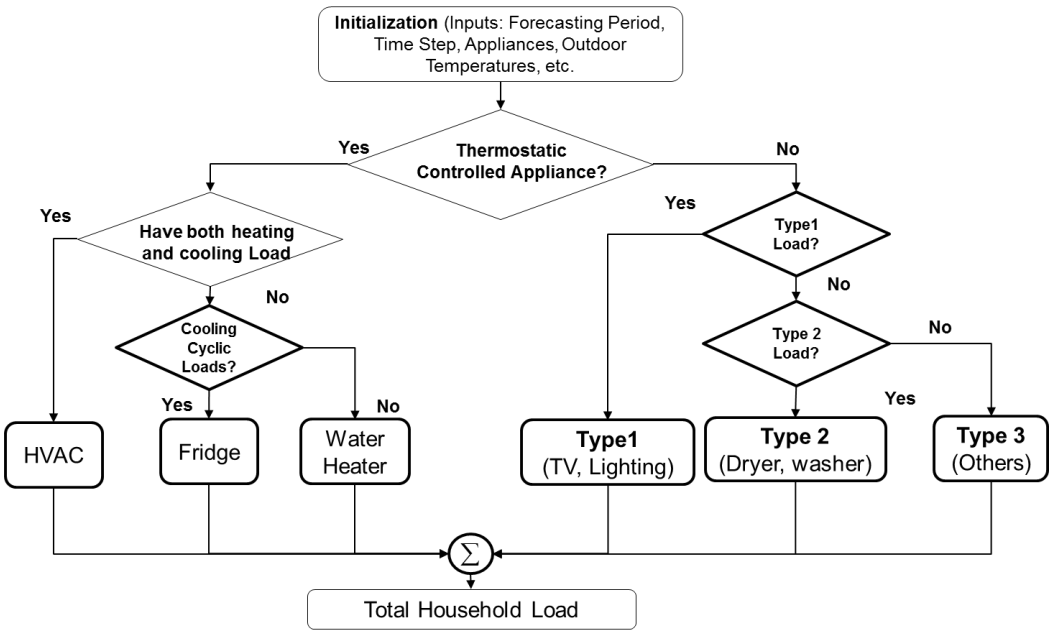

Figure 4-1. Structure of total household load forecasting algorithm

The forecasting algorithms of TCAs are introduced in Section 4.1 and the forecasting algorithms of Non-TCAs are introduced in Section 4.2.

4.1 Thermostatic-controlled Appliance Forecasting Algorithm

The methodology of forecasting algorithms are the same for different TCAs except their measurements are different. So we would like to take HVAC units as an example.

In this chapter, the forecasting algorithms are specifically designed for forecasting the electricity consumption of the traditional HVAC units in a residential house. The fan and pump of a traditional residential HVAC unit are running at constant speeds when the HVAC is ON and will stop if the HVAC status is OFF. Thus, the HVAC is operating at ON/OFF status intermittently. HVACs with variable frequency drives are not considered in this dissertation since the power consumption is not constant when the HVAC is ON.

Before developing load forecasting algorithms, it is important to understand what types of data can be made available to the forecast engine. Commonly measured operation variables

of an HVAC circuit include: voltage, current, and ON/OFF status. Measurements from smart thermostat includes temperature setpoint, T_{set}, the deadband, $T_{deadband} = T^{+} - T^{-}$, and the room temperature, T_{room}. If additional temperature sensors are installed (e.g. the ECOBEE system), the HEM can also receive multiple indoor temperature measurements as well as the outdoor temperature, T_{out}.

If we neglect the dynamics during the startup and shutdown periods of a traditional residential HVAC unit, the HVAC voltage and current can be treated as constants. Thus, the power consumption of the HVAC unit during the ON period is its rated power, P_{rated}. Thus, the HVAC power consumption, P_i, for the i^{th} period can be calculated by

$$P_i = s_i P_{rated} \tag{4.1}$$

where s_i is 1 when HVAC unit is on and 0 when the unit is off.

Because the "ON" and "OFF" of HVAC depend mainly on the thermal dynamics inside a household, there are three sets of data that are critical for tracing the operation status of an HVAC unit: s_i, T_{room} and T_{out}. In this dissertation, we developed two algorithms. The first algorithm uses only s_i as inputs and the second algorithm uses s_i, T_{room} and T_{out} as inputs. Note that for the first algorithm, we only need the thermostat data but for the second algorithm, the HEM needs additional temperature sensors to record the time series data for T_{room} and T_{out}.

Instead of forecasting the parameters of a detailed thermal dynamic model as developed in [25], a simple but robust data-driven approach is developed to build a database of room temperature change rate k_{in} and k_{de} (°F/min) for the ON and OFF cycles with respect to T_{out}.

Note that k_{in} , k_{de} are defined as the ratio of room temperature changes over time changes in a complete ON/OFF cycle, e.g.: $\overline{k_{de}} = -T_{deadband} / \tau_{ON}$ and $\overline{k_{in}} = T_{deadband} / \tau_{OFF}$ for a cooling system.

The forecasting of the room temperature can be done by:

At the i^{th} time step,

$$\begin{aligned} &\text{when } s_i = 1 \\ &T_{room}^{i+1} = T_{room}^{i} + \Delta t * \frac{\Delta T_{room}^{on}}{\tau_{on}^{i}} = T_{room}^{i} + \Delta t * \overline{k_{de}^{i}}\Big|_{T_{out}^{i}} \\ &\text{when } s_i = 0 \\ &T_{room}^{i+1} = T_{room}^{i} + \Delta t * \frac{\Delta T_{room}^{off}}{\tau_{off}^{i}} = T_{room}^{i} + \Delta t * \overline{k_{in}^{i}}\Big|_{T_{out}^{i}} \end{aligned} \tag{4.2}$$

where Δt is the time interval between 2 consecutive time steps (Δt = 1 min in this dissertation). In [34], we have demonstrated the effectiveness of using temperature rates for correcting the forecasting errors for TCA working status. In this dissertation, we extended the study to build a database for the room temperature change rates to forecast the room temperature variations for much longer time periods and reflecting the influence of the variation of ambient temperatures.

4.1.1 Algorithm 1: Without Temperature Measurements

For old HVAC units, the HEM can only detect their ON/OFF status because there is no measurements for T_{room} and T_{out}. According to [25], for a given household, the ON and OFF cycling time, τ_{ON} and τ_{OFF}, are mainly determined by T_{out} if other thermal parameters such as the size of the house, the number of windows, and the thickness of wall, and the type of building materials, are constant. We have done a statistical study on the daily temperature profile. Over 90% of the time, T_{out} will change within 3°F within an hour, as shown in Figure 4-2.

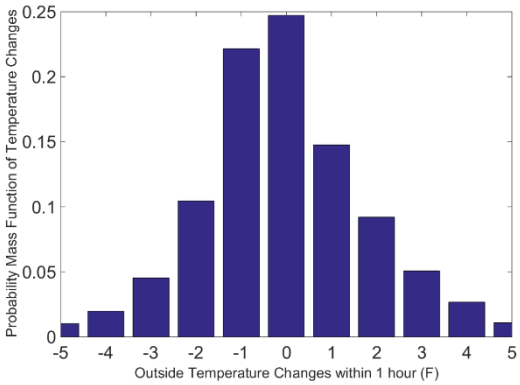

Figure 4-2. A Histogram showing the distribution of temperature changes from May 1, 2013 to Apr 30 2014, Raleigh, NC, USA

Thus, τ_{ON} and τ_{OFF} for the next few cycles can be derived by τ_{ON} and τ_{OFF} for the immediate past 2~3 cycles. Therefore, in Algorithm 1, the most recent τ_{ON} and τ_{OFF} are calculated and used to derive the HVAC status in the next N_p minutes. As shown in Fig. 3, t_1 represents the most recent τ_{ON}; t_0 represents the most recent τ_{OFF}; t_{ON} represents the already "ON" time since last OFF cycle. The future HVAC status can be simple populated by repeating the t_1 and t_0 as the ON and OFF cycles. There will be some cases when $t_{on} \geq t_1$ or $t_{off} \geq t_0$, shown in Figure 4-3(b). If $s_{AC}(i) = 1$ and $t_{on} \geq t_1$, we will assume that the *ON* cycle will end immediately at next time step. Then t_1 will be replaced by t_{on} while t_0 remains unchanged. The forecasted HVAC ON/OFF status will alternate with $\tau_{on} = t_1$ and $\tau_{off} = t_0$. An example of forecasting results is also shown in dashed line in Figure 4-3(b).

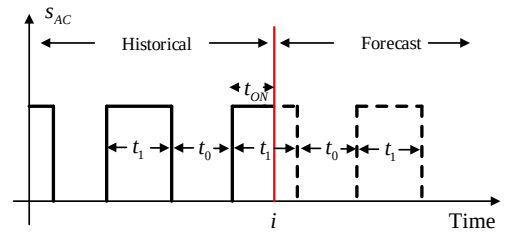

(a)

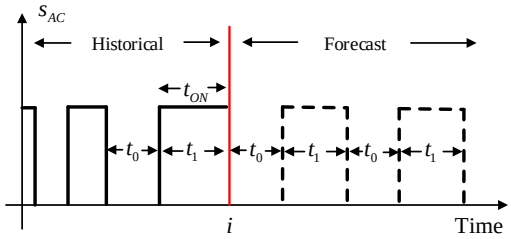

(b)

Figure 4-3. An illustration of Algorithm 1: (a) Forecast ON time is not reached. (b) Forecast ON time is exceeded.

A time-of-the-day adjustment term Δt_a of the ON and OFF time can be added or subtracted from t_1 and t_0 to reflect the expected outdoor temperature influence. For example, in a summer day, the adjustment Δt_0 to the forecasted OFF time t_0 can be 1 minute every two hours and the adjustment term Δt_1 for the forecasted ON time t_1 will increase 1 minutes every three hours from 8:00 a.m. to 3:00 p.m.

4.1.2 Algorithm 2: With Temperature Measurements

In algorithm 2, we assume that historical s_{AC}, T_{room} and T_{out} are available. The reason we carried out the research is to study the value of adding in additional sensors. We want to compare algorithm 1 and 2 to see how much improvement we can make by addition in more temperature sensors to justify the installation of the additional sensors for improving the performance of the HEM algorithms.

Algorithm 2 includes 2 stages: *a training stage* and *a forecasting stage*. The goal of the *training stage* is to build a database for room temperature change rates $\overline{k_{in}}$ and $\overline{k_{de}}$ under

different T_{out}. In the *forecasting stage*, T_{room} will be forecasted based on the database built in the *training stage*. A flow chart which shows the overall process of the algorithm 2 is shown in Figure 4-4.

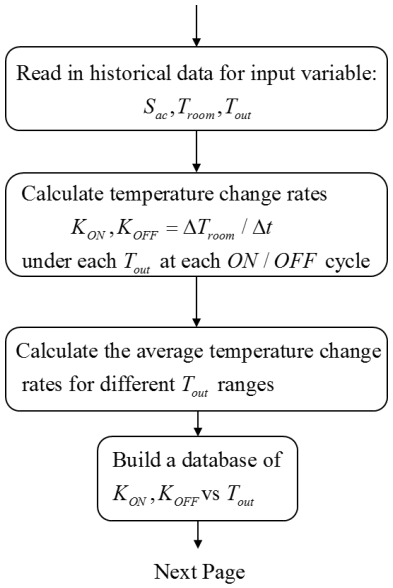

Figure 4-4. Flow charts of the HVAC forecasting algorithm 2: (a) Stage 1

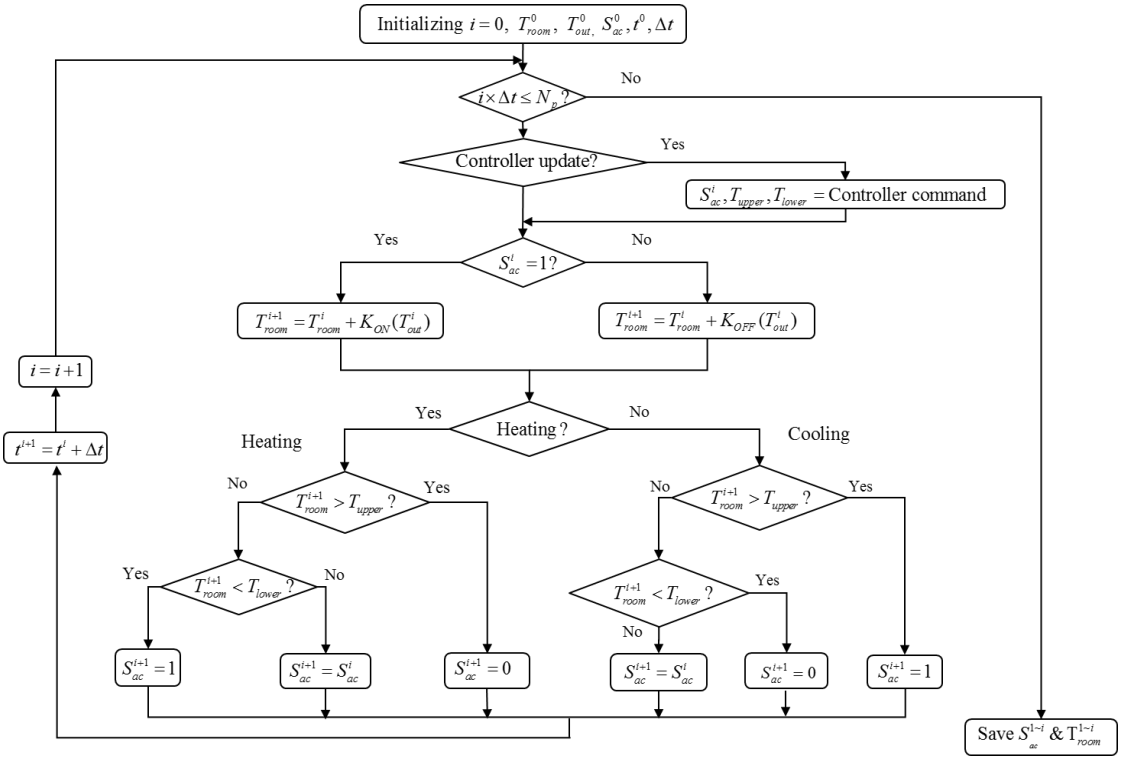

Figure 4-4. Flow charts of the HVAC forecasting algorithm 2: (b) Stage 2

Stage 1: Training Stage

Although T_{room} changes are not linear [25], we can linearize the temperature rising and decreasing curves, since $T_{deadband}$ are usually small enough (≤ 4°F), as shown in Figure 4-5.

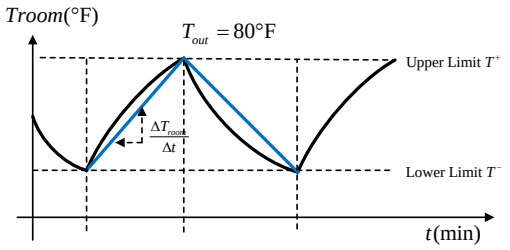

Figure 4-5. An example of linearizing T_{room} in deadbands

Step 1: At the beginning of each ON cycle or OFF cycle, calculate k_{in} or k_{de} under each T_{out}. Record all k_{in} and k_{de} as well as corresponding time length, as shown in Figure 4-6. Note that k in Figure 4-6 refers to either k_{in} or k_{de}.

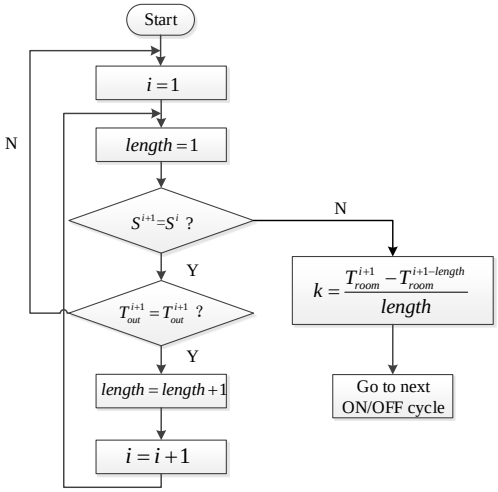

Figure 4-6. A flow chart for calculating k_{in} and k_{de}

Step 2: Calculate the weighted average k_{in} and k_{de} (denoted as $\overline{k_{in}}$ and $\overline{k_{de}}$) under the same T_{out}. The corresponding time length for each k_{in} or k_{de} is used as weights. k_{in} and k_{de} with time length less than N minutes are removed when calculating weighted averages. We use N=10 because when the time length is shorter than 10 minutes, linearizing T_{room} can be inaccurate. An example showing the calculated k_{de} under different time lengths when T_{out} = 80 °F is shown in Figure 4-7.

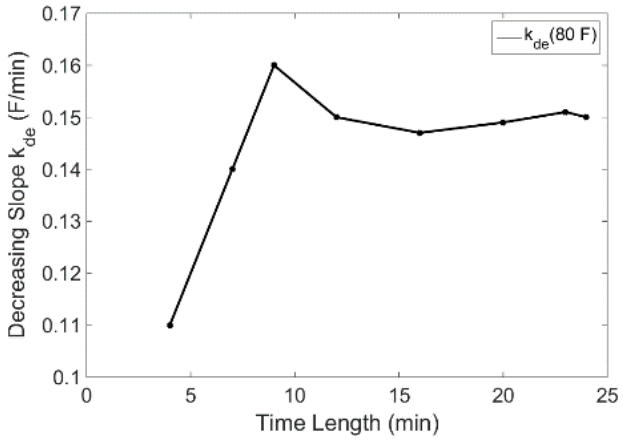

Figure 4-7. An example of calculated T_{room} decrease slope under different time lengths if T_{out}=80°F

Step 3: Use linear regression to do the curve fitting as shown in Figure 4-8 and Table 4-1. Note that when $T_{out} \le T^{-}$, $\overline{k_{in}}$ is considered to be 0.

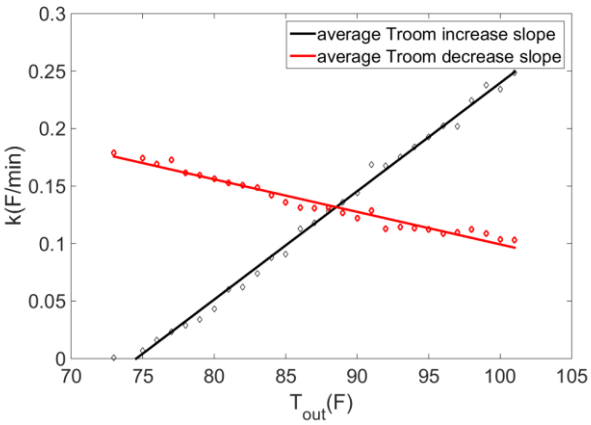

Figure 4-8. An example of $|\overline{k_{in}}|$ and $|\overline{k_{de}}|$ under different T_{out}

Table 4-1. Examples of database built in training stage

T_{out} (°F)	77	78	79	80
$\lvert\overline{k_{in}}\rvert$ (°F / min)	0.0234	0.0291	0.0341	0.0431
$\lvert\overline{k_{de}}\rvert$ (°F / min)	0.1726	0.1617	0.1595	0.1562
T_{out} (°F)	81	82	83	84
$\lvert\overline{k_{in}}\rvert$ (°F / min)	0.0601	0.0602	0.0738	0.0880
$\lvert\overline{k_{de}}\rvert$ (°F / min)	0.153	0.1507	0.1488	0.1422

Stage 2: Forecasting Stage

In this stage, T_{room} will be forecasted based on the database built in *Training Stage*. The following paragraphs show the details of *Forecasting Stage* at each time step *i*:

Step 1: Based on current time step s_i and the forecasted T_{out} at that time step, find the corresponding $\overline{k_{in}}$ or $\overline{k_{de}}$ in the database.

Step 2: Calculate T_{room} based on (4-3).

Step 3: Determine s_{i+1} at next time step using:

$$s_{i+1}=\begin{cases}1 & \\ 0 & \text{if} \\ s_i & \end{cases}\quad\begin{matrix} T_{room}^{i+1} > T^+ \\ T_{room}^{i+1} < T^- \\ T^- \le T_{room}^{i+1} \le T^+ \end{matrix} \tag{4-3}$$

4.2 Non-TCA Forecasting Algorithms

Non-TCAs are divided into 3 categories depending on their own characteristics: type I, type II and type III loads. The forecasting algorithms for each type of Non-TCA are introduced in this section.

4.2.1 Type I load forecasting algorithm

Type I loads refer to the measurable Non-TCAs with potential repetitive patterns, e.g. TVs and lights. For type I loads, we use similar day approach [42] to forecast the power usage. Figure 4-9 shows the flow chart of the forecasting algorithm. If an appliance belongs to type I load, a database of average power consumption at each time step in 24-hour range is first trained based on historical power consumption data of that appliance. Then, depending on the current forecasting time step, the power consumptions of the next N_p time step in the database are used as the forecasting result, where N_p is the number of time steps of the forecasting horizon.

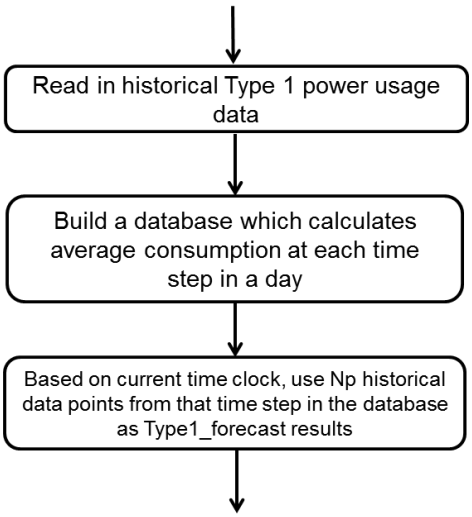

Figure 4-9. Type I loads forecasting algorithm flowchart

4.2.2 Type II load forecasting algorithm

Type II loads refer to the measurable event-triggered loads (e.g. dryers, electric vehicles, ovens, ranges, cookers, etc.). Their power ratings are usually relatively high and usage pattern highly depends on users' personal reference. It is assumed that for these type of loads, once they are turned ON, they will be ON for a period of time at rated power until the work is completed and turned OFF. For these type of loads, without knowing the users' personal habit and preference, it is very hard to forecast when it will be turned ON. A wrong forecasting of Type II appliance turn ON time will lead to a large forecasting error and therefore provide HEMS scheduling algorithm misleading information. Thus, we only forecast the ON period length once it is turned ON. The following figure shows the flow chart of the forecasting algorithm.

The forecasting algorithm for Type II loads has 2 stages: building a database and forecasting. The detailed steps are shown as follows:

- **Step 1**: Build a database which calculates the average turn ON time (t_{AVE}) for the appliance based on historical data is built.

- **Step 2**: If the appliance is OFF at current time step, the status of the appliance for the next N_p time steps $S_{app}^1$to $S_{app}^{N_p}$ is forecasted to be all 0 (OFF). Else, if the appliance is currently ON, go to Step 3.
- **Step 3**: Compare the appliance current ON time length (t_{ON}) with t_{AVE}. If $t_{ON} \geq t_{AVE}$, an incremental ON time is assigned to appliance status at first *m* time steps, where *m* can be selected to be 10% to 20% of $t_{AVE}/\Delta t$. Therefore, $S_{app}^1 \sim S_{app}^m = 1$ and $S_{app}^{m+1} \sim S_{app}^{N_p} = 0$. Else, compare $t_{AVE} - t_{ON}$ with $N_p * \Delta t$. If $t_{AVE} - t_{ON} \geq N_p$, then $S_{app}^1 \sim S_{app}^{N_p} = 1$; else, $S_{app}^1 \sim S_{app}^{t_{AVE}/\Delta t} = 1$ and $S_{app}^{\frac{t_{AVE}}{\Delta t}+1} \sim S_{app}^{N_p} = 0$.

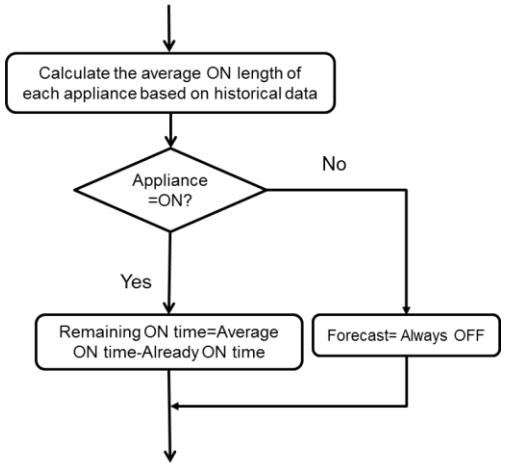

Figure 4-10. Flow chart of Type II load forecasting algorithm

4.2.3 Type III load forecasting algorithm

Type III loads refer to all the remaining appliances that are not included in TCAs, Type I, Type II loads. Type III loads usually include a lot of low power appliances like ventilation, washer, plug-in electronics devices. For the forecasting algorithm, only historical power consumptions of all type III loads and ambient temperature information are available. Since type III loads are generally low power units or less frequently used, even though they are

generally hard to forecast accurately, they actually have less impact on the results of overall household forecasting accuracy.

Generally, we can use multi-linear regression methods, similar day, neural network or time series approaches to forecast type III loads. In this dissertation, we would like to use multi-linear regression method. A general multi-linear forecasting method can be found in [41].

4.3 Simulation Tests

In this section, the proposed data-driven forecasting algorithm is verified in 3 aspects: individual appliance forecasting, total household forecasting and comparison with other forecasting algorithms. In Section 4.3.1, model-generated data and field measurement data of HVAC units and dryers are used to verify the accuracy of TCAs and type II Non-TCAs forecasting algorithms, respectively. Algorithms for other types of loads are not demonstrated since they are commonly seen forecasting algorithms. In Section 4.3.2, a virtual house shown in Table 4-2 is used to verify the forecasting accuracy and potential sensor costs under different number of sensor measurements. In Section 4.3.3, a comparison of the proposed data-driven forecasting algorithm with commonly used forecasting algorithms (Artificial Neural Network and Multi-linear Regression) is demonstrated to show the improvement in forecasting accuracy.

4.3.1 Appliance forecasting results: TCA and Non-TCA Type II loads

In section 4.3.1.1, model-generated data and field measurement data of HVAC units are used to verify the accuracy of TCAs forecasting algorithms. In section 4.3.1.2, model-generated data and field measurement data of dryers are used to verify the accuracy of non-TCA type II load forecasting algorithms. Please note that the data resolution is 1 minute and the forecasting algorithms are updated every 15 minutes.

4.3.1.1 TCA forecasting results

(1) Testing TCA forecasting algorithm 1 using model-generated data

An example of short-term forecast for the HVAC operation status (i.e. 30 minutes ahead forecast, 1 hour ahead forecast and 2 hour ahead forecast) is presented in Figure 4-11. We define the forecast accuracy as the ratio of the total time when the forecasted HVAC status are the same as the actual HVAC status divided by the total forecasting time period. The 30 minutes ahead forecast has an accuracy of 86.7%. However, the forecast accuracy drops sharply as forecasting time length increases. The 1 hour-head forecast has an accuracy of 81.67% but the 2 hour-ahead forecast accuracy is only 56.67%. This is because, the algorithm uses only the most recent ON/OFF cycle lengths without the knowledge of the proper correction for future hours. Thus when outside temperature changes, the mismatches between forecasting results and real values will become large.

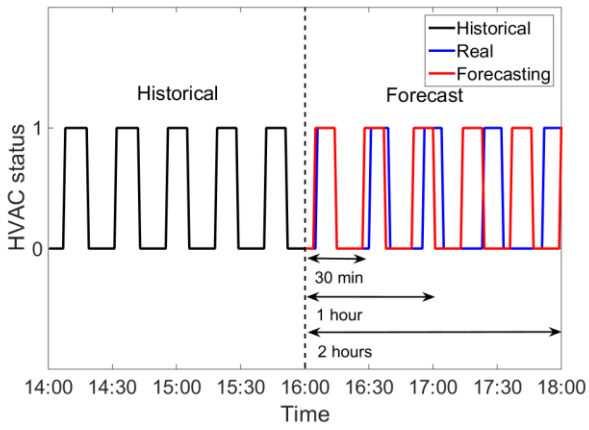

Figure 4-11. An example of the HVAC forecast produced by algorithm 1

In addition, the mismatch will accumulate because of previous mismatches. Therefore, algorithm 1 is only suitable for very short term HVAC forecast (e.g. <=1 hour). This also proves that in the HVAC control algorithms for providing regulation and load following

services, the update rates of HVAC measurement should not exceed 30 minutes for maintaining good performance [34].

(2) Testing TCA algorithm 2 using model-generated data

A week's historical summer data (T_{room}, T_{out} and S) are used for training in order to obtain the database proposed in Section 4.1.2-Stage1-Step 3. The training results are shown in Table 4-1 and Figure 4-7. Two simulation cases are designed to test the performance of algorithm 2 under both normal operation conditions and HVAC cold start process. The normal operation refers to the conditions when T_{room} varies within the deadbands and the cold start process refers to conditions when the HVAC is shut down for a long period of time and is started to bring the temperature down.

The simulation results representing the normal operation conditions are shown in Figure 4-9(a). Forecasting results are compared with actual data when forecast ahead time period $N_p = 30$ minutes, 1 hour and 2 hours. It can be clearly seen that 30 minutes ahead forecasting results are almost the same with actual data in both room temperature and HVAC status. As N_p increases, forecasting accuracy starts to drop slowly, but it still has a fairly good accuracy. In this case, the forecasting accuracy of $N_p = 30$ minutes, 1 hour and 2 hours are 100%, 96.7%, and 93.3%, respectively. If the forecasting algorithm is updated every 15 minutes such that the simulation runs for one week, the average 30 minutes, 1 hour and 2 hours ahead forecast correct rates are 95.4%, 93.7% and 90.2% respectively.

The simulation results representing the cold start process of HVAC are shown in Figure 4-9(b). HVAC is assumed to be turned on at 3:00 while room temperature at that time is $85\,^{\circ}\mathrm{F}$. The current time step is at 3:10. The forecasting correct rates of $N_p = 30$ minutes, 1 hour and

2 hours are 93.3%, 86.7% and 80%, respectively. This shows that the forecasted room temperature curve may have obvious mismatches because the room temperature dropping rate outside the temperature deadbands is different from what can be estimated by the data collected within the deadbands. So, it is recommended that the HEM request more measurements during this process if accuracy is the key to the control algorithms.

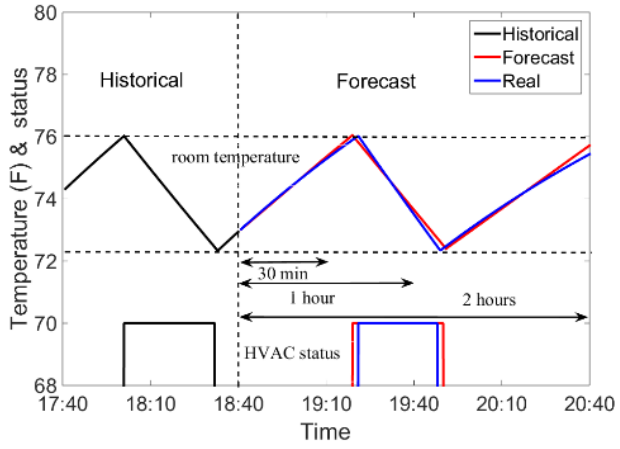

(a)

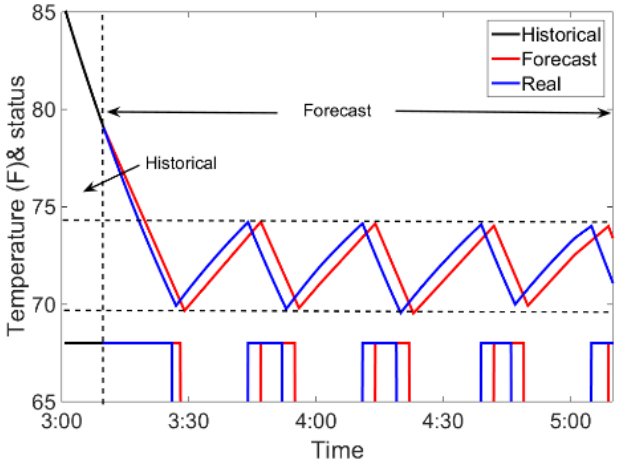

(b)

Figure 4-12. Algorithm 2 performance under (a) normal conditions and (b) cold start process

(3) *Comparison of forecasting accuracy between model-generated data and field measured data*

A comparison between algorithm 1 and 2 using both HVAC model generated data and field measured data is shown in this section. The HVAC model data is generated based on the proposed decoupled-ETP model mentioned in Section 3.1.4. The field-measured data were measured from a residential house located in Raleigh, North Carolina. The 2-floor townhouse was built in 1990s with 1200 square feet. The data were collected from 02/02/2016 to 02/04/2016. Measurements include outside temperature, indoor temperature and HVAC status. The forecasting results are shown in Table 4-2.

Table 4-2. Results: HVAC forecasting on model-generated data and field-measured data

Forecasting Horizon	Forecasting Accuracy			
	Algorithm 1		Algorithm 2	
	HVAC model	Field Data	HVAC model	Field Data
15 min	92.60%	89.50%	97.60%	92.74%
30 min	86.70%	80.13%	95.40%	88.69%
60 min	81.30%	70.50%	93.70%	84.55%
120 min	56.70%	51.10%	90.20%	79.58%

As can be seen in Table 4-2, it is obvious that algorithm 2 outperforms algorithm 1 in all forecasting horizons. Besides, in both algorithms, the forecasting accuracy of model generated data is slightly higher than field measured data. This is because in real life, human activities like door opening, window opening, cooking, party, etc. will have influence on the operation of HVAC units, which makes the ON and OFF cycle vary even under the same outside temperature.

The conclusion is that we recommend algorithm 2 to be the most appropriate forecasting algorithms if outside temperature, indoor temperature and HVAC status or power consumption data are available. Also the forecasting accuracy is good enough for HEM scheduling algorithms and microgrid energy dispatches.

Please note that the algorithms for TCA forecast in Section 4.3.2 are TCA forecasting algorithm 2.

4.3.1.2 Non-TCA forecasting results

Dryer is used as an example to demonstrate the accuracy of Non-TCA type II forecasting algorithm. The model-generated data used in this section are based on the dryer model in [27]. Field-measured data of dryer power consumption were downloaded from house #59 (located in Austin, TX) in www.pecanstreet.org. One month data were used as training data to build the database in 4.2.2-Step 1 and the following one month data are used to verify the forecasting accuracy. Results are shown in Table 4-3.

Table 4-3. Results of dryer forecasting algorithms on model-generated and field-measured data

Forecasting Horizon	Forecasting Accuracy	
	Dryer Model	Field Data
15 min	99.80%	98.77%
30 min	99.60%	97.85%
60 min	99.10%	98.24%
120 min	98.70%	96.97%

As can be seen in Table 4-3, the forecasting accuracy of the Non-TCA type II algorithm is very close to 100% in both model-generated data and field-measured data. The 15 minutes ahead forecast has the highest accuracy, which is essential for short term HEM scheduling algorithm as well as microgrid energy dispatch strategies.

4.3.2 Household forecasting and cost-benefit study

A virtual house with appliances shown in Table 4-4 is used to verify the forecasting accuracy and potential sensor costs under different number of sensor measurements. Section 4.3.2.1 is to demonstrate a study on the relationship between forecasting accuracy of the proposed algorithm under different measurements and the corresponding cost of sensors. Section 4.3.2.2 shows the influence of data resolution on the accuracy on the total household forecasting.

Table 4-4. Characteristics of the Example Virtual House

Appliance	Rated Power (kW)	Quantity and usage
HVAC	3.5	1, always in use
Water Heater	4.5	1, always in use
Fridge	0.3	2, always in use
Dryer	4.5	1, 1 to 4 times per week, turn ON time randomly distributed during 6am to 11 pm; 40 to 60 min per usage
Washer	0.3	
Electric Vehicle	3.3	1, 4 to 7 times per week, charging time randomly distributed during 5 pm to 11 pm during weekday; 1 hour to 3 hours per charge
TV	0.2	2, by actual measurements
Oven	2	1, by actual measurements
Light	0.1	10, by actual measurements
Range	1 or 2	2 at 1kW and 2 at 2 kW, by actual measurements
Micro Oven	0.7	1, by actual measurements
Rice Cooker	0.6	1, by actual measurements
Ventilation	0.3	2, by actual measurements
Desktop	0.3	1, by actual measurements
Miscellaneous	0 to 1	NA, randomly distributed

In terms of evaluation criteria, Mean Absolute Error (MAE) are used to evaluate the accuracy of the proposed forecasting algorithm. Mean Absolute Percentage Error (MAPE) can also be used a reference but not recommended to use because of the following reasons: (1) small error in low power consumption periods may lead to high absolute percentage error, which will further result in misleading MAPE values; (2) there will be cases that the actual values are 0, which is hard to deal with.

The MAE is defined as follows:

$$MAE = \frac{\sum_{i=1}^{N}\sum_{j=1}^{N_p} | P_{forecast,i}^{j} - P_{actual,i}^{j} |}{N * N_p} \tag{4-4}$$

where N is the total number of times of forecast; N_p is the forecasting horizon; $P_{forecast,i}^{j}$ is the j^{th} time step forecasting value at i^{th} forecast; $P_{actual,i}^{j}$ is the actual power consumption corresponding to $P_{forecast,i}^{j}$.

The MAPE is defined as follows:

$$MAE_{CAP} = \frac{\sum_{i=1}^{N}\sum_{j=1}^{N_{CAP}} | P^{j}_{forecast,i} - P^{j}_{actual,i} |}{N * N_{CAP}} \quad (4\text{-}5)$$

where $P^{j}_{forecast,i}$ is the i^{th} time step power usage forecast value at j^{th} forecast if $P^{j}_{forecast,i}$ or $P^{j}_{actual,i} \geq P_{CAP}$; P_{CAP} is the high power cap; $P^{j}_{actual,i}$ is the actual power consumption corresponding to $P^{j}_{forecast,i}$; N_{CAP} is the number of occurrence when $P^{j}_{forecast,i}$ or $P^{j}_{actual,i} \geq P_{CAP}$.

4.3.2.1 Forecasting accuracy and cost of sensors under different measurements of appliance

Sensors are not always the same for measuring different appliances. In order to implement the proposed forecasting algorithm, temperature loggers and power consumption loggers are needed for TCA measurements while Non-TCA measurements only require power consumption loggers. In this case study, it is assumed that all sensors are installed separately such that the overall cost is the sum of all individual sensor costs. For the sake of study, the costs of temperature loggers are $150 each while the costs of power loggers are $60 and $200 each, for power ratings under 1.5 kW and above 1.5 kW respectively.

One may want to know the best combination of measurable appliances such that the cost of sensors installation will be minimized while maintaining at good forecasting accuracy. There will be thousands of measurement combinations. However, TCAs and non-TCA higher power appliances are more worth measuring since they contribute to most of the household power consumptions. Therefore, we designed 4 cases to find the best combination. Available measurements in each case and their corresponding costs are shown in Table 4-5. All the data measurements in this part are in 1 minute resolution.

Table 4-5. Setups of the Case Studies

Case	Measurable appliances in a house	Cost of sensors($)
1	HVAC, water heater	850
2	HVAC, water heater, dryer, electric vehicle	1250
3	HVAC, water heater, dryer, electric vehicle, oven, range	1650
4	All appliances listed in Table I except miscellaneous	2370

The forecasting APEs of the 4 cases during one month simulation are shown in Figure 4-12. Blue, black and magenta dots shows accuracy comparison between each case at 15-minute ahead forecasting, 30 minute forecasting and 60 minute forecasting, respectively. It can be seen that the longer the forecasting horizon is, the less accurate the forecasting algorithm is, regardless of the number of measurable appliances. However, in terms of the forecasting accuracy with respect to number of measurable appliances, more measurements may not always increase the forecasting accuracy. It is concluded that generally 4 to 6 major appliance measurable will give the best results. More appliances measurable will not increase the accuracy while increasing installation costs.

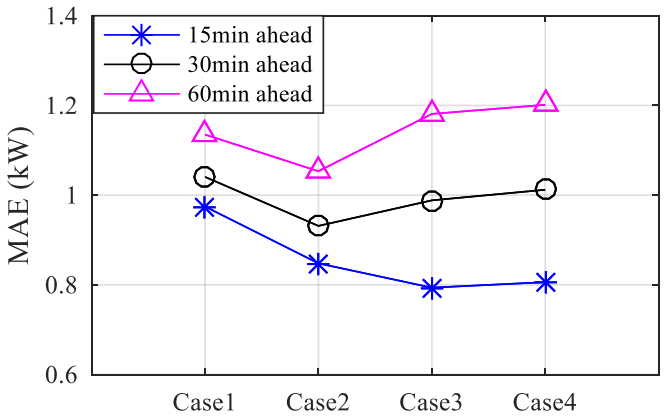

Figure 4-13. Forecasting accuracy of the virtual house in summer

4.3.2.2 Forecasting accuracy under different measurement resolution

The resolution of the measurement data is another important factor which may

influence the accuracy of the forecasting algorithm. All previous cases studies are based on 1-minute resolution measurements. In this section, we want to see the comparison of the forecasting accuracy if we increase the measurement resolution from 1 minute to 5 minutes.

Please note that according to the Nyquist Theorem [47], the sampling frequency (measurement resolution) must be no less than twice of highest frequency in the original signal. Therefore, 5 minute resolution data is not suitable for those appliance with periods less than 10 minutes. Due to the reason that ON/OFF cycles of TCAs like HVACs or fridges are sometimes short, (e.g. in a very hot summer day, the OFF time length of an HVAC may be less than 5 minutes), 5 minutes resolution measurement data are not suitable for TCAs, but suitable for most of the high power Non-TCA units (e.g. dryers, electric vehicles, washers, ovens etc). Therefore, the TCAs will remain 1 minute measurement in the 2 cases shown below.

A comparison study is conducted on the same virtual house shown in Table 4-5. The 2 forecasting algorithms both are both tested in a summer month. In this case, we assume 4 appliances are measured (Case 2 in Table 4-5). The forecasting accuracy comparison is shown in Table 4-6.

Table 4-6. MAE of total household forecasting, under different forecasting horizon and data resolution

Forecasting Horizon	Data Resolution	
	1 minute	5 minutes
15-min MAE(kW)	0.6044	0.5981
30-min MAE(kW)	0.7733	0.7309
60-min MAE(kW)	0.9227	0.8729

It is observed that the 5 minutes resolution measurement gives lower forecasting MAE than 1 minute resolution. The reasons can be: 1) 5 minutes resolution data is the average of 1 minute resolution data in every 5 minutes, which will flatten the load curves; 2) less data points are forecasted in 5 minutes resolution data compared with 1 minute resolution data, e.g: 15

minutes ahead forecast only requires 3 points forecast for 5 minutes resolution.

4.3.3 Comparison with other forecasting algorithms

This section demonstrates the forecasting error comparison between the proposed data-driven forecasting algorithm and other commonly used forecasting approaches: Neural Network and Multi-linear Regression. The results are shown in Table 4-7. Note that all the forecasting algorithms applies 1 minute data resolution.

It can be seen that under 15 minutes, 30 minutes and 60 minutes ahead forecasting, the proposed data-driven forecasting algorithm has much lower MAE and MAPE than the other 3 approaches. This shows that the proposed data-driven algorithm is much more appropriate for short-term household load forecasting, which is essential for scheduling and control in home energy management and microgrid operations.

Table 4-7 Forecasting accuracy comparison between the data-driven approach, neural network (NN) and multi-linear regression (MLR)

Horizon	MAE(kW)			MAPE (%)		
	Data-Driven	NN	MLR	Data-Driven	NN	MLR
15 min	0.7133	2.9	1.97	48%	149%	109.7%
30 min	0.7571	2.92	1.98	51%	165%	110%
60 min	0.8134	2.98	1.98	54%	159%	110%

4.4 Conclusion

This chapter introduces a data-driven algorithm for single household load forecasting. Different from traditional forecasting methods, the data-driven algorithm split the measurable appliances in a house into different categories. An individual forecasting algorithm for each type of appliance is then introduced. The data-driven forecasting algorithm is verified in 3 aspects. First, individual algorithms of TCA and non-TCA type II loads are verified using both model-generated data and field-measurement data. Second, a virtual single house data is used

to validate the data-driven forecasting algorithm under different measurements and different data resolution. At the end, we also compare the data-driven forecasting algorithm with some commonly-used existing algorithm. Results show that the 4-6 major appliances are recommended to be measured to maintain the balance of forecasting accuracy and installation costs. Results also show that the data-driven forecasting algorithms outperforms than the traditional forecasting algorithms in household forecasting areas, which is more suitable for scheduling and control in home energy management and microgrid operations.

CHAPTER 5 A Microgrid Commitment Algorithm for Dispatching DG and DR Resources in Hybrid Community-Level Microgrid under Islanding Operations

Commercial-residential hybrid buildings (e.g. Figure 5-1) are commonly seen in high population density cities, especially in Asian countries, like China, Korea and Japan [3]. With rapid growth of microgrid development, a community-level hybrid microgrid consisted of DG resources (e.g. CHP units, PVs, ES units) and DR resources, commercial-residential hybrid buildings, will become possible in the future. However, how to optimally dispatch of all the resources while maintaining the electrical demands and thermal demands in such a microgrid during islanding conditions will become an issue.

In this chapter, a microgrid system which is consisted of several commercial-residential hybrid buildings, and scheduled to operate under islanding conditions for a period of time is studied. A microgrid commitment (MC) algorithm is designed to optimally dispatch the DG resources (PV and ES) as well as the DR resources while maintaining the electrical and thermal balance of the microgrid system. Compared with previous published papers [55]-[57], the contribution of our paper lies in the following aspects: (1) this is the first paper that researches on the optimal dispatch strategy of commercial-residential hybrid microgrids under islanding operations. (2) our paper depicts the generation of exhaust heat and fuel efficiency more accurately such that the thermal balance can be modeled in a more practical way; (3) controllable loads, especially TCAs can bid in the market such that demand response will not create an aftermath peak after being controlled.

The structure of this paper is shown as follows: Section 5.1 introduces the nomenclature; Section 5.2 introduces configuration of the microgrid system; Section 5.3

describes the Microgrid Commitment (MC) algorithm; Section 5.4 shows the simulation case studies; Section 5.5 is the conclusion.

5.1 **Nomenclature**

N_g:	Number of CHP units in the microgrid
$P_e^i(t)$:	Electrical output (kW) of i^{th} CHP unit at time step t
$P_{e,max}^i$, $P_{e,min}^i$:	Maximum/ minimum electrical output (kW) of i^{th} CHP unit
$E_{fuel}^i(t)$:	Remaining fuel left (kWh) of i^{th} CHP unit at the end of time step t
A^i, B^i:	Coefficients of generation costs of CHP i
a^i, b^i,c^i, d^i:	Waste heat calculation Coefficients of CHP i
COP_{abs}^i:	Coefficients of performance of absorption chiller i
COP_{ec}^i:	Coefficients of performance of electric chiller i
N_{es}:	Number of energy storage units in the microgrid
$P_{es}^j(t)$:	Charging (if positive) or discharging (if negative) rate of j^{th} energy storage unit at time step t
$P_{es,max}^j$, $P_{es,min}^j$:	Maximum charging or discharging rate (kW) of j^{th} energy storage unit
$E_{es}^j(t)$:	Remaining energy left (kWh) of j^{th} energy storage unit at the end of time step t
N_{pv}:	Number of PV systems in the microgrid
$P_{pv}^m(t)$:	Generation (kW) of m^{th} PV system at time step t
$P_{ec}^i(t)$:	Electrical chiller output (kW) at i^{th} hybrid building
$P_{abs}^i(t)$:	Absorption chiller output (kW) at i^{th} hybrid building

$P_{th}^{i}(t)$: Commercial thermal load demand (kW) at i^{th} hybrid building at time step t

$P_{re}^{i}(t)$: Sum of non-bid-in loads of all residential users of hybrid building i at time step t

$P_{com}^{i}(t)$: Sum of non-thermal loads of all commercial users of hybrid building i at time step t

$P_{base}(t)$: Baseload (kW) at time step t, aka, sum of all non-bid-in loads (kW) of residential users and non-thermal loads (kW) of commercial users (kW) at time step t

N_l: Number of types of controllable loads in the microgrid

$P_l^k(t)$: Total demand (kW) of controllable load type k at time step t

$T_{out}(t)$: Outside temperature at time step t

Δt: Duration (minute) of each time step

5.2 Configuration of mircogrids

The configuration and assumptions of the microgrid is introduced in this section.

An example of a community-level hybrid microgrid is shown in Figure 5-1. We consider the microgrid consisting of hybrid buildings that contain both residential and commercial users, CHP units, ES units and PVs. For residential users, controllable loads like HVACs and water heaters can participate in the microgrid islanding operation market as demand response resources. In this dissertation, we assume that each type of controllable loads must bid in price as blocks. The MC algorithm will consider the controllable bid-in prices as penalty costs. An example of the controllable loads bid-in prices is shown in Figure 5-3. For commercial users, their thermal loads are assumed to be non-controllable, but can be supplied

by both electricity (electric chiller) and waste heat generated by CHP unit (absorption chiller), but waste heat has higher priority. Non bid-in loads of residential users and non-thermal loads of commercial users are considered to be baseloads, and can only be shut down when electrical and thermal balance cannot be met even after all controllable loads are shut down. If baseloads have to be shut down, they will generate a high penalty cost. Other assumptions are made as follows:

(1) Electrical output of all CHP units, ES units and PVs will supply the whole microgrid electrical demands.

(2) The thermal output of the CHP (absorption chiller) can only be used to supply the demand of its corresponding commercial thermal loads. Besides, these thermal loads will first be supplied by the absorption chiller and any unmet thermal loads will be supplied by the electrical systems.

(3) Each hybrid building has one CHP unit, and the exhaust heat of the CHP unit can only be used to supply commercial thermal loads at its own building.

(4) All control strategies are considered to be direct load control, which means the controller can determine the ON/OFF status of controllable loads directly at any time.

(5) ES units and PVs have no operation, penalty or generation costs.

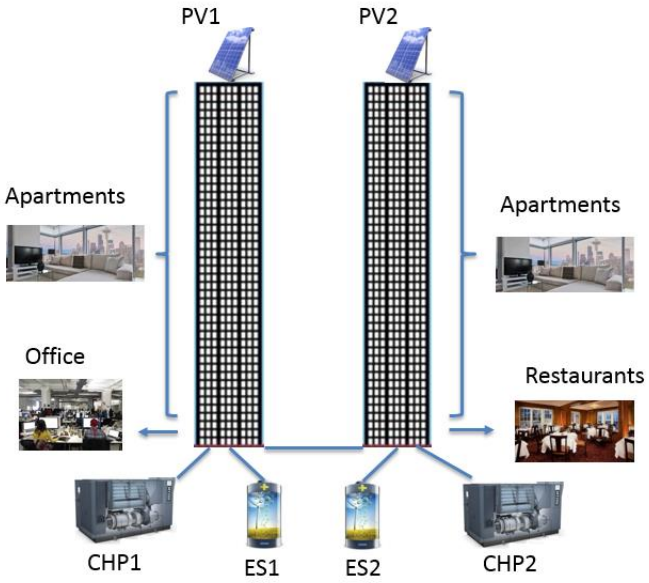

Figure 5-1. An example of a community-level microgrid

5.3 The MC Algorithm

5.3.1 Description of the MC algorithm

When islanding operation begins, as shown in Figure 5-2, the central controller will run the MC algorithm in this section based on the input information, e.g. load and PV forecast, remaining fuel of each CHP unit, remaining energy of each ES unit and other time-invariant information etc. Then the central constroller will determine the dispatch the electrical power output reference of each CHP unit, the charging/discharging rate of each ES unit, the power reference command of each type of controllable loads and whether or not the baseloads need to be cut off based on the MC algorithm results. Then, the local controller will then determine the ON/OFF status of each controllable load at each time step. In this dissertation, we only discuss the optimization algorithm in the central controller. As the local controller algorithms can be found in other papers [58]. Please note that the central controller can rerun the MC algorithm and update the dispatch commands every certain time period.

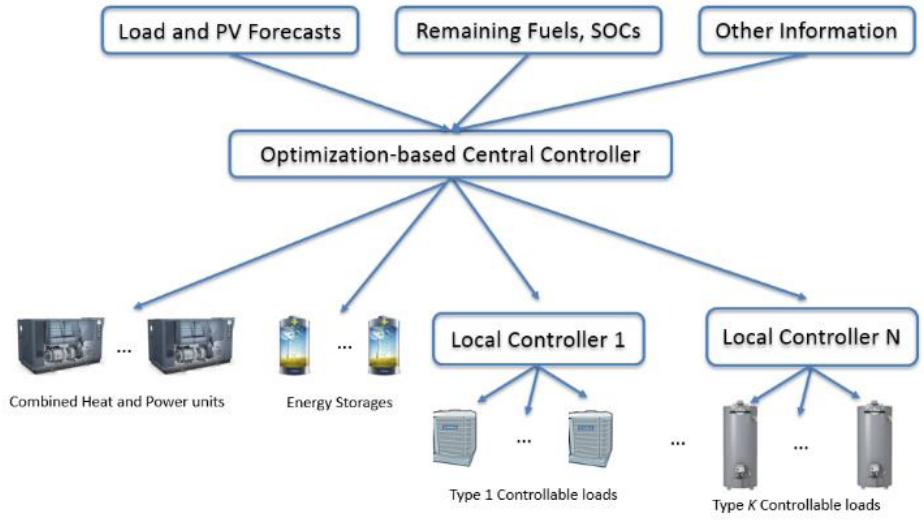

Figure 5-2. Control framework of the microgrid

The **MC algorithm** is introduced as follows:

Step 1: Read in all time-invariant known information, including N_g, $P^i_{e,max}$, $P^i_{e,min}$, A^i, B^i, a^i, b^i,c^i, d^i, COP^i_{abs}, COP^i_{ec}, N_{es}, $E^i_{es,max}$, $P^j_{es,max}$, $P^j_{es,min}$, N_{pv}, N_l, Δt.

Step 2: Update all time-variant known information, including N_h, $T_{out}(t)$, $E^i_{fuel}(0)$, $E^j_{es}(0)$, $P^i_{re}(t)$, $P^i_{com}(t)$, $P^i_{th}(t)$, $P^m_{pv}(t)$, $i = 1,2,\dots N_g$, $t = 1,2,\dots N_h$, $j = 1,2,\dots N_{es}$and $m = 1,2,\dots N_{pv}$.

Step 3: Based on the information in Step 1 and 2, formulate the MC primary problem using (5.1)-(5.19) in Section 5.3.2.1.

Step 4: Solve the MC primary problem using methods in Section 5.3.2.2. If feasible solution is found, go to Step 6. Else, assume $p\% = 10\%$ and go to Step 5.

Step 5: Formulate and solve the Secondary MC problem in Section IV. If feasible solution is found, go to step 6. Else, $p\% = p\% + 10\%$ and go back to Step 5.

Step 6: Send the CHP generation dispatch commands, ES charging/discharging dispatch commands and controllable load operation schedules, baseloads cut off commands to

the central controller.

The formulation and solutions of the primary and secondary MC problem is shown in Section 5.3.2. Please note that in this dissertation, the term "thermal loads" only refers to the thermal loads of commercial users. Residential thermostatic controlled appliances will be mentioned as HVAC units, water heaters or fridges. "Baseloads" are the sum of all commercial electrical loads and residential electrical loads excluding thermal loads and residential controllable loads.

5.3.2 The MC Primary Problem

The MC Primary Problem formulates an optimization problem based on the existing information at the beginning of each dispatch and tries to solve it using either Mix Integer Programming (MIP) or Linear Programming (LP). It does a 1st round check of the problem to see whether or not the problem can be solved without shutting down or cutting off baseloads.

5.3.2.1 Problem Formulation

- Objective Function

The objective function of the optimization problem is to minimize the total generation cost of the CHP units and penalty cost by shutting down controllable loads of the community-level microgrid under islanding conditions for a certain period of time, as shown in (5.1):

$$\text{Total Cost} = \min\{\sum_{t=1}^{N_h}\sum_{i=1}^{N_g} cost^i\left(P_e^i(t)\times\Delta t\right) + \sum_{k=1}^{N_l}[Penalty^k(E_{l,max}^k - E_l^k)\times(E_{l,max}^k - E_l^k)]\} \quad (5.1)$$

In (5.1), $\sum_{t=1}^{N_h}\sum_{i=1}^{N_g} cost^i\left(P_e^i(t)\times\Delta t\right)$ refers to the total generation cost of all CHP units and $\sum_{k=1}^{N_l}[Penalty^k(E_{l,max}^k - E_l^k)\times(E_{l,max}^k - E_l^k)]\}$ refers to the total penalty costs of all types of controllable loads.

The generation cost curve of i^{th} CHP unit is defined as:

$$cost^i(x) = A^i \times x + B^i \tag{5.2}$$

where x is the power generation of the i^{th} CHP and A^i, B^i are the linear cost curve coefficients. The cost curve is considered to be linear because the power output range of a microgrid CHP is limited to several hundred kWs, where linear cost curve fits the best [61].

The penalty cost curves of shutting down controllable loads are defined as a piecewise constant function:

$$Penalty^k(x^k) = \begin{cases} Price^k(1) & if\ x_0^k \le x^k < x_1^k \\ \dots & \dots \\ Price^k(n^k) & if\ x_{n^k-1}^k \le x^k < x_{n^k}^k \end{cases} \tag{5.3}$$

where x^k is the total shutting down energy of all type k controllable loads; $Penalty^k(x^k)$ is the corresponding penalty cost(\$/kWh) at x^k; n^k is the number of penalty cost levels of controllable load type k. $Price^k(1), Price^k(2), \dots, , Price^k(n^k), x_1^k, x_2^k, \dots, x_n^k$ are constants. An example of penalty cost of shutting down HVAC units and water heater units are shown in Figure 5-3.

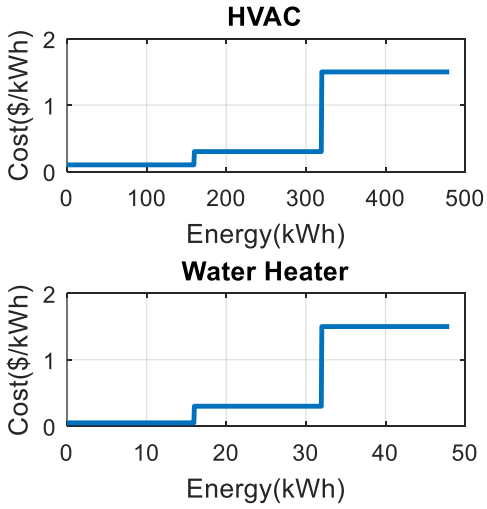

Figure 5-3. Example penalty costs of shutting down controllable loads

- Constraints:

The unknown variables in the optimization problem include: the electrical output of the i^{th} CHP unit at time step t, $P_e^i(t)$; the actual total demand of controllable load type l at time step t, $P_l^k(t)$; the amount of energy left in j^{th} ES unit at the end of time step t, $E_{es}^j(t)$; the charging/discharging rate of j^{th} ES unit at time step t, $P_{es}^j(t)$; the equivalent thermal output of the i^{th} absorption chiller at time step t, $P_{abs}^i(t)$; the i^{th} electrical demand of electric chiller at time step t, $P_{ec}^i(t)$; the amount of fuel left of i^{th} CHP unit at the end of time step t, $E_{fuel}^i(t)$.

The constraints of the optimization problem can be summarized into equipment limits, electrical balance, energy calculations, thermal constraints, ES limits and controllable load limits, which are introduced as follows:

(1) Equipment limits:

$$P_{e,min}^i \le P_e^i(t) \le P_{e,max}^i \tag{5.4}$$

$$P_{es,min}^j \le P_{es}^j(t) \le P_{es,max}^j \tag{5.5}$$

$$0 \le E_{es}^j(t) \le E_{es,max}^j \tag{5.6}$$

$$P_{abs}^i(t) \ge 0 \tag{5.7}$$

$$0 \le P_{ec}^i(t) \le P_e^i(t) \tag{5.8}$$

$$E_{fuel}^i(t) \ge 0 \tag{5.9}$$

$$i = 1,2,\dots N_g; j = 1,2,\dots N_{es}; t = 1,2,\dots N_h$$

The equipment limits include of CHP electrical outputs limits, ES charging/discharging rates limits, energy storage energy limits, CHP thermal output limits, thermal loads supplied by electricity limits and CHP remaining fuel limits.

(2) Electrical balance:

$$\sum_{i=1}^{N_g} P_e^i(t) + \sum_{j=1}^{N_{es}} P_{es}^j(t) + \sum_{m=1}^{N_{pv}} P_{pv}^m(t) = P_{base}(t) + \sum_{k=1}^{N_l} P_l^k(t) + \sum_{i=1}^{N_g} P_{ec}^i(t) \tag{5.10}$$

$$P_{base}(t) = \sum_i P_{re}^i + \sum_i P_{com}^i \tag{5.11}$$

$$t = 1,2, \dots N_h$$

(5.10) refers to the electrical balance between supply and demand. All of the sources (CHP, ES and PV) needs to supply the electrical demand of baseloads, controllable loads and the thermal loads if needed at any time step. Here baseloads include all electrical loads of the residential users excluding controllable loads (HVACs and water heaters) and all electrical loads of commercial users excluding thermal loads.

(3) Energy calculation:

$$E_{es}^j(t) = E_{es}^j(0) + \sum_{\tau=1}^{t} P_{ec}^i(\tau) \tag{5.12}$$

$$E_{fuel}^i(t) = E_{fuel}^i(0) + \sum_{\tau=1}^{t} P_{fuel}^i(\tau) \tag{5.13}$$

$$i = 1,2, \dots N_g; j = 1,2, \dots N_{es}; t = 1,2, \dots N_h$$

The remaining ES energy and CHP fuel energy at the end of each time step are determined based on their initial energy and the consumptions at each time step.

(4) ES limits

$$\frac{E_{es}^j(t) - E_{es,max}^j}{\Delta t} \le P_{es}^j(t) \le \frac{E_{es}^j(t)}{\Delta t} \tag{5.14}$$

$$k_{es,1} \times \frac{\sum_{t=1}^{N_h} P_{es}^j(t)}{N_h} \le P_{es}^j(t) \le k_{es,2} \times \frac{\sum_{t=1}^{N_h} P_{es}^j(t)}{N_h} \tag{5.15}$$

$$j = 1,2, \dots N_{es}; t = 1,2, \dots N_h$$

(5.14) refers that the charging/discharging rate of ES units are limited by its current remaining energy and the maximum ES energy. (5.15) is designed to ensure that the ES units will not deplete very soon, where $k_{es,1}$ and $k_{es,2}$ are constants.

(5) Controllable load limits

$$0 \leq \sum_{t=1}^{N_h}(P_l^i(t) \times \Delta t) \leq E_{l,max}^i \tag{5.16}$$

$$k_{l,1} \times \frac{\sum_{t=1}^{N_h} P_l^k(t)}{N_h} \leq P_l^k(t) \leq k_{l,2} \times \frac{\sum_{t=1}^{N_h} P_l^k(t)}{N_h} \tag{5.17}$$

$$i = 1,2,\dots N_g; k = 1,2,\dots N_l; t = 1,2,\dots N_h$$

(5.16) refers that the total controllable loads consumption are limited to $E_{l,max}^i$, where $E_{l,max}^i$ is estimated by the number, power ratings, outside temperature of the controllable load type *l*. (5.17) is designed to ensure that the controllable loads will not change too much during the whole dispatch period, where $k_{l,1}$ and $k_{l,2}$ are constants.

(6) Thermal constraints

$$P_{abs}^i(t) = \frac{COP_{abs}^i}{COP_{ec}^i} \times \left(\frac{a^i \times T_{out}(t) + b^i}{\eta^i(T_{out}(t))} \times P_e^i(t) + c^i \times T_{out}(t) + d^i\right) \tag{5.18}$$

$$P_{abs}^i(t) + P_{ec}^i(t) \geq P_{th}^i(t) \tag{5.19}$$

$$i = 1,2,\dots N_g; t = 1,2,\dots N_h$$

(5.18) shows the equivalent exhaust heat calculation based on [21], [63]. An example of CHP efficiency [20] with respective to outside temperature is shown in Figure 5-4. (5.19) ensures that each thermal demand can be supplied by exhaust heat and electricity.

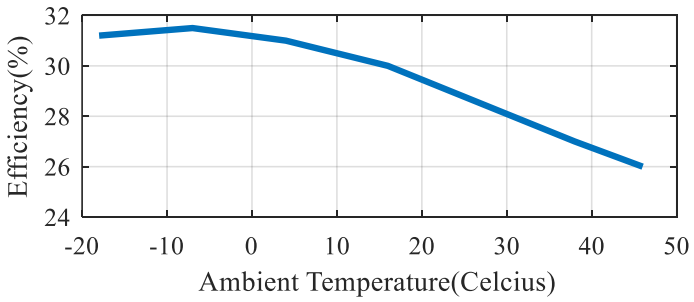

Figure 5-4. Example fuel efficiency curve of a 250kW CHP under different ambient temperatures

5.3.2.2 Solutions

As is shown in (5.4)-(5.19), all the constraints are considered to be linear and continuous. The only non-linear and non-continuous term in the problem is the penalty cost functions in the objective function shown in (5.3). In order to make the problem acceptable by existing software, e.g. MATLAB [65], GAMS [66], in this dissertation, we provide 2 ways to reformulate the problem to convert to either a mixed integer programming (MIP) problem or a linear programming (LP) problem.

(1) Method 1: Converting to an MIP problem

Define $x^k = E_{l,max}^k - E_l^k$ to represent the total amount of shut down energy of controllable load type *k*. We also define a series of binary variables $u_1^k, u_2^k, \ldots, u_{n^k}^k \in \{0,1\}$, $k = 1,2, \ldots N_l$. The following constraints are added into the original problem formulation:

$$u_1^k + u_2^k + \cdots + u_{n^k}^k = 1 \tag{5.20}$$

$$\begin{cases} u_1^k \times \left(x^k - x_0^k\right) \geq 0 \\ u_2^k \times \left(x^k - x_1^k\right) \geq 0 \\ \cdots \\ u_{n^k}^k \times \left(x^k - x_{n^k-1}^k\right) \geq 0 \end{cases} \tag{5.21}$$

$$\begin{cases} u_1^k \times x^k \leq x_1^k \\ u_2^k \times x^k \leq x_2^k \\ \cdots \\ u_{n^k}^k \times x^k \leq x_{n^k}^k \end{cases} \tag{5.22}$$

$$k = 1,2, \ldots N_l$$

The objective function (5.1) can then be reformulated as:

$$\text{Total Cost} = \min\{\sum_{t=1}^{N_h} \sum_{i=1}^{N_g} cost^i\left(P_e^i(t) \times \Delta t\right) + \sum_{k=1}^{N_l}[(Price^k(1) \times u_1^k + Price^k(2) \times u_2^k + \cdots + Price^k(n^k) \times u_{n^k}^k) \times x^k]\} \tag{5.23}$$

After Method 1, the optimization problem is converted into a standard non-linear mix

integer programming problem, which can be solved by existing solvers [65], [66].

(2) Method 2: Converting to a LP problem

Another way of solving the optimization problem is to divide the original optimization problem (5.1)-(5.19) into a series of sub LP problems. The detailed conversion is introduced as:

Suppose there are N_l types of controllable loads and each type of controllable load has n^k, $k = 1,2, \dots N_l$ levels of penalty cost price (\$/kWh), if we select only one penalty cost price of each type of controllable load, there will be $N_{sub} = n^1 \times n^2 \times \dots \times n^{N_l}$ combinations in total, where each one of the problem can be solved as a LP problem.

For each one of the LP problem, the formulation is introduced as:

$$\text{Total Cost} = \min\{\sum_{t=1}^{N_h} \sum_{i=1}^{N_g} cost^i\left(P_e^i(t) \times \Delta t\right) + \sum_{k=1}^{N_l}[(Price^k(i^k) \times (E_{l,max}^k - E_l^k)]\} \tag{5.24}$$

$$i^k \in \{1,2, \dots, n^k\}$$

Subject to:

$$x^k = E_{l,max}^k - E_l^k \tag{5.25}$$

$$x_{i^k-1}^k \le x^k < x_{i^k}^k \tag{5.26}$$

$$k = 1,2, \dots N_l$$

where $Price^k(i^k)$ is the penalty cost price of controllable load type k when $x_{i^k-1}^k \le x^k < x_{i^k}^k$. The other constraints are the same with (5.4)-(5.15) and (5.17)-(5.19).

After solving each of the N_{sub} LP problems formulated as above, the one that gives the minimum Total Cost will be the optimal solution.

An example is shown as below:

Assuming only two types of loads (HVACs and Water Heaters) are controllable and their penalty costs are defined as:

$$Penalty^1(x^1) = \begin{cases} 0.1 & if\ 0 \le x^1 \le 160 \\ 0.3 & if\ 160 \le x^1 < 320 \\ 1.5 & if\ 320 \le x^1 < 480 \end{cases} \tag{5.27}$$

$$Penalty^2(x^2) = \begin{cases} 0.05 & if\ 0 \le x^2 \le 16 \\ 0.5 & if\ 16 \le x^2 < 32 \\ 3 & if\ 32 \le x^2 < 48 \end{cases} \tag{5.28}$$

where x^1 refers to the total shutting down energy of HVAC units and x^2 refers to the total shutting down energy of water heater units. By applying Method 2, the optimization problem can be reformulated into the following 9 LP sub-problems shown in Table 5-1.

Table 5-1 LP Sub-problems of the Example

LP problem index	Total Penalty Costs	Constraints		
		HVAC	Water Heater	Others
1	$0.1 \times x^1 + 0.05 \times x^2$	$0 \le x^1 \le 160$	$0 \le x^2 \le 16$	Same with (4)-(15) and (17)-(19)
2	$0.1 \times x^1 + 0.3 \times x^2$	$0 \le x^1 \le 160$	$16 < x^2 \le 32$	
3	$0.1 \times x^1 + 1.5 \times x^2$	$0 \le x^1 \le 160$	$32 < x^2 \le 48$	
4	$0.3 \times x^1 + 0.05 \times x^2$	$160 < x^1 \le 320$	$0 \le x^2 \le 16$	
5	$0.3 \times x^1 + 0.3 \times x^2$	$160 < x^1 \le 320$	$16 < x^2 \le 32$	
6	$0.3 \times x^1 + 1.5 \times x^2$	$160 < x^1 \le 320$	$32 < x^2 \le 48$	
7	$1.5 \times x^1 + 0.05 \times x^2$	$320 < x^1 \le 480$	$0 \le x^2 \le 16$	
8	$1.5 \times x^1 + 0.3 \times x^2$	$320 < x^1 \le 480$	$16 < x^2 \le 32$	
9	$1.5 \times x^1 + 1.5 \times x^2$	$320 < x^1 \le 480$	$32 < x^2 \le 48$	

Both Method 1 and Method 2 can be used to find the optimal solution of the primary MC problem. However, when the types and penalty cost levels of controllable loads are small, method 2 is recommended to save computational time.

5.3.3 The Secondary MC Problem

Due to some reasons, e.g. incorrect forecasting, inappropriate sizing of ES or PVs, insufficient fuels in CHP units or energy in ES units, there will be cases when the Primary MC formulation is unsolvable. This means that the baseloads and thermal loads cannot be met even

if all controllable loads are fully shut down. As a result, baseloads and thermal loads must be shut down partially in order to ensure supply and demand balance.

5.3.3.1 Problem Formulation

Assume that baseloads and thermal loads need to be shut down by $p\%$, the Secondary MC problem will be formulated as:

$$\text{Total Cost} = \min\{\sum_{t=1}^{N_h}\sum_{i=1}^{N_g} cost^i\left(P_e^i(t) \times \Delta t\right) \quad (5.29)$$

Subject to:

$$P'_{base}(t) = P_{base}(t) \times (1 - p\%) \quad (5.30)$$

$$\sum_{i=1}^{N_g} P_e^i(t) + \sum_{j=1}^{N_{es}} P_{es}^j(t) + \sum_{m=1}^{N_{pv}} P_{pv}^m(t) = P_{base}(t) + \sum_{k=1}^{N_l} P_l^k(t) + \sum_{i=1}^{N_g} P_{ec}^i(t) \quad (5.31)$$

All other constraints are the same with (5.4)-(5.9), (5.11)-(5.15), (5.18)-(5.19).

5.3.3.2 Solutions

This is an LP problem and can be easily solved by existing methodologies, like *Simplex* [71]. If the problem has feasible solutions, then the feasible solution is guaranteed to be optimal.

5.4 Simulation Studies

A series of simulation study cases representing a virtual microgrid system consisted of 2 residential-commercial hybrid buildings is shown in this section. The assumption of the microgrid system is the same with Section 5.2.

Table 5-2 shows all time-invariant variables of the microgrid system. A 4-hour islanding operation is assumed to happen on a summer day, starting from 12 PM to 4 PM. A 4-hour, 15-minute resolution and 15-minute updated microgrid dispatch simulation is demonstrated in this case to show the performance of the algorithm. The PV sizes and output are estimated based on [54], [68]. The parameters of the CHP units shown in Table II are obtained by [63]. The

commercial load data and thermal loads data are obtained by [70]. The residential load data, including both controllable loads and baseloads, are obtained through PECANSTREET.ORG [54].

Table 5-3 shows the time-variant variables at the 1st dispatch time step and the actual 15-minute load and PV information. In this section, 3 cases are designed to show the performance of the algorithm.

Table 5-2. Time-invariant Variables of the Microgrid

Variables	Descriptions	Values of each unit
N_g	Number of CHPs	2
$P^i_{e,max}$	Maximum i^{th} CHP output (kW)	250,250
$P^i_{e,min}$	Minimum i^{th} CHP output (kW)	25,25
A^i	Cost coefficient of i^{th} CHP($/kWh)	0.0329,0.0329
B^i	Cost coefficient of i^{th} CHP($)	1.482,1.482
a^i	Exhaust heat calculation coefficients of i^{th} CHP	2.8E-4,2.8E-4
b^i	Exhaust heat calculation coefficients of i^{th} CHP	0.2067,0.2067
c^i	Exhaust heat calculation coefficients of i^{th} CHP	2.161,2.161
d^i	Exhaust heat calculation coefficients of i^{th} CHP	66.564,66.564
COP^i_{abs}	COP of i^{th} absorption chiller	1.6,1.6
COP^i_{ec}	COP of i^{th} electric chiller	4,4
N_{es}	Number of ES units	2
$E^j_{es,max}$	Capacity of j^{th} ES (kWh)	100,100
$P^j_{es,max}$	Maximum charging rate of j^{th} ES (kW)	50,50
$P^j_{es,min}$	Minimum charging rate of j^{th} ES (kW)	50,50
N_{pv}	Number of PVs	2
N_l	Number of controllable load types	2
Δt	Duration of each time step (min)	15

Table 5-3. Time-variant Variables of the Microgrid

Variables	Descriptions	Values
N_h	Number of time steps to dispatch	16
$T_{out}(t)$	Outside temperature at each time step (°C)	32,32,32,32,32,32,32,32, 32,32,32,32,32,32,32,32
$E_{fuel}^{i}(0)$	Initial remaining fuel of i^{th} CHP (kWh)	500, 500
$E_{es}^{j}(0)$	Initial remaining energy of j^{th} ES (kWh)	100, 100
$P_{base}(t)$	Actual baseloads at each time step (kW)	153,163,168,180,180,172, 166,166,174,178, 177, 190
$P_{th}^{1}(t)$	Actual thermal loads of 1st building at each time step (kW)	40,46,44,48,49,49,48,48, 54,56,63,52,53,64,58,50
$P_{th}^{2}(t)$	Actual thermal loads of 2nd building at each time step (kW)	57,51,64,55,58,69,53,50, 51,54,71,63,49,50,61,52
$P_{pv}^{1}(t)$	Actual PV outputs of 1st building at each time step (kW)	66,67,69,70,71,71,71,71, 70,69,68,66,64,62,59,57
$P_{pv}^{2}(t)$	Actual PV outputs of 2nd building at each time step(kW)	66,67,69,70,71,71,71,71, 70,69,68,66,64,62,59,57

5.4.1 Case 1: Primary MC problem at each dispatch is solvable

In this case, a 16-step dispatch simulation is shown to verify the performance of the algorithm when there is feasible solution at each dispatch of the MC formulation. Every time when a dispatch happens, the controller will base on (1) forecasting on PVs, thermal demands and baseloads; (2) remaining energy of ES units and remaining fuel of CHP units; (3) information in shown in Table 5-2 and Table 5-3 to formulate and solve the MC primary problem in 5.3.2, and if the MC primary problem is solvable, then send out dispatch and control commands to ES units, CHP units and controllable loads. The components of baseloads, thermal demands (commercial) at 15-minute interval are shown in Figure 5-5. Note that since the 2 buildings are geographically very close to each other, the solar radiations on PV panels are assumed to be identical. The forecasting absolute percentage errors (MAPE) of PVs, thermal demands and baseloads at each time is 10% and the maximum forecasting error is 20%.

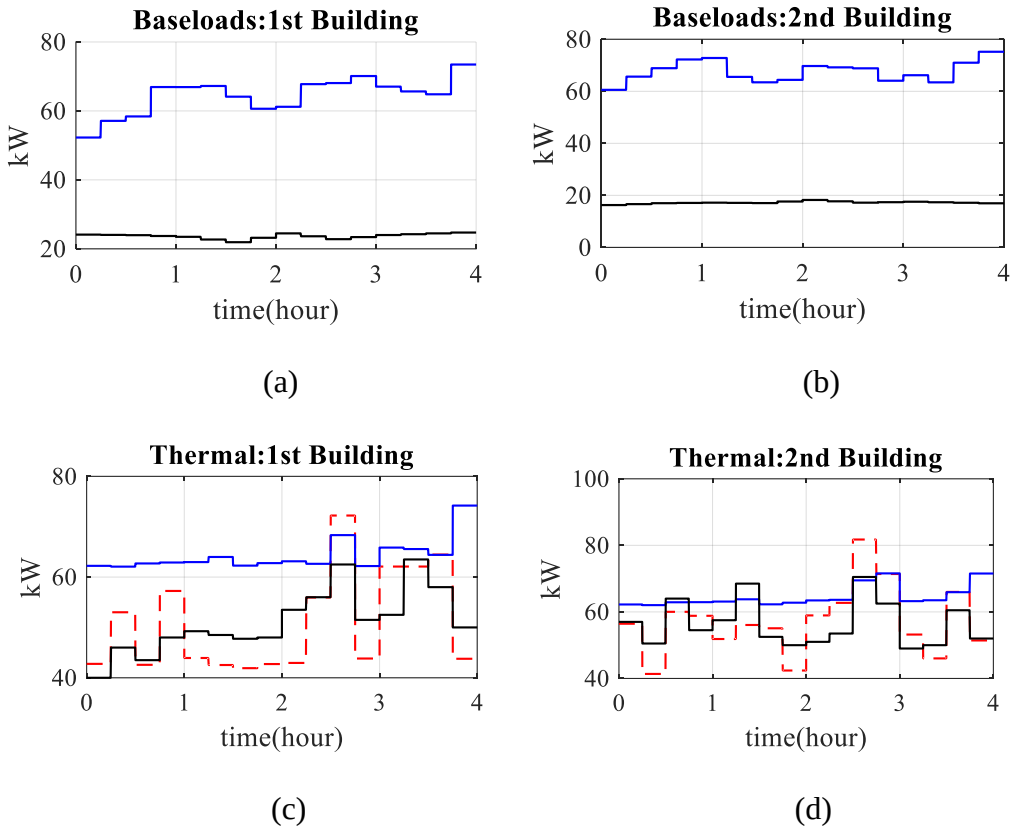

Figure 5-5. Baseloads, thermal supply and demand: (a) 15.min resolution actual load curves of residential (blue) and commercial baseloads (black) at 1st building; (b) 15.min resolution load curves of residential (blue) and commercial baseloads (black) at 2nd building; (c) thermal supply from 1st CHP unit P_{abs}^{1} (blue) and thermal demand of 1st building thermal load P_{th}^{1} (actual in black and forecasted in red); (d) thermal supply from 2nd CHP unit P_{abs}^{2} (blue) and thermal demand of 2nd building thermal load P_{th}^{2} (actual in black and forecasted in red)

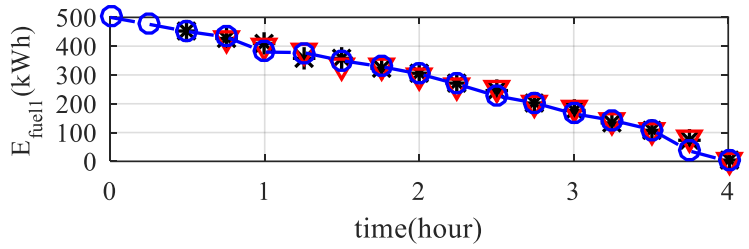

(a)

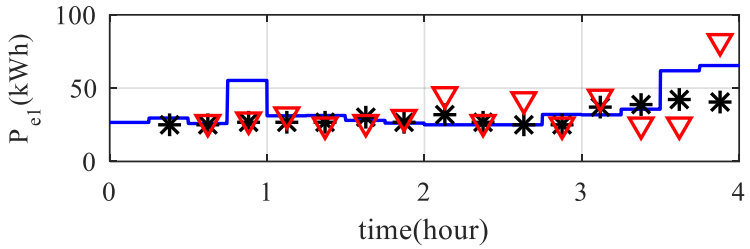

(b)

Figure 5-6. Actual dispatch results vs anticipated dispatch of CHP 1: (a) Actual remaining fuel at each time step (blue), anticipated remaining fuel at 1 step (black) and 2 steps ahead (red); (b) actual CHP power output dispatch command at each time step (blue), anticipated remaining fuel at 1 step (black) and 2 steps ahead (red)

It can be seen from Figure 5-5 (b) that the algorithm is trying to supply the commercial thermal loads by waste heat as much as possible. This is because using waste heat does not increase the cost of generation, while using electricity to supply thermal loads will increase generation costs. The gap between black and blue curve when black curve is above blue curve in Figure 5-5 (c) and (d) represents the amount of electricity P_{abs}^{i}needed to supply thermal loads.

Dispatch results of CHP and ES units are shown in Figure 5-6 to Figure 5-7. Since the dispatch result curves of 2 CHP units are very similar, we only show the results of 1 CHP unit dispatch results. For the same reason, we also only show the results of 1 ES unit dispatch results. Figure 5-8 shows the dispatch commands to controllable loads. Except from demonstrating the actual dispatch results at each time step, one and two steps ahead dispatch

results are also drawn (in black and red) to compare the changes of dispatch commands with respect to time. The deviation is generated because of the forecasting error since forecasting is updated at the beginning of each dispatch.

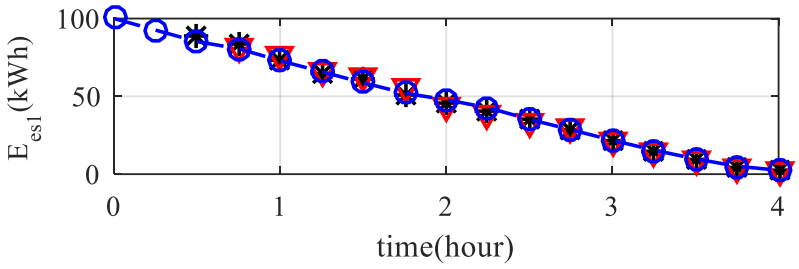

(a)

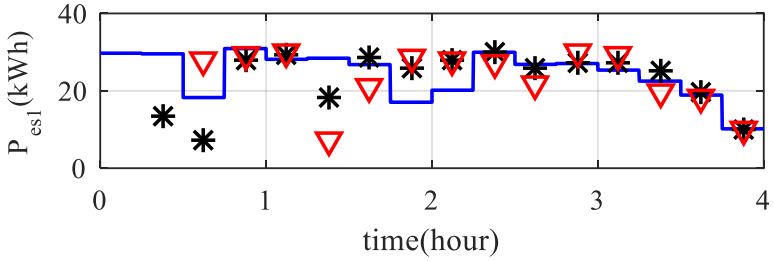

(b)

Figure 5-7. Actual dispatch results vs anticipated dispatch of ES 1. (a) Actual remaining energy at each time step (blue), anticipated remaining fuel at 1 step (black) and 2 steps ahead (red); (b) actual ES power output dispatch command at each time step (blue), anticipated remaining fuel at 1 step (black) and 2 steps ahead (red)

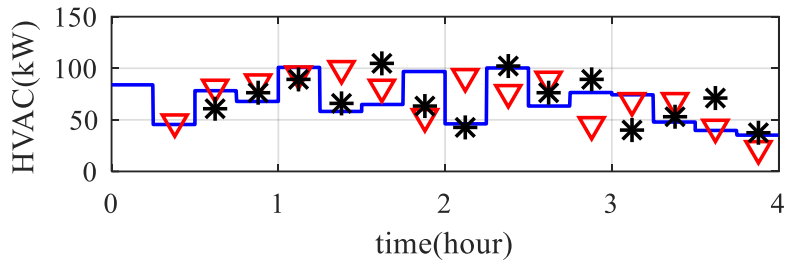

(a)

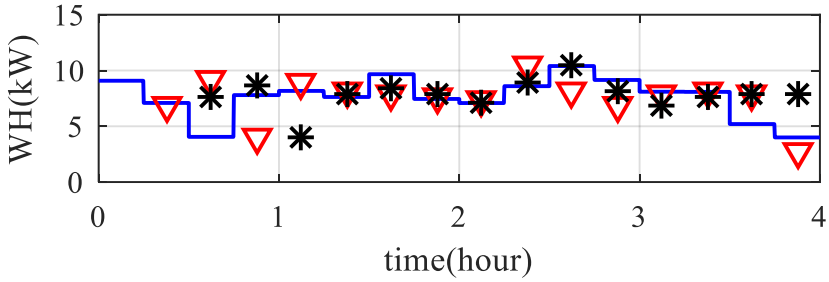

(b)

Figure 5-8. Actual dispatch results vs anticipated dispatch of controllable loads. (a) Actual operation schedule at each time step (blue), anticipated at 1 step (red) and 2 steps ahead (black) of HVAC units; (b) actual operation schedule at each time step (blue), anticipated at 1 step (black) and 2 steps ahead (red) of water heater units

The controllable loads commands are shown in Figure 5-8. One and two steps ahead dispatch commands are also drawn (in black and red) for comparison. It is easy to see that HVAC units can provide more potential capabilities than water heaters. This is because of the average turn-on time of a water heater is generally much less than an HVAC unit even though their rated power may be similar.

5.4.2 Case 2: MC primary formulation at certain dispatch is insolvable

Due to some reasons, e.g. incorrect forecasting, inappropriate sizing of ES or PVs, insufficient fuels remaining in CHP units or energy in ES units, there will be cases when the MC formulation is unsolvable. In this case, we are showing a condition when the MC formulation has no feasible solution at certain step and the corresponding response of the controller. All the setups are the same with Case 1 except that forecasting MAPE of PVs,

thermal demands and baseloads at each time step is 25%, which the maximum forecasting error is 50%.

An infeasible solution was found at time step 13. Figure 5-9 to Figure 5-11 shows the dispatch results at each step in this case. The dispatch commands at step 13 were marked as magenta. Because of the forecasting error at step 13, the baseloads and thermal loads cannot be met even if all controllable loads are fully shut down. As a result, baseloads and thermal loads must be shut down partially in order to ensure supply and demand balance. Based on Step 5 of MC algorithm, it is finally found that baseloads and thermal loads were forced to shut down by 10%.

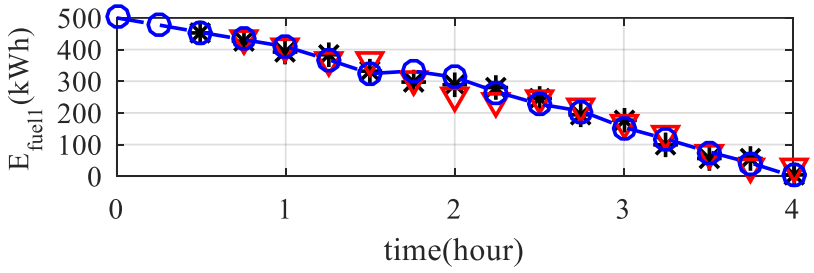

(a)

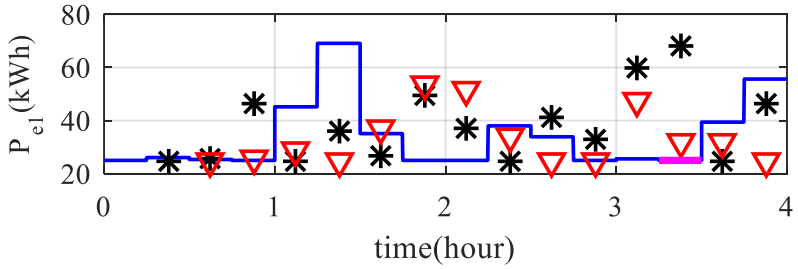

(b)

Figure 5-9. Dispatch results of CHP 1. (a) Actual remaining fuel at each time step (feasible in blue, infeasible in magenta), anticipated remaining fuel at 1 step (black) and 2 steps ahead (red); (b) actual CHP power output dispatch command at each time step (blue), anticipated remaining fuel at 1 step (black) and 2 steps ahead (red)

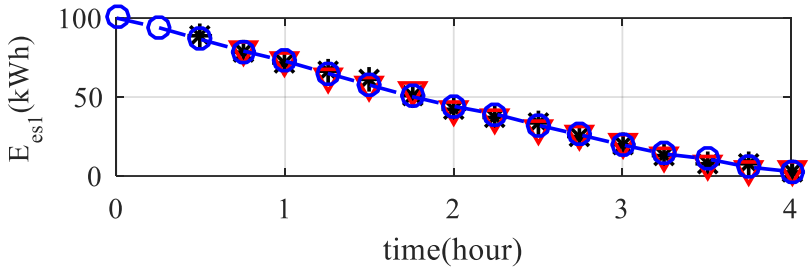

(a)

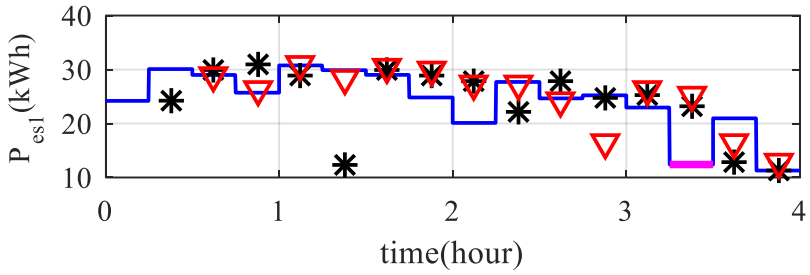

(b)

Figure 5-10. Actual dispatch results vs anticipated dispatch of ES 1. (a) Actual remaining energy at each time step (feasible in blue, infeasible in magenta), anticipated remaining fuel at 1 step (black) and 2 steps ahead (red); (b) actual ES power output dispatch command at each time step (blue), anticipated remaining fuel at 1 step (black) and 2 steps ahead (red)

It is also observed that due to no feasible solution to the MC formulation at time step 13, the total cost for this case is $384.75, which is much higher than the total cost $128.8 in Case 1. This implies that if the forecasting accuracy is good enough, controllable loads may not be needed to be fully shut down and no actions need to be taken to baseloads. Therefore, Case 3 is shown to observe the influence of forecasting errors on the MC problem.

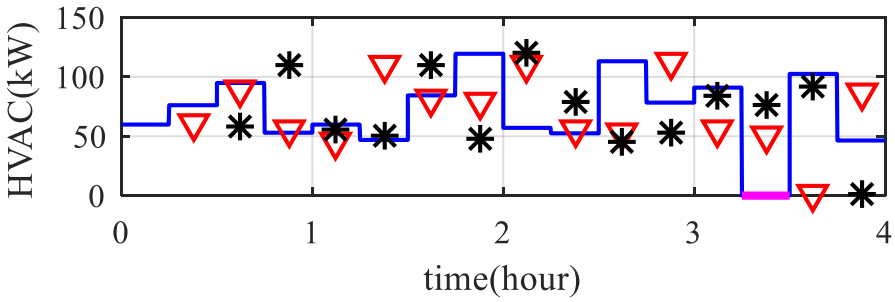

(a)

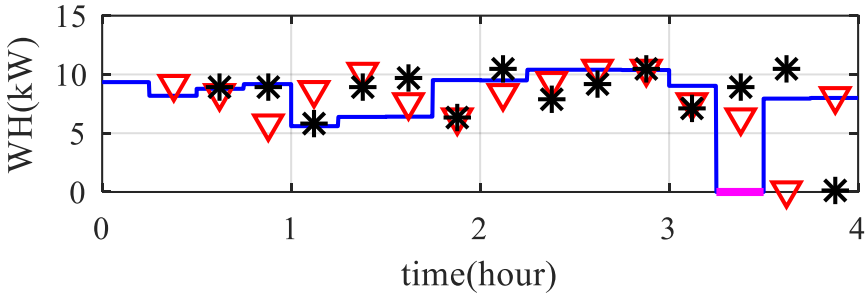

(b)

Figure 5-11. Actual dispatch results vs anticipated dispatch of controllable loads. (a) Actual operation schedule at each time step (feasible in blue, infeasible in magenta), anticipated at 1 step (red) and 2 steps ahead (black) of HVAC units; (b) actual operation schedule at each time step (blue), anticipated at 1 step (black) and 2 steps ahead (red) of water heater units

It is also observed that due to no feasible solution to the MC formulation at time step 13, the total cost for this case is \$384.75, which is much higher than the total cost \$128.8 in Case 1. This implies that if the forecasting accuracy is good enough, controllable loads may not be needed to be fully shut down and no actions need to be taken to baseloads. Therefore, Case 3 is shown to observe the influence of forecasting errors on the MC problem.

5.4.3 Case 3: Influence of forecasting accuracy on MC problem

A Monte-Carlo simulation showing the influence of forecasting accuracy on the MC problem is demonstrated in this case. All the setups are the same with Case 1 except that forecasting APE of PVs, thermal demands and baseloads at each time step follows different levels of uniform distributions $UNIF(0,10\%), UNIF(0,20\%), UNIF(0,30\%)$, and $UNIF$

(0,40%). At each level, 1000 simulation is performed to study the statistical results of the influence of forecasting accuracy on the MC problem. At each level of forecasting accuracy, the following statistics are recorded: forecasting MAPE, mean, standard deviation, maximum and minimum of total cost, percentage of having infeasible solutions of the primary MC formulation, percentage of average number of occurrence of having infeasible solutions of primary MC formulation. The table summarizing the above information is shown in Table 5-4.

A scenario which assumes no forecasting error is also shown in Table 5-4 for comparison purpose. As can be seen in Table 5-4, generally, the higher the forecasting accuracy is, the less likely that primary MC formulation will have infeasible solutions, and therefore, less likely to shut down baseloads. Meanwhile, it can be seen that under 10% forecasting MAPE, no baseloads were shut down. This means that the MC commitment algorithm is most effective in a certain range of forecasting accuracy. However, in different scenarios, this forecasting accuracy may be different.

Table 5-4. Influence Different Levels of Forecasting Accuracy on the MC Problem

Forecasting MAPE	Max forecasting error	Total Cost($)				Percentage of infeasibility	Average Occurance of infeasiblity
		mean	std	max	min		
0%	0%	76.8	-	-	-	0	0
5%	10%	83.3	2.5	90.1	69.7	0	0
10%	20%	89.3	19.2	141.9	60	0	0
15%	30%	107.6	43.6	437.4	63.9	6%	0.06
20%	40%	214.7	188.3	920.9	63	40%	0.45

5.5 Conclusions

This chapter researches on the dispatch problem of a community level microgrid, which is consisted of DG, and DR resources, e.g. residential HVAC and water heater units and

commercial-residential hybrid buildings. A MC algorithm is proposed to optimally dispatch all DG and DR resources while supplying both electrical and thermal loads under islanding operations. The MC algorithm formulates 2 sub-optimization problem to deal with the conditions when DG and DR resources can or cannot supply baseloads. Three cases are performed to verify the effectiveness of the MC algorithm and the influence of forecasting accuracy on the MC algorithm.

CHAPTER 6 Summary

This dissertation researches on a commercial-residential hybrid community-level microgrid in 2 major areas: modeling and control.

In terms of modeling, a dynamic, integrated combined heat and power unit (CHP) for microgrid applications is first developed. The CHP unit is a Simulink-based model, but is able to run under real time test system, e.g. OPAL-RT. A Zero-SSE isochronous governor used in islanding conditions is proposed. The advantages of the Zero-SSE governor include: (1) no steady-state error in frequency regulation; (2) providing a capability of sharing load changes between multiple generation units. Besides, the derating effects of ambient temperatures on fuel efficiency, maximum power output, exhaust heat output are also modeled to improve the accuracy of the CHP model. A series of simulation studies are performed to validate the proposed model.

Then, a data-driven decoupled modeling methodology for Thermostatic Controlled Appliances (TCA) is proposed. In this section, an optimization-based method is proposed to systematically estimate the RCQ parameters for 1st order ETP model. Then, a decoupled-ETP model which decoupled the parameters in ON/OFF cycles is proposed to improve the modeling accuracy of ETP model. Then, an adjusted decoupled-ETP model is proposed to improve the modeling accuracy of TCAs for whole-day use if only midnight data can be available or usable. Simulation studies show that the decoupled-ETP has the best performance when whole-day data are usable, while adjusted decoupled-ETP model works the best for whole-day operation applications when only midnight data are usable.

Load forecasting is essential for control and scheduling. A data-driven algorithm is proposed to forecast the short-term household load energy usage. Compared with traditional methods, temperature and power measurement sensors are added for major appliances in the house such that individual algorithm for different types of appliances can be applied to improve the forecasting accuracy. A series of studies are performed to validate the effectiveness of the data-driven algorithm. Studies show that the proposed data-driven greatly improved the forecasting accuracy of household loads compared with traditional techniques, like neural network, multi-linear regression. Cost-benefit studies also show that 4-6 major appliances measurable will be enough for forecasting purpose while not generating very high sensor installation costs. Studies also show that TCAs must have no more than 1 minute resolution data and non-TCAs can go up to 5 minute resolution in terms of measurement accuracy.

Last, a microgrid commitment algorithm is proposed for dispatching DG and DR resources in hybrid community-level microgrid under islanding operations. This is considered to be the 1st time research on dispatching and scheduling of such a microgrid system. Computational costs are minimized by: (1) designing a decentralized control scheme (a central controller and several local controllers) such that central controller does not need to know the status of each controllable load; (2) considering DR resources as block bid-in penalty costs into the dispatch strategy; (3) modeling most constraints as linear functions. Simulation results show that the MC algorithm is able to optimally dispatch all the resources in the microgrid system. Meanwhile, there exists a threshold value of forecasting accuracy under which the MC algorithm works the best.

References

[1]. US Department of Energy, “Microgrid Portfolio of Activities”, 2017, [Online] https://energy.gov/oe/services/technology-development/smart-grid/role-microgrids-helping-advance-nation-s-energy-syst-0

[2]. Berkeley Lab, “Microgrid Concepts”, 2017, [Online], https://building-microgrid.lbl.gov/microgrid-concept

[3]. URBANLAND, A hybrid building for a new way of life, 2017, [Online]. Available: https://urbanland.uli.org/planning-design/a-hybrid-for-a-new-way-of-life-the-home-office-building/

[4]. L. Martirano, S. Fornari, A. Di Giorgio and F. Liberati, "A case study of a commercial/residential microgrid integrating cogeneration and electrical local users," 2013 12th International Conference on Environment and Electrical Engineering, Wroclaw, 2013, pp. 363-368

[5]. S. Massucco, A. Pitto and F. Silvestro, "A gas turbine model for studies on distributed generation penetration into distribution networks," IEEE Trans. Power Syst., vol. 26, no. 3, pp. 992–999, Aug. 2011.

[6]. A. Lazzaretto and A. Toffolo, "Analytical and Neural Network Models for Gas Turbine Design and Off-Design Simulation," International Journal of Thermodynamics, vol. 4, pp. 173–182, 2001.

[7]. L. N. Hannett and A. H. Khan, "Combustion turbine dynamic model validation from tests," IEEE Transactions on Power Systems, vol. 8, pp. 152-158, 1993.

[8]. H. Asgari, X. Chen and R.Sainudiin, "Considerations in modelling and control of gas turbines — A review," in Control, Instrumentation and Automation (ICCIA), 2011 2nd International Conference on, 2011, pp. 84-89.

[9]. M. R. Faieghi and S. M. Azimi, "Design an Optimized PID Controller for Brushless DC Motor by Using PSO and Based on NARMAX Identified Model with ANFIS," in International Conference on Computer Modelling and Simulation, 2010, pp. 16-21.

[10]. F. P. D. Mello, D. J. Ahner, F. P. D. Mello, and D. J. Ahner, "Dynamic models for combined cycle plants in power system studies," IEEE Transactions on Power Systems, vol. 9, pp. 1698-1708, 1994.

[11]. M. Nagpal, A. Moshref, G. K. Morison, and P. Kundur, "Experience with testing and modeling of gas turbines," in Power Engineering Society Winter Meeting, 2001, pp. 652-656 vol.2.

[12]. S. K. Kim, H. A. Thompson and P. J. Fleming, "Fuzzy modeling of a gas turbine engine using clustering and multi-objective optimization," in Control Applications, 2003. CCA 2003. Proceedings of 2003 IEEE Conference on, 2003, pp. 564-569 vol.1.

[13]. N. Chiras, C. Evans and D. Rees, "Nonlinear gas turbine modeling using NARMAX structures," IEEE Transactions on Instrumentation & Measurement, vol. 50, pp. 893.898, 2001.

[14]. W. I. Rowen, "Simplified Mathematical Representations of Heavy-Duty Gas Turbines," Journal of Engineering for Gas Turbines & Power, vol. 105, pp. 865.869, 1983.

[15]. M. H. L. and R. B. G., "Utility experience with gas turbine testing and modeling," in Power Engineering Society Winter Meeting, 2001. IEEE, 2001, pp. 671-677 vol.2.

[16]. S. K. Yee, F. M. Hughes and J. V. Milanovic, "Comparative Analysis and Reconciliation of Gas Turbine Models for Stability Studies," in Power Engineering Society General Meeting, 2007. IEEE, 2007, pp. 1-8.

[17]. S. R. Guda, "Modeling and power management of a hybrid wind microturbine power generation system", thèse de master de l'université de Bozeman, Monata. Juillet. 2005.

[18]. S. K. Yee, J. V. Milanovic and F. M. Hughes, "Overview and Comparative Analysis of Gas Turbine Models for System Stability Studies," IEEE Transactions on Power Systems, vol. 23, pp. 108 - 118, 2008.

[19]. N. Chiras, C. Evans, D. Rees, "Nonlinear modelling and validation of an aircraft gas turbine engine," Nonlinear Control Systems 2001 (IFAC Symposia Series), pp. 871–876. 2001.

[20]. I. Rand, "MT250 Series Microturbine,", 2009. [Online]. Available: http://www.ingersollrandproducts.com/energy/_catalogs/Ingersoll%20Rand%20MT250%20Microturbine%20Product%20Spec%20080LTb.pdf.

[21]. L. Yi, "Research on Hybrid Micro/Small-turbine Based CCHP-Groundwater Heat Pump System,": Chinese Academy of Sciences, 2010.

[22]. MathWorks, "Synchronous Machine,", 2016. [Online]. Available: http://www.mathworks.com/help/physmod/sps/powersys/ref/synchronousmachine.html.

[23]. S. C. G. Company, "Absorption Chiller Guideline,", 1998. [Online]. Available: http://web.stanford.edu/group/narratives/classes/0809/CEE215/ReferenceLibrary/Chillers/AbsorptionChillerGuideline.pdf.

[24]. P. Palensky, D.Dietrich, "Demand Side Management: Demand Response, Intelligent Energy Systems, and Smart Loads," IEEE Transactions on Industrial Informatics, vol. 7, pp. 381-388, 2011.

[25]. N. Lu, “An Evaluation of the HVAC Load Potential for Providing Load Balancing Service,” IEEE Transactions on Smart Grid, vol. 3, pp. 1263.1270, 2013.

[26]. M. Pipattanasomporn, M. Kuzlu, S. Rahman, “An Algorithm for Intelligent Home Energy Management and Demand Response Analysis,” IEEE Transactions on Smart Grid, vol. 3, pp. 2166-2173, 2013.

[27]. S. Shao, M. Pipattanasomporn, S. Rahman, “Development of physical-based demand response-enabled residential load models,” IEEE Transactions on Power systems, vol. 28, pp. 607-614, 2013.

[28]. Y. Ozturk, D. Senthilkumar, S. Kumar, G. Lee “Demand Response Optimization for Smart Home Scheduling Under Real-Time Pricing,” IEEE Transactions on Smart Grid, vol. 3, pp. 1812-1821, 2012.

[29]. K.M Tsui, S.C Chan “An Intelligent Home Energy Management System to Improve Demand Response,” IEEE Transactions on Smart Grid, vol. 4, pp. 694-701, 2013.

[30]. M. A. Abu-El-Magd, N. K. Sinha, "Short-Term Load Demand Modeling and Forecasting: A Review," IEEE Transactions on Systems, Man and Cybernetics, vol. 12, pp. 370-382, 1982

[31]. N. Amjady, "Short-term hourly load forecasting using time-series modeling with peak load estimation capability," IEEE Transactions on Power Systems, vol. 16, pp. 798-805, 2001.

[32]. J. F. Chen, W. M. Wang, and C.-M. Huang, "Analysis of an adaptive time series autoregressive moving-average (ARMA) model for short-term load forecasting," Electric Power Systems Research, vol. 34, pp. 187-196, 1995.

[33]. T. Hong, "Short Term Electric Load Forecasting," Ph.D. dissertation, ECE Dept., North Carolina State University, Raleigh, North Carolina, 2010.

[34]. M. Vanouni.; N. Lu, "Improving the Centralized Control of Thermostatically Controlled Appliances by Obtaining the Right Information," in Smart Grid, IEEE Transactions on, vol.6, no.2, pp.946-948, March 2015

[35]. A. G. Ruzzelli, C. Nicolas, A. Schoofs and G. M. P. O'Hare, "Real-Time Recognition and Profiling of Appliances through a Single Electricity Sensor," 2010 7th Annual IEEE Communications Society Conference on Sensor, Mesh and Ad Hoc Communications and Networks (SECON), Boston, MA, 2010, pp. 1-9.

[36]. S. Makonin, F. Popowich, L. Bartram, B. Gill and I. V. Bajić, "AMPds: A public dataset for load disaggregation and eco-feedback research," 2013 IEEE Electrical Power & Energy Conference, Halifax, NS, 2013, pp. 1-6.

[37]. M. Weiss, A. Helfenstein, F. Mattern and T. Staake, "Leveraging smart meter data to recognize home appliances," 2012 IEEE International Conference on Pervasive Computing and Communications, Lugano, 2012, pp. 190-197.

[38]. M. Dong, P. C. M. Meira, W. Xu and C. Y. Chung, "Non-Intrusive Signature Extraction for Major Residential Loads," in IEEE Transactions on Smart Grid, vol. 4, no. 3, pp. 1421-1430, Sept. 2013.

[39]. A. I. Cole and A. Albicki, "Data extraction for effective non-intrusive identification of residential power loads," IMTC/98 Conference Proceedings. IEEE Instrumentation and Measurement Technology Conference. St. Paul, MN, 1998, pp. 812-815 vol.2.

[40]. H. Najmeddine et al., "State of art on load monitoring methods," 2008 IEEE 2nd International Power and Energy Conference, Johor Bahru, 2008, pp. 1256-1258.

[41]. R. Torkzadeh, A. Mirzaei, M. M. Mirjalili, A. S. Anaraki, M. R. Sehhati and F. Behdad, "Medium term load forecasting in distribution systems based on multi linear regression & principal component analysis: A novel approach," *2014 19th Conference on Electrical Power Distribution Networks (EPDC)*, Tehran, 2014, pp. 66-70

[42]. X. Zhang, X. Zhang and F. Fang, "Power forecasting of solar photovoltaic power systems based on similar day and M5' model trees," *2017 36th Chinese Control Conference (CCC)*, Dalian, 2017, pp. 9238-9243.

[43]. S. Karthika, V. Margaret and K. Balaraman, "Hybrid short term load forecasting using ARIMA-SVM," *2017 Innovations in Power and Advanced Computing Technologies (i-PACT)*, Vellore, India, 2017, pp. 1-7.

[44]. G. Acuña, C. Ramirez and M. Curilem, "Comparing NARX and NARMAX models using ANN and SVM for cash demand forecasting for ATM," *The 2012 International Joint Conference on Neural Networks (IJCNN)*, Brisbane, QLD, 2012, pp. 1-6.

[45]. X. Hua, Y. Le, W. Jian and V. Agelidis, "Short-term power forecasting for photovoltaic generation based on wavelet neural network and residual correction of Markov chain," *2015 IEEE PES Asia-Pacific Power and Energy Engineering Conference (APPEEC)*, Brisbane, QLD, 2015, pp. 1-5.

[46]. S. Katipamula and N. Lu, “Evaluation of residential HVAC control strategies for demand response programs,” ASHRAE Trans., vol. 1, no. 12, pp. 1–12, 2006.

[47]. C.E. Shannon, "Communication in the presence of noise". Proceedings of the Institute of Radio Engineers. 37 (1): 10–21, Jan 1947

[48]. S. Ihara and F. C. Schweppe, “Physically based modeling of cold load pickup,” IEEE Trans. Power App. Syst., vol. PAS-100, no. 9, pp. 4142–4150, Sep. 1981.

[49]. E. Agneholm and J. Daalder, “Cold load pick-up of residential load,”Proc. Inst. Elect. Eng., Gen., Transm.,Distrib., vol. 147, no. 1, pp.44–50, Jan. 2000.

[50]. J. Yan, Q. Zeng, Y. Liang, L. He and Z. Li, "Modeling and Implementation of Electroactive Smart Air-Conditioning Vent Register for Personalized HVAC Systems," in IEEE Access, to be published, doi: 10.1109/ACCESS.2017.2664580

[51]. A. Gomes, C. H. Antunes, and A. G. Martins, “Physically-based load demand models for assessing electric load control actions,” in Proc. IEEE Bucharest PowerTech, Jul. 2009.

[52]. R. E.Mortensen and K. P. Haggerty, “A stochastic computer model for heating and cooling loads,” IEEE Trans. Power Syst., vol. 3, no. 3, pp. 1213–1219, Aug. 1988.

[53]. N. Lu, “An evaluation of the HVAC load potential for providing load balancing service,” IEEE Trans. Smart Grid, vol. 3, no. 3, pp. 1263–1270, Sep. 2012

[54]. Pecan Street Inc., "Dataport", 2017. [Online]. Available: http://www.pecanstreet.org/

[55]. J. M. Sohn, "Generation Applications Package for Combined Heat Power in On-Grid and Off-Grid Microgrid Energy Management System," in *IEEE Access*, vol. 4, pp. 3444-3453, 2016

[56]. W. Z., G. W., W. R., Y. X., and L. W., "Economic optimal schedule of CHP microgrid system using chance constrained programming and particle swarm optimization," in 2011 IEEE Power and Energy Society General Meeting, 2011, pp. 1-11.

[57]. X. Lin, P. Li, J. Ma, and Y. Tian, "Dynamic optimal dispatch of combined heating and power microgrid based on leapfrog firefly algorithm," in IEEE International Conference on Networking, Sensing and Control, 2015, pp. 416-420

[58]. X. Wu, J. He, Y. Xu, J. Lu, N. Lu and X. Wang, "Hierarchical Control of Residential HVAC Units for Primary Frequency Control," in IEEE Transactions on Smart Grid, vol. PP, no. 99, pp. 1-1.

[59]. N. Lu and Y. Zhang, “Design considerations of a centralized load controller using thermostatically controlled appliances for continuous regulation reserves,” IEEE Trans. Smart Grid, vol. 4, no. 2, pp. 914-921, Jan. 2013.

[60]. Department of Energy, "Absorption Cooling Basics", 2017. [Online]. Available: https://energy.gov/eere/energybasics/articles/absorption-cooling-basics

[61]. Diesel Service & Supply, “Approximate Natural Gas Consumption Chart”, 2017, Available: http://www.dieselserviceandsupply.com/Natural_Gas_Fu-el_Consumption.aspx

[62]. PPINYS, “2015 Average price of natural gas”, 2015, [Online]. Available: http://www.ppinys.org/reports/jtf/naturalgas.html

[63]. T. Sun, J. Lu, Z. Li, D. Lubkeman and N. Lu, "Modeling Combined Heat and Power Systems for Microgrid Applications," in IEEE Transactions on Smart Grid, vol. PP, no. 99, pp. 1-1.

[64]. X. Ke, N. Lu and C. Jin, "Control and size energy storage for managing energy balance of variable generation resources," 2014 IEEE PES General Meeting | Conference & Exposition, National Harbor, MD, 2014, pp. 1-5.

[65]. MATLAB 2017a, The MathWorks, Inc., Natick, Massachusetts, United States.

[66]. GAMS Development Corporation. General Algebraic Modeling System (GAMS) Release 24.2.1. Washington, DC, USA, 2013.

[67]. J. Currie and D. I. Wilson, "OPTI: Lowering the Barrier Between Open Source Optimizers and the Industrial MATLAB User," Foundations of Computer-Aided Process Operations, Georgia, USA, 2012

[68]. SUNPOWER, "How Many Solar Panels Do You Need: Panel Size and Output Factors", 2017, [Online]. Available: https://us.sunpower.com/blog/how-many-solar-panels-do-you-need-panel-size-and-output-factors

[69]. National Fuel Cell Research Center, "Commercial Office Building Measurements and Dynamic Integrated Distributed Energy Resource Application, Analyses, and Control", 2016, [Online]. Available: http://www.nfcrc.uci.edu/3/research/researchsummaries/DynamicModeling/DYNAMIC-MODELING_CommBldgData-Analyses.pdf

[70]. ENERGY.GOV, "Reference Buildings by Building Type", 2017, [Online]. Available: https://energy.gov/eere/buildings/downloads/reference-buildings-building-type-medium-office

[71]. Xinda Ke, "Solution Methods of Large-Scale Power System Resource Scheduling and Dispatch Problems," Ph.D. dissertation, North Carolina State University, 2016

[72]. X. Ke, D. Wu and N. Lu, "A Real-Time Greedy-Index Dispatching Policy for using PEVs to Provide Frequency Regulation Service," IEEE Trans. Smart Grid, vol. PP, no. 99, pp. 1-1.

[73]. J. E. Beasley, editor. Advances in Linear and Integer Programming. Oxford Science, 1996. (Collection of surveys)

[74]. X. Ke, N. Lu and C. Jin, "Control and Size Energy Storage Systems for Managing Energy Imbalance of Variable Generation Resources," *IEEE Trans. Sustainable Energy*, vol. 6, no. 1, pp. 70-78, Jan. 2015.

[75]. X. Ke, N. Lu and C. Jin, "Control and size energy storage for managing energy balance of variable generation resources," *2014 IEEE PES General Meeting | Conference & Exposition*, National Harbor, MD, 2014, pp. 1-5.

[76]. P. Du et al., "Probabilistic-Based Available Transfer Capability Assessment Considering Existing and Future Wind Generation Resources," *IEEE Trans. Sustainable Energy*, vol. 6, no. 4, pp. 1263-1271, Oct. 2015

[77]. Xinda Ke, Anjie Jiang and Ning Lu, "Load profile analysis and short-term building load forecast for a university campus," *2016 IEEE Power and Energy Society General Meeting (PESGM)*, Boston, MA, 2016, pp. 1-5.